2021

Co-axial printing of growth factor-laden microspheres for pancreatic islet transplantation

Ane Urigoitia Asua

UNIVERSITY
OF WOLLONGONG
AUSTRALIA

Co-axial printing of growth factor-laden microspheres for pancreatic islet transplantation

Ane Urigoitia Asua

Supervisors:
(University of Wollongong) Dr. Zhilian Yue, Dr. Xiao Liu, Prof. Gordon Wallace
(Utrecht University) Dr. Yang Li

This thesis is presented as part of the requirement for the conferral of the degree:
Double degree in Biofabrication (University of Utrecht)

University of Wollongong / Utrecht University

August 2021

Double degree in Biofabrication

This project is part of the double degree Master in Biofabrication, held between the University of Utrecht (the Netherlands) and the University of Wollongong. The experimental work on the project "Co-axial printing of growth factor-laden microspheres for pancreatic islet transplantation" lasted for one year. The experimental part of the master was completed with another eight-month project at the University of Utrecht, "Bioresin development for 3D lithography". The report of the work done in Utrecht is shown at the end of the thesis, in Annex 1.

Abstract

Type I diabetes is an autoimmune disease affecting millions of people in the world. It occurs when the pancreas cannot produce insulin, resulting in episodes of hyperglycaemia that can lead to heart attacks, renal failure, or death. The main cause is the auto destruction of beta cells that produce insulin, located in the pancreatic islets (or islets of Langerhans). Current treatments include insulin injections that decrease the blood glucose level. However, it can sometimes generate hypoglycaemia or insulin resistance on the patients. Bioprinting allows controlled engineering of pancreatic islets with hydrogel scaffolds and transplanting them into the patients. Nevertheless, immunotolerance of the grafted constructs has yet to be achieved. Currently, the islets are implanted together with immunosuppressors to avoid the rejection, but these affect the functionality of the beta cells. Co-transplanting regulatory T cells (Tregs) that regulate the autoimmune response could be the solution to immune rejection. Thus, co-axial extrusion printing is a promising approach, as it allows printing two types of bioinks. Pancreatic islets can be printed in the core of the structure and Tregs in the shell, protecting the islets. This project was mainly focused on the development of the bioink for the shell. The ink consists of a hydrogel that promotes cell growth and allows bioprinting (2% alginate/7.5% gelatin methacrylolyl (GelMA)/3.5% gelatin), and growth factors for Treg functionality (IL-2). The growth factors were encapsulated in GelMA microspheres for a sustained release inside the ink. The release rate of IL-2 was studied, as well as the ink properties and printability.

Laymen's Summary

Type I diabetes affects millions of people in the world. It is an autoimmune disease, where the patient's own immune system attacks the body. It occurs when the immune system destroys the beta cells that are responsible for generating insulin, located in the pancreatic islets. Insulin regulates and reduces the sugar level in the blood stream when it is too high. However, type 1 diabetic people have a lack of this hormone, therefore, they present episodes of hyperglycaemia (high levels of sugar in blood). This can lead to heart attacks, renal failure or death. Current treatments include insulin injections that decrease the blood glucose level. However, its extensive use can sometimes generate hypoglycaemia (low levels of sugar in blood) or insulin resistance on the patients.

Bioprinting is an emerging technology where 3D printing is applied to the biology, providing the opportunity to assemble cells with or without biomaterials in a spatially controlled manner. It allows engineering pancreatic islets in scaffolds and transplanting them into the patients. Nevertheless, immunotolerance of the grafted constructs has yet to be achieved. The immune system could attack the transplanted constructs because the cells and materials used are foreign and/or because in type 1 diabetes, the pancreatic islets are generally attacked. Currently, the islets are implanted together with immunosuppressors to mitigate the rejection and provide some immunotolerance. However, these suppressors affect the functionality of the beta cells. Co-transplanting regulatory T cells (Tregs) that regulate the autoimmune response could be the solution to immune rejection. Thus, co-axial extrusion printing is a promising approach, as it allows printing two types of bioinks. Extrusion printing works delivering the material through a needle (called nozzle) and depositing it into 3D constructs with desired coordination. In the co-axial variety, the nozzle has two inputs (one for each material). These two materials are extruded simultaneously, one inside the other one. In the approach for bioprinting a solution for type 1 diabetes, pancreatic islets could be printed in the core of the structure (inside) and Tregs in the shell (outside), protecting the islets.

This project was mainly focused on the development of the bioink (the supporting biomaterial for the cells, responsible for providing mechanical structure and environment for the cells) for the shell. The ink consisted of a hydrogel, a material rich in water that promotes cell growth and allows bioprinting (2% alginate/7.5% gelatin methacrylolyl (GelMA)/3.5% gelatin). Furthermore, some growth factors necessary for Treg functionality (interleukin-2 or IL-2) were needed. The growth factors were encapsulated in GelMA microspheres for a sustained release inside the ink. The microspheres are sub-micron to micron sized hollow spheres, often used for drug encapsulation. In the project, the release rate of IL-2 from the microspheres was studied, as well as the ink properties and printability.

Acknowledgements

I would like to acknowledge and express my gratitude to my supervisors, Dr. Zhilian Yue and Dr. Xiao Liu, for their help and guidance throughout the project. I would also like to thank Prof. Gordon Wallace and Prof. Michael Higgins, for contributing to the establishment of the double degree between Utrecht and Wollongong, and for allowing me make use of the Australian Institute for Innovative Materials (AIIM), specifically The Intelligent Polymer Research Institute (IPRI), for my experimental work. Besides, I would like to acknowledge the collaborators at the University of Adelaide in the group of Professor Coates, especially Juewan Kim.

Furthermore, I would like to thank the two previous students who worked in characterising the ink and the printing parameters for the islet printing project, Sarah Carter and Max Renes. Special thanks to Narangerel Gantumur, for showing me the technique of microsphere formation and exchanging valuable information for the development of the project.

I would like to extend my thanks to the AIIM-IPRI team for their assistance throughout my project, specifically to Cameron Angus, Dr Andrew Nattestad, Dr Holly Warren and pHd students Alex Nagle, Aida Naseri, Jeremy DiNoro and Malachy Maher. Finally, I would like to thank my fellow master students, Ane Albillos, Borja Sanz and Jacopo Bani, for their advice and support.

Certification

I, Ane Urigoitia Asua, declare that this thesis submitted in fulfilment of the requirements for the conferral of the degree Double degree in Biofabrication, from the University of Wollongong, is wholly my own work unless otherwise referenced or acknowledged. This document has not been submitted for qualifications at any other academic institution.

_____

Ane Urigoitia Asua

24th August, 2021

List of Names or Abbreviations

APC: anaphase-promoting complex

APS: ammonium persulfate

β cells: beta cells

D_2O: deuterium oxide

DoF: degree of functionalisation

EPC: endothelial progenitor cell

GelMA: gelatin methacrylolyl

IL-2: interleukin-2

Irgacure: 2-hydroxy-1-[4-(2-hydroxyethoxy)phenyl]-2-methyl-1-propanone

LAP: lithium phenyl-2,4,6-trimethylbenzoylphosphinate

MA: methacrylic anhydride

MHC: major histocompatibility complex

MPs: microparticles (microspheres)

NaOH: sodium hydroxide

NMR: nuclear magnetic resonance

PBS: phosphate-buffered saline

PLGA: poly(lactic-co-glycolic acid)

RGD: arginine-glycine-aspartate

T1D: type 1 diabetes

T2D: type 2 diabetes

Teff: effector T cell

TEMED: tetramethylethylenediamine

TERM: tissue engineering and regenerative medicine

Treg: regulatory T cell

UV: ultraviolet

Table of contents

List of Figures and Illustrations

Chapter 1

1. Introduction

1.1 Diabetes

Diabetes mellitus is a metabolic illness affecting millions of people worldwide. The cases of diagnosed diabetes in the world have increased drastically on the recent years, for instance, only in the United States the number of patients with type 2 diabetes has increased from 1.5 million to 24 million from 1958 to 2015 (Figure 1). It occurs when the pancreas does not function correctly (more information about the pancreas is shown in Box 1). The pancreas consists of different types of cells (Figure 2), which produce different hormones (Table 1). These cells include beta cells that generate insulin, a hormone that controls glucose levels in the blood stream. When patients generate insufficient insulin, they present elevated blood sugar levels (hyperglycaemia). This leads to complications such as risk of heart attack, kidney failure, cornea and nerve damage, etc (1–3). Its prevalence has increased significantly over the past decades, especially in developed and developing countries (4,5): 180 million were affected in 1980, rising to 422 million in 2014 (3,6). For instance, in the United States, the percentage of the diagnosed disease has increased from less than 1% to almost 8% in the past 60 years (7).

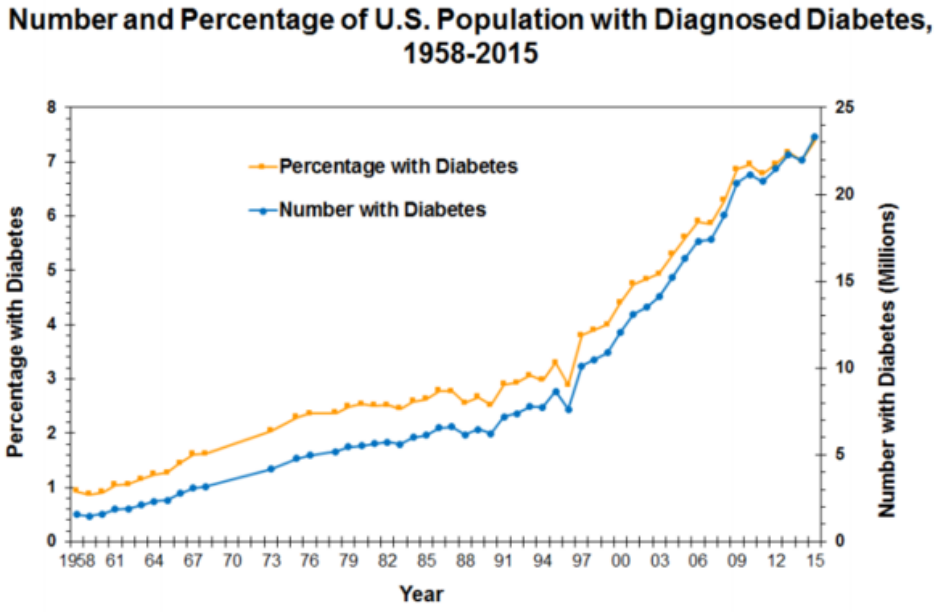

Figure 1. Evolution of diagnosed type II diabetes cases over the last 60 years in the United States (7).

Box 1. Structure and function of pancreas.

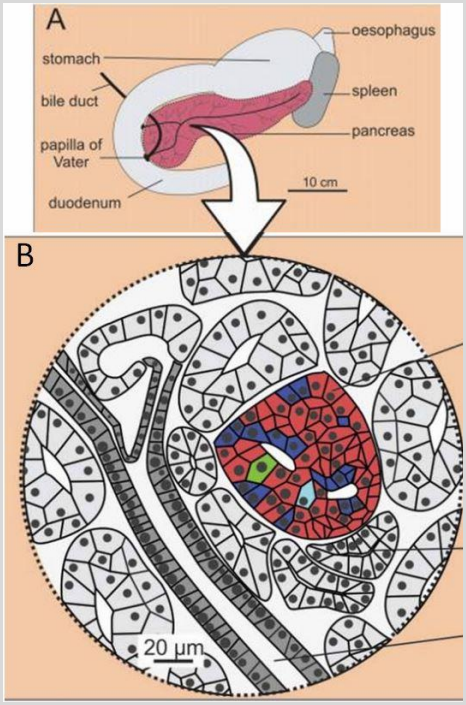

Figure 2. Structure of the human macroscopic (A) and microscopic (B) pancreas (modified from (8)). Figure 2B shows the cell distribution in the islets of Langerhans, which make up to 5% of the whole organ.

The pancreas is composed of two main components. One of them is the **exocrine** pancreas, which includes ductal and acinar cells. These generate enzymes that are delivered to the small intestine for the digestion. The other one is the **endocrine** pancreas, which represents less than 5% of the whole organ but is of vital importance.

The endocrine pancreas consists of the pancreatic islets or islets of Langerhans, formed by thousands of endocrine cells and a strong vasculature (1,8). There are 5 types of cells, each of them synthesising a different hormone:

Table 1. Summary of the quantity and hormone produced by each cell type in the islets (8,9).

Cells	% of cells in islets	Hormone produced
Beta	50-70%	Insulin
Alpha	20-40%	Glucagon
Delta	< 10% together	Somatostatin
PP		Pancreatic polypeptide
Epsilon	< 1%	Ghrelin

Insulin and glucagon are the two enzymes regulating glucose levels in blood. While insulin decreases the blood glucose level when it is high, glucagon increases it when it is low.

There are two main types of diabetes: type 1, also called insulin-dependent or juvenile diabetes; and type 2, also known as non-insulin-dependent or adult diabetes (3,10). Table 2 summarises the features of each type.

Table 2. Characteristics and differences of type 1 and 2 diabetes.

	Type 1 Diabetes	*Type 2 Diabetes*
People affected	- 5-10% of diabetics (40 million) (1–3) - Usually young population (>85% under the age of 20) (5)	- 90-95% of diabetics (380 - 400 million) (11) - Generally adult people (3,12) - Recently in younger ages as well (related to increase in sedentarism and obesity) (5)
Mechanism	- Beta cell destruction (insulin generating cells) by patient's own immune system (1,13) - No insulin secretion (or very low)	- Insulin resistance: even if insulin is created, target organs are resistant, keeping blood glucose levels high (10,14,15) - Insufficient compensatory insulin secretion (2)
Cause	- Autoimmune (10,16) - Combination of genetic, immunologic and environmental factors, although not fully understood yet (17)	- Genetic, environmental and lifestyle factors, obesity (18–21)
Consequences	- Risk of cardiovascular disease, neuropathy, retinopathy, nephropathy (1,13)	- Increased risk of stroke and heart attack (22,23), kidney failure (24), blindness, nerve damage (9) and limb amputations (25,26)
Treatment	- Daily insulin injections to decrease blood glucose levels (1,13)	- Lifestyle changes: diet, more exercise… in early stages (6) - Insulin injections in advanced stages (10)

As Table 2 shows, the two types are different. For better understanding, the difference in the mechanism between them is shown schematically in Figure 3. Even if fewer people are affected by it, T1D is more dangerous: it is a chronic autoimmune disease that destroys the insulin producing beta cells. As a consequence, they need daily controls to measure their blood glucose level, and a lifetime treatment to keep it in a normal range (1,27). Whereas Type 2 diabetes is mainly prevalent in the adulthood, more children suffer from the Type 1. Meanwhile, early T2D occurs when the

target tissues such as liver, fat or muscle are resistant to the insulin produced (10,28,29). This means that the problem is not the lack of insulin in the body, even if they lose beta cells in the advanced stages of the disease, producing less insulin than healthy individuals (10,30,31). Therefore, their condition can be initially improved by changing their lifestyle and acquiring healthier habits, to the point of not needing any treatment (or not as often as the T1D patients). For this reason, this work was focused on Type 1 diabetes.

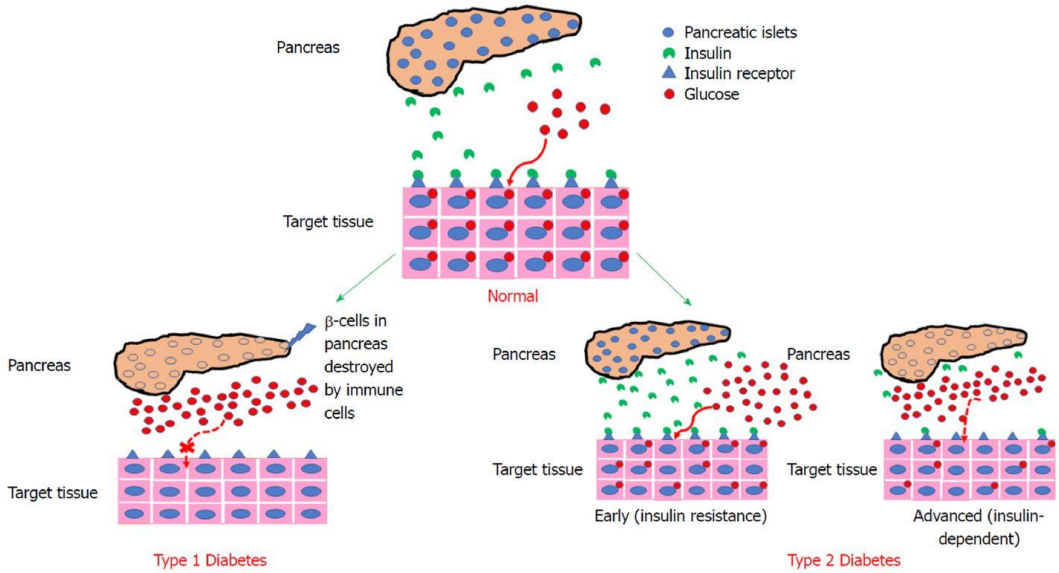

Figure 3. Schematic representation of the mechanism of type 1 and 2 diabetes (10). When the β-cells are destroyed, the insulin is not produced and glucose cannot be carried inside the cells, accumulating in the blood stream (T1D). However, type 2 diabetes starts when the β-cells produce insulin, but the target tissues are resistant, accumulating the part of the glucose in the blood stream. In later stages, less insulin is produced and T2D also becomes insulin dependent.

1.1.2 Current treatments for Type 1 diabetes

Type 1 diabetes occurs when the immune system of the patients attacks and destroys the insulin-producing beta cells (located in the Langerhans islets). People affected by it present various symptoms such as polydipsia (extreme thirstiness), polyphagia (increased appetite) and polyuria (large production of urine), as well as the already mentioned hyperglycaemia (27). The lack of treatment would result in serious consequences, especially cardiovascular events (stroke, myocardial infarction, etc), which might lead to limb amputations (27). Moreover, other dangerous effects are retinopathy, nephropathy and neuropathy (1,3).

Regeneration of the exocrine pancreas can be achieved naturally; however, the islets and the beta cells have a limited regenerative capacity (28). Therefore, T1D is a chronic disease: the symptoms usually appear when 90-95% of the beta cells are destroyed (1,27) and these cells are incapable of self-regeneration. For this reason, T1D must be tackled externally. The most widely spread method to treat diabetes is the use of insulin injections. These consist of subcutaneous administration of insulin to the patient in a controlled way. The insulin decreases the blood glucose level, taking it to a normal range. However, the exact dose and administration time might not match the functional

rhythms, and the intensive use can generate hypoglycaemia (3,32). Hypoglycaemia occurs when the glucose in blood is below the normal range. It can be as dangerous as hyperglycaemia, and it can occur if there is too much insulin in the blood stream (due to overusing the treatment). Hence, the main goal of the insulin administration (keeping blood glucose in a normal range) could fail on some occasions (33). Currently there are some measurements to improve this treatment, by using insulin analogues, insulin pumps or continuous glucose monitors (27). Additionally, the need of a daily insulin administration results in a high cost for the treatment (estimated 14.5-14.9 billion USD were spent in the USA in 2007 in T1D (34)). This leads to the treatment not being accessible for people in lower social-economical situations or regions.

Pancreas transplants have been considered as a solution to daily insulin injections and constant glucose monitoring. However, donor shortage and the frequent post-operatory complications are the main reasons limiting the wider application of this treatment option (35).

Another possible solution is the transplantation of the endocrine islets (36). This method has been previously proven as an effective therapy, by using allogenic pancreatic islets from deceased donors (37,38). Tissue engineering and biofabrication approaches can be used to engineer personalised islet constructs suitable for each patient.

1.2 Biofabrication and bioprinting

Biofabrication is a fast-evolving research field used increasingly on tissue engineering and regenerative medicine (TERM) (39). It is defined as the "*automated generation of biologically functional products with structural organization from living cells, bioactive molecules, biomaterials, cell aggregates such as micro-tissues, or hybrid cell-material constructs, through Bioprinting or Bioassembly and subsequent tissue maturation processes*" (39). These materials often include either biological components or living cells, or both. Bioprinting is under the umbrella of biofabrication. It incorporates the use of 3D printing (also known as additive manufacturing), to deposit living materials in a specific 2D or 3D pattern (40). Therefore, bioprinting allows for the precise deposition of materials, biomaterials, cells and growth factors, in a layer-by-layer fashion, generating complex structures for TERM. A schematic representation of biofabrication and TERM is shown in Figure 4.

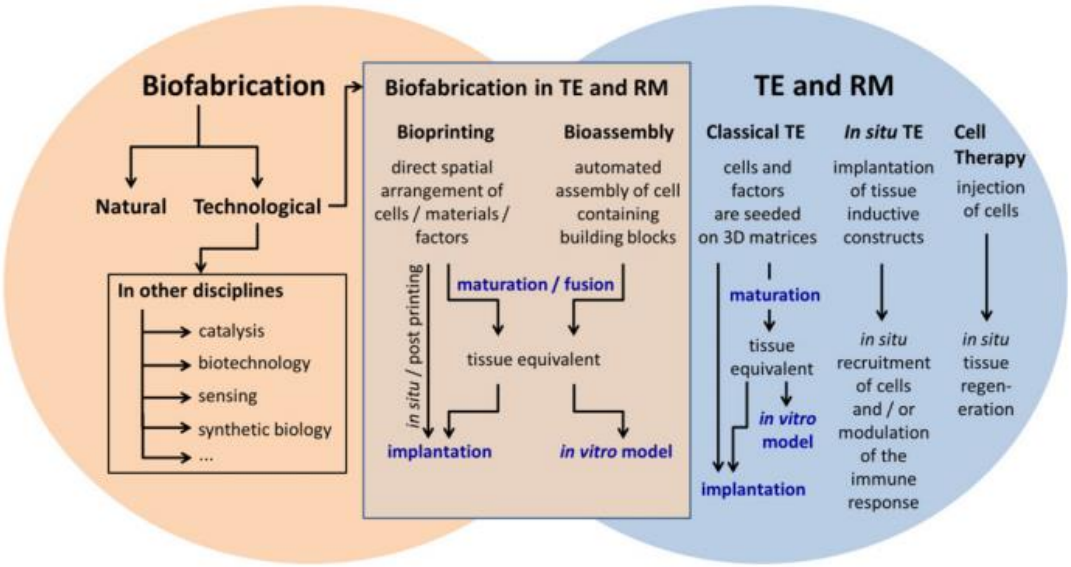

Figure 4. Scheme explaining biofabrication and its implication in TERM (39). On the one hand, biofabrication can occur naturally or technologically in many different disciplines (biotechnology, synthetic biology, etc). On the other hand, there are many different techniques that can be applied in tissue engineering and regenerative medicine: classical tissue engineering, where cells are seeded and matured in scaffolds or matrices for implantation; *in situ* tissue engineering, where biomaterials or inductive constructs are implanted to induce regeneration; and cell therapy, where cells are injected on the host to induce regeneration. However, biofabrication can also be applied in TERM. The main difference between using biofabrication or conventional TERM technologies is the ability to spatially arrange materials, which is a huge advantage for complex tissues.

The two main biofabrication techniques in TERM are bioprinting and bioassembly. The first one is a top-down manufacturing method and the second one, a bottom-up method (41). Top-down methods dispense small units of the biomaterial to build the structure, whereas bottom-up ones use blocks of materials and cell droplets as a starting point (42,43). This project will be focused on bioprinting for TERM only.

Figure 5 shows a schematic representation of bioprinting. The two most important parts for bioprinting are bioink and printing technique, which are introduced in detail. Depending on the organ or tissue, the bioink will be different. Besides, depending on the characteristics of the print (a model, a functional tissue and the type or size of tissue, etc), the printing method used will also be different.

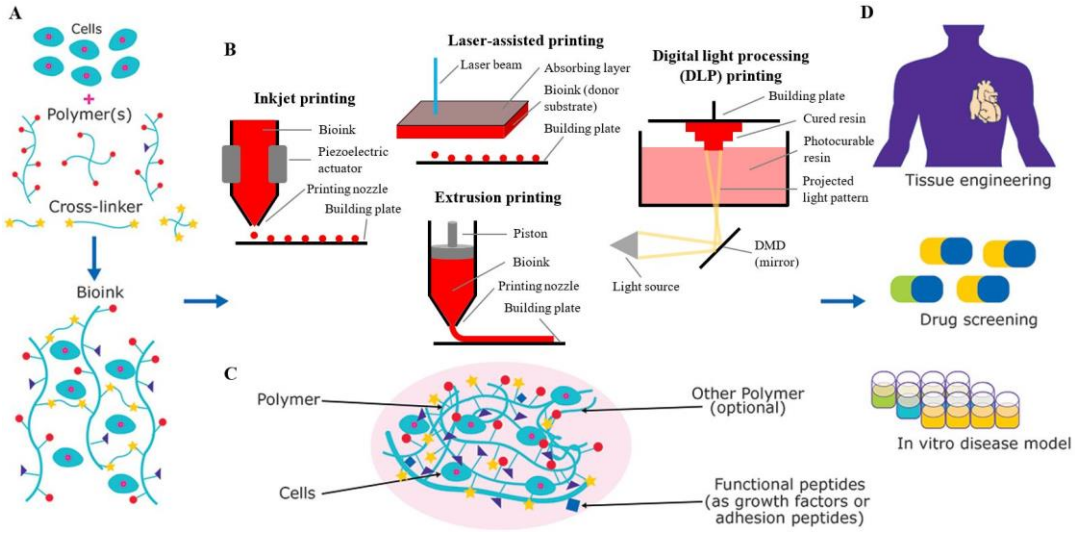

Figure 5. Graphical representation of the bioprinting process (modified from (44)). First, the bioink, a mixture of cells, polymers and crosslinkers, is chosen (A). Then, the bioink is printed, and different printing techniques can be used depending on the bioink used or the desired characteristics for the final result (B). While printing, the ink is crosslinked, generating a solid or gel-like composite comprising the polymers, cells and crosslinkers (C). Finally, these printed constructs can be used in many different areas, such as tissue engineering, drug testing or disease modelling (D).

1.2.1 Bioink

The mixture of components used in bioprinting (Figure 5) is referred as bioink. The bioink is generally composed of the polymers, cells and functional peptides such as growth factors other biological cues. Polymers work as a scaffold for cells. They support the desired structure of the printed construct and can be printed as porous materials, for nutrient and oxygen exchange between cells and the environment (45). The structure and composition of polymers vary depending on the type of tissue, the mechanical properties and degradability that need to provide, as well as the method of printing used (46,47). They can be natural, synthetic or a mixture of both. The cells added to the mixture can be fully differentiated or not. Also, several types of cells can be printed simultaneously, as well as cell clusters (aggregates). Finally, bioactive molecules (functional peptides), generally growth factors or signalling molecules are added to the bioink to regulate cell behaviour, phenotype and functions.

1.2.2 Bioprinting techniques

Different types of 3D printing technologies can be used for bioprinting. The main methods are mentioned in Figure 5B: inkjet printing, laser-assisted printing, extrusion printing and digital light processing (48,49).

- **Inkjet printing**. The mechanism came from the conventional 2D ink printers (50). Bioink droplets are expelled from the cartridge with a thermal or piezoelectric actuator (46,51).
- **Laser-assisted printing**. A laser pulse hits the donor layer (absorbing layer + bioink) in a certain position. The absorbing layer absorbs the energy of the laser, generating heat,

evaporating part of the bioink adhered to the absorbing layer and creating a high-pressure bubble. Then, a bioink droplet is ejected to the building plate (51).

- **Digital light processing (DLP) printing**. There are two types of stereolithography (SLA): laser-direct writing and mask-image projection printing. The second one is known as DLP printing. It uses a defined mask image, which is projected on the surface of the photocurable bioink, crosslinking an entire layer at a time (52,53).
- **Extrusion printing**. The bioink is continuously extruded, depositing cylindrical filaments with precision (51). The ink can be extruded with 3 different mechanisms: pneumatic, piston or screw-based (54).

Table 3 shows some features, advantages and disadvantages of different bioprinting techniques.

Table 3. Summary of advantages and disadvantages of the 4 main bioprinting techniques.

Printing modalities	*Advantages*	*Disadvantages*
Inkjet printing	High resolution (< 50 µm) (46,51).	Liquid or low viscosity bioinks only (<0.01 Pa·s), low cell density (< 10^7 cells/ml) (55)
Laser-assisted printing	Medium cell densities (<10^8 cells/ml), high bioink viscosity (1-300 mPa·s) (51).	High cost, limited ink availability (51).
DLP printing	High resolution (50 µm), fast, easy fabrication of complex geometries (51,53).	Use only for photocurable materials, limited biocompatible resins, cytotoxicity of photoinitiators (51,52).
Extrusion printing	High cell densities (no limitation) (46,56), wide range of bioinks available (51).	Relatively lower resolution (100-200 µm), limited printing conditions due to high shear stress (46,51).

In summary, 3D bioprinting presents a promising avenue to treatment of diabetes. Islets of Langerhans or insulin-producing beta cells could be 3D printed in a biological scaffold for TERM purposes. After maturation of the printed constructs, they could be transplanted in diabetic patients. In this way, the issue of donor shortage would be overcome, and the patients would be able to re-establish the insulin-producing system in their body. They would be in no need of more daily insulin injections. However, all the tissue-printing solutions, including islet printing, are still in research phase.

1.3 3D printing of bioink for pancreatic islet transplantation

1.3.1 Limitations for islet transplantation

Previous studies showed that infusions of islets via the patients' portal vein were successful as a treatment for diabetes (38,57). These islets were administered with immunosuppressors and most of the patients were insulin-independent for at least 5 years after several islet injections (58). However, one of the main issues of this technique is the immune reaction. The infusion of islets into the portal vein activates an innate immune response (10,59). In some cases, the islets could get trapped into blood clots, become hypoxic and generate a bigger immune reaction (59–61). This reaction, together with the side effects of the immunosuppressive drugs in the islets (62), contributes to the poor survival rate of the islets initially transplanted (therefore the need of several infusions to succeed) (36,63,64). Subcutaneous and gastric submucosa have been studied as alternative islet transplantation methods, with a higher success rate when compared to portal vein infusion (65,66). However, the three methods share the need of immunosuppressors (62,65,66).

Furthermore, type 1 diabetes patients have the immune system activated against the β cells, presenting immune reactions for even autologous islet transplants (67). Figure 6 explains the immune mechanism of T1D. A genetic defect in the bone marrow or thymus can present self-antigens (such as the ones of β cells) as harmful, generate autoreactive lymphocytes or have defects in lymphocyte precursors, which results in the immune system attacking β cells. Moreover, the immune system can also present anomalies that result in the immune cells attacking the islets and β cells: defective immune regulation, production of autoreactive antibodies, etc. Finally, β cells can also be defective. They can produce cytokines and chemokines that activate immune response, present high quantities of antigens or have a limited potential for replication, resulting in a low β cell renewing. For all these reasons, achieving immune tolerance is an essential requirement for islet transplantation in T1D.

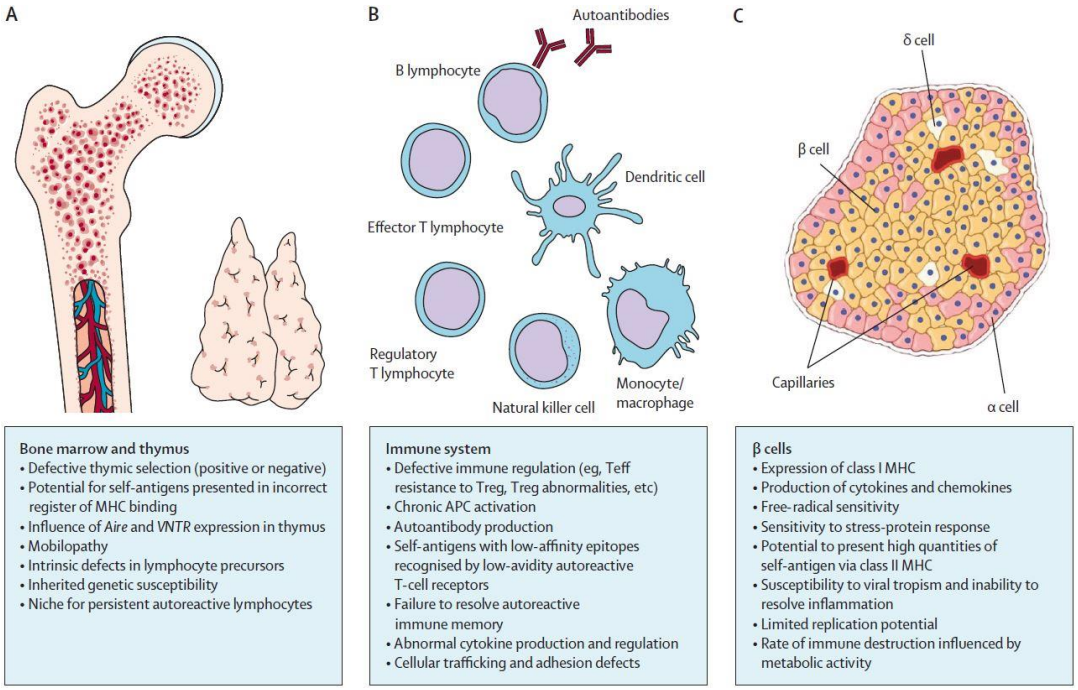

Figure 6. Molecular and metabolic processes that occur in type 1 diabetes (27). Insulin deficiency and T1D are caused by genetic and metabolic defects in the bone marrow and thyme (A), in the immune system (B) and in the β cells (C). Teff = effector T cell, Treg = regulatory T cell, APC = anaphase-promoting complex, MHC = major histocompatibility complex.

1.3.2 Achieving immune compatibility

The method previously explained uses a deceased donor (with no diabetes), mechanically and enzymatically digests the pancreas, and isolates the islets. These islets are then transplanted into the patient. However, this method has shown limited therapeutic outcome due to compromised islet functions as a result of the following two aspects:

- The infusion activates the innate immune response, killing the islets and creating blood clots and other complications.
- The use of immunosuppressors reduces β cell functionality as well as having other detrimental effects (risk of infection, organ toxicity, etc) (35,62).

Hence, a promising solution could be the transplantation of bioprinted constructs made of islets and supporting material to avoid the adverse reactions as a result of direct contact with blood flow. Besides, the immunosuppressors could be replaced with an alternative approach by means of providing immune-tolerant islet constructs. Two strategies have shown promise in reducing immune rejection. The first strategy involved coating islets with hydrogels, which create a barrier against the immune system (36). For example, alginate is an indigestible hydrogel in the human body, which has been proven to be non-immunogenic (68,69). It has been used to encapsulate islets (in micro- or macrocapsules), retaining islet functionality for over 10 months in human trials (36). However, the thickness of the capsules could determine the viability of the transplanted islets. If the alginate coating is too thin, the transplant could still trigger the immune rejection on the host. But if it is too

thick, the diffusion of nutrients and oxygen into the islets could be compromised, resulting in a poor cell viability (70,71). As a solution, various types of hydrogels, some of them are porous, could be mixed to provide a scaffold to facilitate oxygen and nutrient exchange. Gelatin methacrylolyl (GelMA), for instance, would provide tuneable mechanical properties, high degradability and RGD sequences that alginate lacks (72). Alternatively, other types of cells that provide immune tolerance could be co-transplanted together with the islets. Regulatory T cells (Tregs) are known to help suppressing the autoimmune reaction (37).

1.3.2.1 Regulatory T cells (Tregs)

Regulatory T cells are a type of lymphocytes. Their function is to promote tolerance to antigens (self or foreign) and maintain immune homeostasis (73), suppressing effector T cell responses up to a point (13,74). There are various types of Tregs that participate in the immunoregulation (75). Type 1 diabetes and a poor Treg function have been correlated, either due to an imbalance between effector T cells (Teffs) and Tregs (76), or because the Tregs are deficient or dysfunctional (77). The imbalance between Teffs and Tregs occurs when Teffs become resistant to Treg-mediated-immunosuppression over time (78). Therefore, the addition of Tregs at the site of the transplanted islets has been proven to improve their performance and longevity in vivo. Treg migration to the transplanted area resulted to be an issue (79). Hence, Tregs need to be localised at the site of the implanted islets to achieve their immunosuppression. This has been already tested by infusing both cell types (islets and Tregs) together or adding growth factors that attract Tregs migration to the islets (80).

Tregs need growth factors to proliferate and maintain their function. Interleukin-2 (IL-2) is a growth factor for Treg cells, taking part in their development, proliferation and immunosuppressive function (81). It is essential for Treg lineage stability and their survival (82), as defects in IL-2 production result in a reduced number of Tregs in the islet area (83). Thus, the addition of IL-2 in the bioink is crucial for Treg survival and islet function in the transplanted site.

1.3.3 Extrusion bioprinting

As briefly discussed in 1.2.2, extrusion 3D printing consists of extruding a continuous flow of ink through a nozzle when applying pressure (which can be pneumatic, piston or screw (84,85)). The ink is deposited in the pre-designed coordinates to obtain a 3D structure. Moreover, temperature, printing speed and flow can be controlled (by varying the pressure applied to the bioink cartridge) (86). Extrusion-based printers have been widely used for bioprinting, as its main advantages are the scalability of the process, relatively low price, high variety of bioinks printable, ability to print with high cell densities, high ink viscosities and larger constructs (46,54,87). For this reason, hydrogels, which may be viscous, and high cell densities that contribute on the increasing of the viscosity, can be used. Even if it the relatively low resolution is one of the main disadvantages of this technique, it might not be essential in this case, as human islets are <100-700 μm in diameter (8), being the printing resolution 100-200 μm (46).

Pancreatic islets have been previously bioprinted using extrusion bioprinting (36,86). The viability of the islets decreased when the printing conditions entailed more stress to the cells (more pressure, higher shear stress when printing) (86). The bioprinted islets were capable of maintaining their structure and functionality, by reacting to glucose stimulation and generating insulin (36).

1.3.3 Co-axial bioprinting

Co-axial bioprinting is a type of extrusion printing where 2 different bioinks are printed at the same time. One ink, known as the core, is printed inside the second ink, known as the shell. Previous studies demonstrated the possibility to print very soft hydrogels in the core of the ink (88). The core-shell like structure is crosslinked after printing. Figure 7 shows a schematic representation of the co-axial printing nozzle, and the way the ink is deposited, with the core (blue in Figure 7D) inside the shell (red in figure 7D).

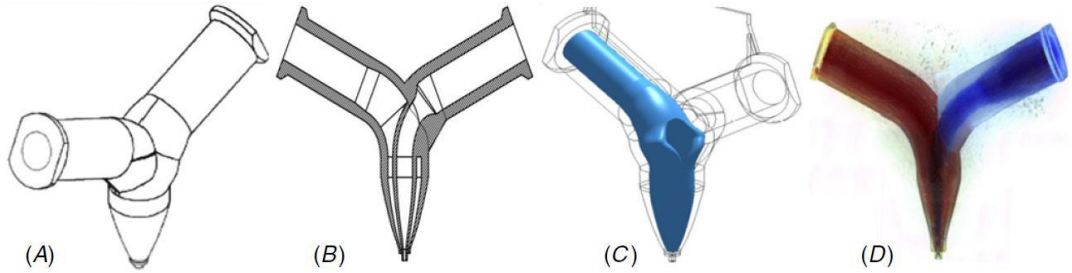

Figure 7. Schematic mechanism the co-axial nozzle (89). It shows the schematic configuration of the nozzle (A-C), as well as the distribution of the ink on it (D), being the blue ink in the core (inside) and the red one in the shell (outside).

In summary, co-axial bioprinting is an interesting approach to print islets with their supporting cells. The Langerhans islets could be printed in the core (inner side) together with endothelial cells to achieve vascularisation, and Tregs in the shell (outer layer) to act as an immunological barrier for the islets (Figure 8). Moreover, the growth factor for the Tregs (IL-2) could be encapsulated and added to the shell.

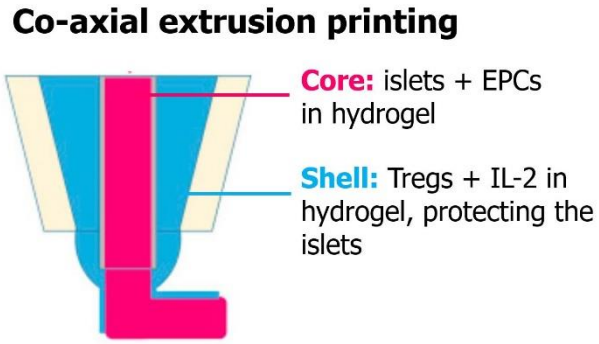

Figure 8. Distribution of cells in the islet co-axial bioprinting approach. Endothelial progenitor cells (EPCs) could also be incorporated in the core for vascularisation.

1.3.3.1 Custom-made printer

The co-axial extrusion printer used in this study was developed in house by the Translational Research Initiative for Cell Engineering and Printing group (TRICEP) at the University of Wollongong. The software used was also developed there. The XYZ axes, printing speed, flow rate, core:shell ratio and temperature could be controlled with the software. Furthermore, simple squared scaffolds (lattices) could be printed by introducing the scaffold width, length and height, number of layers and number of lines in the X and Y directions (Figure 9E). A G-code could also be introduced to print more complex structures. This was the second generation of a printer developed after the Biopen. It featured two different extruders controlled by motors, one for the core and one for the shell, which applied pressure on the core and shell syringes. These syringes were connected to a custom-made titanium nozzle fabricated using SLS (selective laser sintering). The co-axial nozzle is highlighted in Figure 9C and 9D, where the two inks were extruded, resulting in the core ink being encapsulated by the shell ink. The printer had temperature regulation units surrounding the syringes, therefore the temperature of the inks could be controlled before extruding them. However, the temperature could not be controlled neither in the nozzle nor in the printing base.

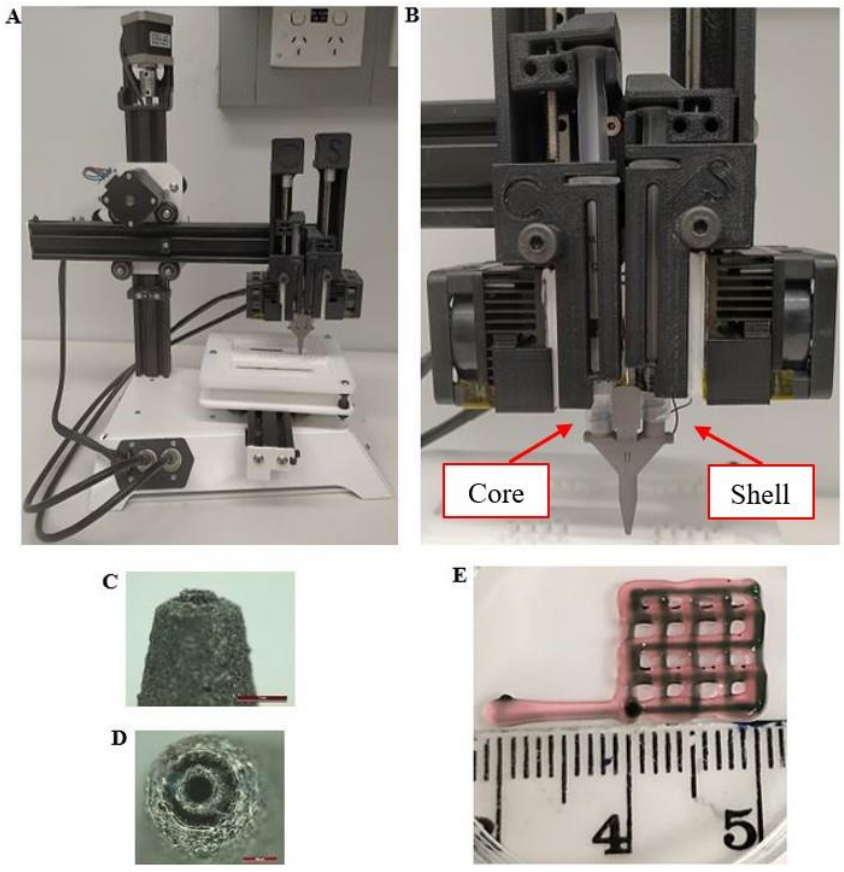

Figure 9. Co-axial printer from TRICEP™. The printer (A) and a zoom in the core-shell system (B) can be observed, being C for core (left) and S for shell (right) (pointed with arrows). The syringes with loaded bioink are screwed in the nozzle, and the pistons press the ink through the nozzle. A close-up of the tip of the nozzle is also shown (C-D), with the core-shell separation (scale-bars: 1 mm (C), 500 µm (D)). Finally, an example of a scaffold printed with the pre-made scaffold coding of the software (E), with blue ink in the core and pink ink in the shell.

When the print started, the printing arm moved to the starting point (X, Y, Z coordinates). The printing arm would then start pressing the core and shell syringes (seen in Figure 9B) to get the ink extruded through the nozzle (the core in the inner part, the shell in the outer part as shown in Figure 9D). The pressure applied on each of the syringes would determine the printing flow and the core:shell ratio, controlled by the software (more pressure, more flow; more pressure on the core syringe and less on the shell syringe, more core-shell ratio and vice-versa). The higher the flow, the more ink came out of the nozzle per second, and vice-versa. The printer would then start moving to the coordinates written on the G-code of the software, while extruding the ink. The speed it moved while printing was determined by the printing speed on the software. The faster it moved, the fewer ink it deposited at the same point and vice-versa. The excess of speed, or too little flow could make the prints too thin and brittle, whereas a low speed or too high flow could make the prints thick and lose resolution. The correct print thickness (like the one shown in Figure 9E) could be achieved by finding a balance between the printing flow and speed. Once a layer was finished, the printing arm would go a few millimetres up to start printing the next layer.

1.3.4 Bioink for pancreatic islet printing purposes

A bioink is essential for bioprinting. It provides cells with a structure and gives them mechanical strength. The materials used as a bioink can vary depending on the aim and function of the tissue. Generally, hydrogels are used. They are hydrophilic polymers that resemble the extracellular matrix. Most of the hydrogels present high cytocompatibility and biocompatibility (90). They have tuneable chemical and physical properties, and they also absorb 90-99% of their dry weight in water (important for the biocompatibility) (91). Generally, this gelation occurs with crosslinking, which can be induced chemically, by temperature or light (at a specific wavelength). Among these gelation techniques, photopolymerisation is an attractive crosslinking method as the polymerisation is short-timed and controllable, and with no need for extreme pH or temperature that could harm cells (92,93). Different hydrogels have been previously used for bioprinting purposes: alginate, gelatin, collagen, fibrin/fibrinogen, gellan gum, hyaluronic acid (HA), agarose, chitosan, silk (94). These are 3D bioprintable, and complex morphologies can be engineered with this technique (95,96). The immediate crosslinking after bioprinting stabilises the printed structures, maintaining their shape. The choice of biomaterials or hydrogels depends on the target tissue or the mechanical properties aimed to achieve. GelMA, alginate and gelatin are the constituents of the bioink used in this study, and they will be introduced in the following part.

1.3.4.1 GelMA, alginate and gelatin

Gelatin methacrylolyl (GelMA) is a chemically modified gelatin. Gelatin is an inexpensive material that can be extracted from various animals (97). It derives from the hydrolysis of collagen, which is one of the most abundant proteins in the body (98). It has lower immunogenicity than collagen (99,100) and it contains RGD sequences (arginine-glycine-asparagine) that support cell attachment to the material (99–101).

The phase behaviour of the aqueous solution of gelatin can be thermoreversible, becoming a gel in cooler temperatures and liquid in warmer temperatures. Unfortunately, it is liquid at physiological temperature (37ºC), hence, not useful for cell culturing (99,102). On the other hand, GelMA, a derivative of gelatin, retains the thermoresponsive phase behaviour, and can be chemically crosslinked to improve the structural stability. This makes gelMA an ideal substitute for gelatin and one of the most widely used hydrogels in TERM. It has been proven to be biocompatible and suitable for long-term cell culture (41,103). One of the most frequently used methods for crosslinking GelMA hydrogels is photocrosslinking. GelMA is photocured in the presence of light (visible or UV) using molecules called photoinitiators. Upon photo-irradiation, the photoinitiator produces free radicals, initiating the polymerisation (102,104). Currently Irgacure 2959 remains one of the most frequently used photoinitiators in 3D printing. It works under a broad spectrum, for cell printing, a wavelength of 365 nm or below is required (93). However, the use of UV light in long-term exposure is detrimental to cells (105). Therefore, alternative initiators are preferable. Lithium phenyl-2,4,6-trimethylbenzoylphosphinate (LAP) is another commonly used photoinitiator which absorbs photons in the near-visible light (106). LAP is a water-soluble molecule with relatively high molar extinction coefficient. Its maximum absorption is at 375 nm wavelength, however, it has been proven to be a successful photoinitiator at 405 nm (106). Figure 10 shows the absorption peaks of LAP at different wavelengths. Even if LAP is cytotoxic at high concentrations, it is efficient at low concentrations where there is no cytotoxicity (0.05% or 0.067% are enough for crosslinking) (105).

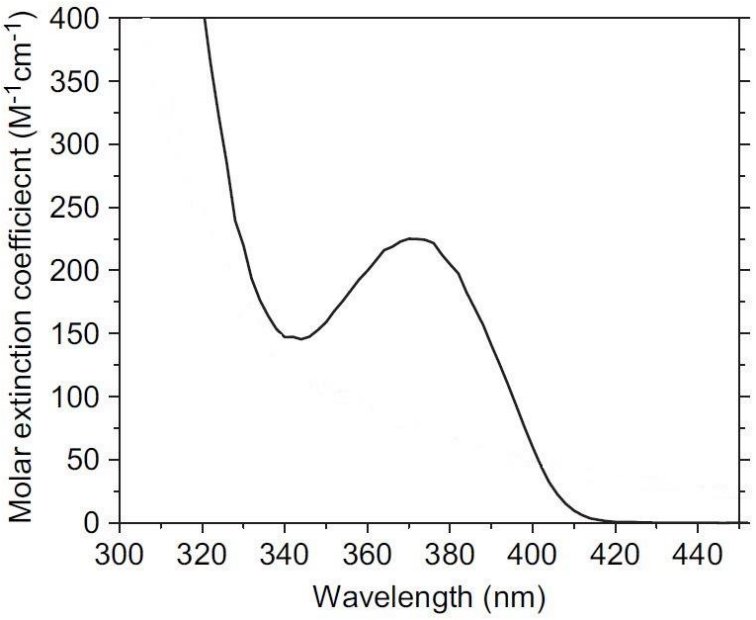

Figure 10. Molar extinction coefficient of lithium phenyl-2,4,6-trimethylbenzoylphosphinate (LAP) at a function of wavelengths (modified from (106)). Even if the peak is at 375 nm (meaning the LAP is most efficient with that wavelength), its molar extinction coefficient of 405 nm is >50 $M^{-1}cm^{-1}$. Hence, this molecule can be used to initiate polymerisation at near-UV visible lights.

Another commonly used hydrogel is alginate, due to its low toxicity, ease of crosslinking and relatively low cost (107). This polysaccharide is extracted and purified from brown algae. It is an anionic polymer which crosslinks by divalent cations such as Ca^{+2} (36,69,107). It has been

previously used to encapsulate various cell types, including islets that remained functional for over 10 months in humans (36,108). Alginate is non-biodegradable in the human body, and non-immunogenic when high purity alginates are employed (68,69). This polysaccharide is composed of mannuronic and guluronic acid. It is immunoprotective when the guluronic acid is predominant, as the mannuronic acid has some mitogenic properties (109). The 3D crosslinked structure and charge distribution of alginate might be the reason why smaller molecules than the pore size of the scaffold are unable to penetrate it (67). This property might be related to the immune protection that alginate provides.

Finally, the hydrogel precursors must be 3D printable by extrusion printing. In extrusion printing, the material needs to be in gel-state in order to retain its shape after printing (if it is too rainy, the construct will merge into a drop before crosslinking it). This can be achieved by modifying the printing temperature (the cooler, the more gel GelMA and alginate are). However, one of the aims of this project is to print at room temperature. The gelation behaviour of the bioink can be modulated by adding gelatin to the bioink formulation and varying its concentration. Gelatin has previously been blended with other hydrogels to improve the printability of bioinks (110). Figure 11 explains the gelation process of GelMA, gelatin and alginate.

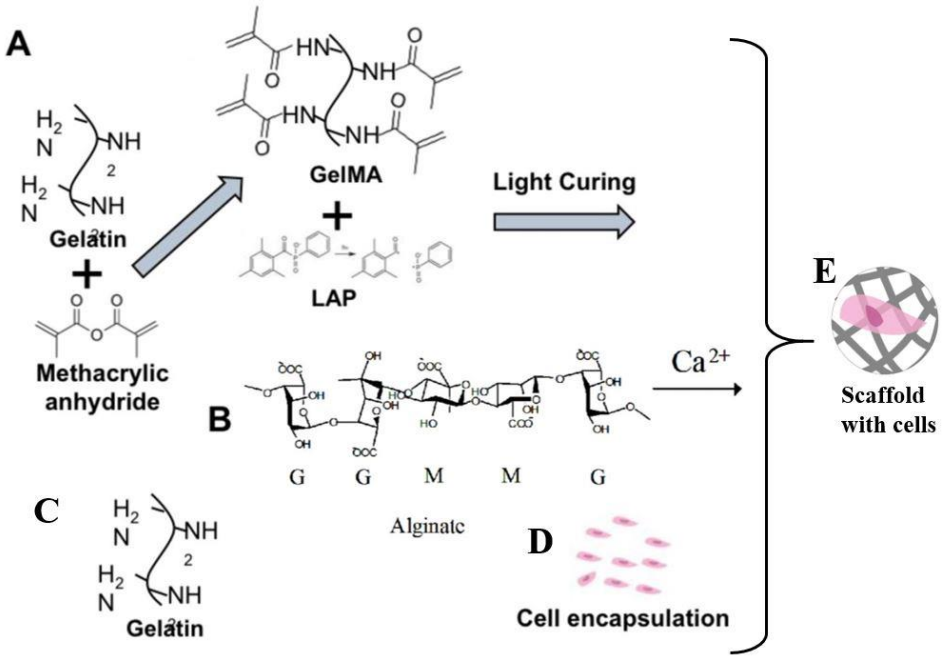

Figure 11. Gelation process of GelMA, alginate and gelatin (modified from (105)). GelMA, which derives from gelatin, crosslinks under light exposure with LAP (A). Alginate crosslinks with calcium ions (B). Gelatin (C) and cells (D) are also added to generate a scaffold with entrapped cells (E).

Finally, biological cues can also be added to the biomaterials apart from cells. In this case, IL-2 can be used to promote Treg function and recruitment. This growth factor can be entrapped inside microspheres to obtain a sustained release over time and avoid constantly adding growth factors to the medium.

1.3.4.2 Microspheres

Microspheres or microparticles (MPs) are microsized structures often used in pharmaceutical engineering, medical applications and TERM for the delivery and sustained release of bioactive molecules (111,112). Apart from delivering drugs and growth factors, appropriately designed structures can also provide binding sites for cell attachment (111). Diverse materials, such as poly(lactic-co-glycolic acid) (PLGA), gelatin, GelMA, alginate or collagen, have been employed for the generation of MPs (111,113–116). Gelatin microspheres using glutaraldehyde as a crosslinker were widely used in the past (113), but cytotoxicity is a major limitation of this crosslinker (114). Using GelMA as a source for crosslinking is less toxic and provides a broader range of crosslinking densities, as well as a better controlled reaction (117). The capability of these MPs to retain and release growth factors has also been proven (114).

GelMA microspheres can be generated in water-in-oil emulsion. They can be crosslinked in situ (when the emulsification is occurring) or after they are formed (post-crosslinking). Finally, the growth factors are added after the generation and crosslinking of the spheres. Therefore, the IL-2 could be encapsulated in the GelMA microspheres after the creation of the MPs, and then incorporated to the bioink.

Chapter 2

2. Preliminary work

This project was a continuation of previous projects in the field of bioprinting for pancreatic islets. Previous students characterised the ink and did preliminary cell studies. Sarah worked on the ink characterisation for encapsulating islets, concluding on the use of 2% alginate/7.5% GelMA as the best formulation in terms of mechanical properties, gel degradability and cell viability. After her, Max optimised the printing conditions and studied the effect of the printing on cell viability. However, he used the first generation of the customised printer, so these tests should be repeated on the new printer. The most critical difference between the first and the second-generation printers was that the latter lacked a temperature control unit at the printing plate, meaning that once the ink was extruded it would be at room temperature. Max used the same bioink as Sarah and printed at 15ºC. However, in this project the printing was done at room temperature, as the printer did not allow for a complete temperature control from when the ink was in the printing cartridge to after extruding the ink.

The University of Wollongong is closely working with the Royal Hospital of Adelaide (South Australia) in the bioprinting for pancreatic islets. All the cell work and animal studies are performed there, while the university of Wollongong is focused on the characterisation and optimisation of the ink and the printing parameters.

The new steps to be taken building upon the previous students were:

- Use of new co-axial printing (optimisation of printing parameters)
- Optimise printability at room temperature
- Optimisation of core and shell formulations to the targeted cell types respectively (Tregs in shell, endothelial progenitor cells (EPCs) and islets in core)
- Introduction of microspheres with growth factors for sustained release

Due to time constraints (10 months as part of the double degree at Utrecht University), the focus of this project was placed on the optimisation of the shell ink. The ink was characterised with encapsulation of microspheres pre-loaded with IL-2. Gelatin was added to the ink to make it printable at room temperature. Optimisation of the core ink was undertaken by another biofabrication Master student (Narangerel).

Chapter 3

3. Aim

The aim of this project was to characterise and optimise a GelMA/alginate/gelatin ink for co-axial extrusion printing, which served as the shell ink. This ink contained GelMA microspheres loaded with IL-2, and the release of the IL-2 was studied. The main objectives were separated in 3 main blocks:

- Preparation and characterisation of GelMA microspheres. GelMA microspheres were generated using a water-in-oil emulsion method and post-crosslinked with ammonium persulfate (APS) and tetramethylethylenediamine (TEMED).
- Characterisation and optimisation of the shell ink for extrusion printing. The gelatin concentration was optimised, and rheological studies were performed to determine the ink characteristics. Finally, the printing parameters were established.
- Release study of IL-2 from the GelMA microspheres.

The outcome of these experiments could be further used through collaboration to co-print Tregs and pancreatic islets and test the behaviour, insulin-producing capacity and immunosuppression abilities of the constructs in animal models.

Chapter 4

4. Materials and methods

4.1 GelMA microspheres

4.1.1 Generation of GelMA microspheres

4.1.1.1 Water-in-oil emulsion

GelMA microspheres were prepared using a water-in-oil emulsion method. A 15% w/v GelMA solution (82% Degree of Functionalisation (DoF), TRICEP™, Australia) in deionised water, previously heated at 37°C, was added drop by drop in olive oil (1:8 v/v) and homogenised at 5000 rpm for 5 minutes. Afterwards, samples were cooled down to induce gelation with ice and they were homogenised for other 10 minutes. After the homogenisation, the water-in-oil emulsion was transferred to a magnetic stirrer, in an ice bath. The stirring was kept at 800 rpm for 40 minutes, then, chilled acetone (half the volume of the oil employed) was added. The stirring continued for another 30 minutes, and the microspheres were collected. The oil was removed from the mixture by 3 washes with acetone, centrifuging the samples at 500 rpm for 7 minutes. Afterwards, the microspheres were vacuum dried overnight.

The dried particles were weighed (m_1) and the yield of the process was calculated (Y_1):

$$Y_1 = \frac{m_1}{m_0} \cdot 100 \quad (1)$$

m_0: initial GelMA weight

4.1.1.2 Crosslinking of GelMA microspheres

The GelMA microspheres were chemically crosslinked using ammonium persulfate (APS, 228.2 g/mol, Chem-Supply, Australia) and N,N,N',N'-Tetramethylethylenediamine (TEMED, 99% purity, Sigma-Aldrich, USA). APS and TEMED were dissolved in a water:acetone mixture (20:80 v/v) at a final concentration of 0.25% w/v and 0.5% v/v respectively, and added to the suspension of GelMA microspheres (10% w/v). After adding the mixture to the microspheres, they were crosslinked for 16 hours (overnight) on an orbital shaker.

The next day, the spheres were washed 3 times with water/acetone (20:80 v/v) and then acetone to eliminate the APS and TEMED and stop the reaction. They were centrifuged at 500 rpm for 5 minutes. The samples were then vacuum dried for 2 hours and weighed (m_2). Then, the yields of this part of the process (Y_2) and of the whole process until that point (Y_3) were calculated:

$$Y_2 = \frac{m_2}{m_1} \cdot 100 \quad (2)$$

$$Y_3 = \frac{m_2}{m_0} \cdot 100 \quad \text{or} \quad Y_3 = Y_1 \cdot Y_2 \div 100 \quad (3)$$

4.1.1.3 Crosslinking efficiency

Once the microspheres were crosslinked, they were washed with water. To do so, water was added to the mixture, waited for 10 minutes, and centrifuged for 5 minutes at 500 rpm. Another wash was made with water, and other 2 with acetone, to substitute the water for it. Finally, the samples were again vacuum dried for 2 hours and weighed (m_3). The crosslinking efficiency (Y_4) and the yield of the whole process (Y_5) were calculated. The microspheres were stored at -20ºC until use.

$$Crosslinking\ efficiency\ (Y_4) = \frac{m_3}{m_2} \cdot 100 \quad (4)$$

$$Total\ yield\ (Y_5) = \frac{m_3}{m_0} \cdot 100 \quad \text{or} \quad Y_5 = Y_3 \cdot Y_4 \div 100 \quad (5)$$

4.1.2 Particle size analysis

2 mg GelMA MPs were suspended in 300 µl PBS and analysed under a Leica DFC310-FX microscope. These were imaged and the diameter of the particles was manually measured with ImageJ software. Afterwards, a histogram was plotted with all the data of the diameters to obtain a distribution of the population. 3 samples were analysed, and 10 images of different regions were taken per sample.

4.1.3 Microsphere degradation

GelMA microspheres were subjected to a degradation study. 5 mg of MPs were suspended in a solution of 2 U/ml type I collagenase (≥ 125 U/mg lyophilised powder, Sigma-Aldrich, USA) in PBS. They were left on an orbital shaker and timepoints were taken at day 1, 2, 4, 6, 10, 15, 20 and 28. The samples were centrifuged for 1 minute at 1000 rpm and washed twice with DI water to remove the salts of the PBS. Afterwards, they were freeze dried and the dry weight was recorded. The degradation profile was calculated with the following equation:

$$Remaining\ gel, day\ x\ (\%) = \frac{w_x}{w_0} \cdot 100 \quad (6)$$

The experiment was done in triplicate, and the degradation medium was changed every two days to prevent the collagenase from losing activity.

4.2 Bioink characterisation

The bioink for printing consisted of three different materials: alginate (medium viscosity, Sigma-Aldrich, UK), GelMA (synthesized) and gelatin (300 bloom, type A from porcine skin, Sigma-Aldrich, USA).

4.2.1 GelMA synthesis

10% (w/v) gelatin (175 bloom, type A from porcine skin, Sigma-Aldrich, USA), dissolved in PBS and autoclaved, was used for methacrylation. The sterile solution was heated in sterile conditions at 50ºC while stirring at a medium speed (600-800 rpm). Afterwards, methacrylic anhydride (Sigma-

Aldrich, USA) was added drop by drop, at a concentration of 0.06% (v/v) (0.6 ml methacrylic anhydride per gram gelatin). The reaction was left for 4 hours, after which the unreacted methacrylic anhydride was removed by centrifugation (5 minutes, 3000 rpm). The pH of the solution was adjusted to 7.0 with 5M sodium hydroxide (NaOH). Finally, the solution was dialysed for 4 days at 37-40ºC and freeze dried. The samples were stored at -20ºC until use.

4.2.1.1 NMR

^{1}H-NMR was used to assess the purity and methacrylation degree of GelMA. GelMA and gelatin were dissolved in deuterium oxide (D_2O) at a concentration of 10 mg/ml each. The solutions were transferred to NMR tubes and analysed on the Ultrashield™ 400 Plus machine (Bruker, USA). The data was analysed with the Bruker TopSpin 4.0.5 software. Table 4 summarises the settings for the measurements.

Table 4. Solvents and settings used for the NMR measurements.

Settings	*Test*
Type of test	^{1}H-water suppression zgpr
Solvent	D_2O
Number of scans	64
Sample temperature (K)	300

4.2.2 Bioink preparation

2% alginate was dissolved in PBS at 37°C overnight. Afterwards, GelMA was added to a final concentration of 7.5%. The mixture was vigorously vortexed for 1-2 minutes and warmed up at 37°C until complete dissolution and blending of both materials. Finally, gelatin powder was added and the same steps of vortexing and warming up were taken until a uniform blend of the 3 materials was obtained. All the steps were performed sterilely (in a laminar flow cabinet, using sterile tweezers and PBS, and UV-irradiating the materials before dissolving them).

Prior to printing, the ink was mixed with LAP photoinitiator (lithium phenyl(2,4,6-trimethylbenzoyl)phosphinate, > 98%, Tokyo Chemical Industry, Japan) to a final concentration of 0.06% w/v. The ink was vortexed to obtain a uniform mixture. Microspheres (if needed) were added to the gel and distributed throughout the ink with a positive displacement pipette. The resulting mixture was then transferred to 3 ml syringes with the same pipette (maximum of 2.5 ml for printing). The syringes were then left at 37ºC for 15 minutes to remove air bubbles generated due to the mixing process, and they were then taken outside the incubator to get the room temperature before printing. During the procedure, the samples were covered with aluminium foil to avoid contact with light and pre-mature crosslinking.

4.2.3 Preliminary printing characterisation

The printing was done with an in-house built co-axial printer (shown on the Introduction section, part "*1.3.3.1 Custom-made printer*"). The initial characterisation was performed using a single cartridge (setting the core:shell ratio at 1:0). The ink formulations containing gelatin were extruded at room temperature, whereas the ink without gelatin was extruded at 15°C.

4.2.3.1 Filament test

The printing nozzle was placed far from the printing platform (x, y, z = 50, 50, 70) and the material was extruded. The process of extrusion was recorded on a phone camera and the length of the extruded ink was measured. The experiment was done in triplicate. Figure 12 shows an example of the filament test.

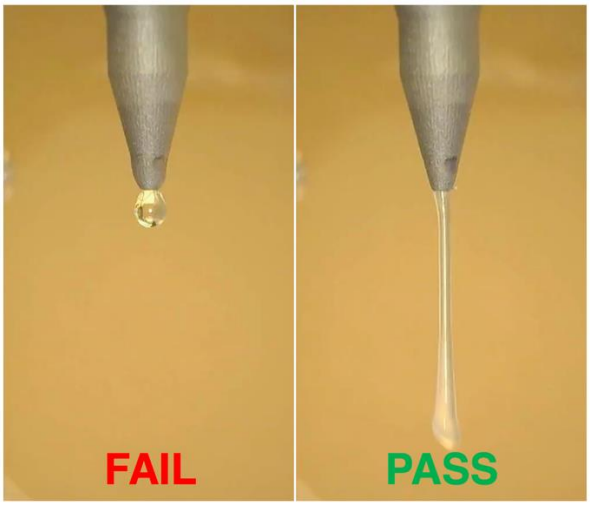

Figure 12. Example of filament test. If the ink is too rainy, it will deposit droplets instead of extruding a line, which makes it unsuitable for extrusion printing.

4.2.3.3 Filament fusion test

Lattices of a single layer, with an increasing distance between filaments, were printed. 0.23 ml/min flow and 140 mm/min speed were used. The structure of the printed scaffolds is shown in Figure 13, together with the G-code. The resulting scaffolds and spacing between the filaments were measured with ImageJ and compared to theoretical values.

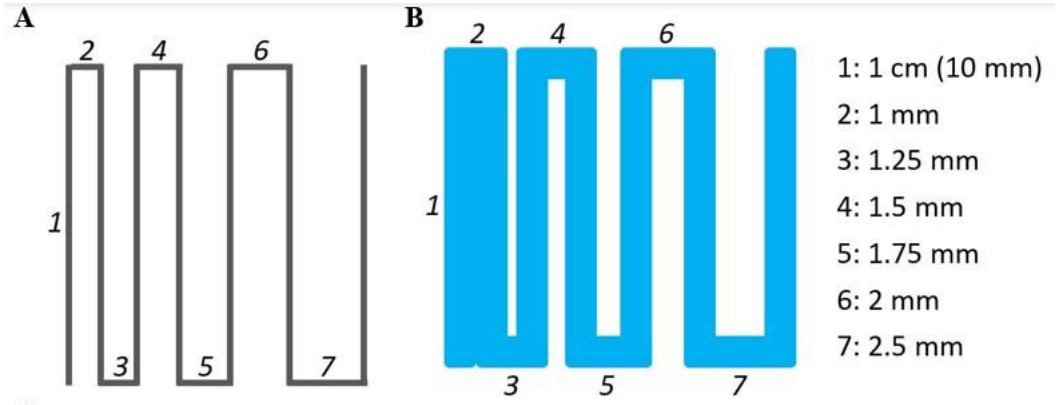

C

G-code:

M400	…	…
G91	M400	G1 Y10 E0.122667
G1 E0.3	G1 Y-10 E0.122667	G1 X2 E0.0245333
G1 X5 E0.184001 F140	G1 X1.25 E0.0153333	M400
M400	G1 Y10 E0.122667	G1 Y-10 E0.122667
G1 F140	G1 X1.5 E0.0184000	G1 X2.5 E0.0306667
G1 F140	M400	M400
M400	G1 Y-10 E0.122667	G1 Y10 E0.122667
G1 Y10 E0.122667	G1 X1.75 E0.0214667	M400
G1 X1 E0.0122667	M400	G1 E-0.2
…	…	G1 Z10

Figure 13. Scheme of the printed scaffolds and their dimensions. The scaffold on the left (A) shows the design, the one on the right (B) shows the outcome if the ink had a perfect shape fidelity (1 mm diameter filaments). Figure C displays the G-code used for the filament fusion test.

4.2.3.4 Layer stacking test

Pre-coded lattices were printed, with dimensions of 10 x 10 mm, and 5 strands with spacing of 2.5 mm between them (both in x and y direction). Each layer was 0.6 mm thick (Z), with a number of layers increasing in pairs from 2 to 10 (thus, the height of the scaffolds ranged from 1.2 to 6 mm).

4.2.4 Rheology

The bioink was subjected to rheological studies in the AR-G2 Rheometer (TA Instruments), fitted with at 40 mm cone plate (2° angle). The tests were performed in triplicate and the results were recorded with the TA Rheology Advantage Instrument Control software. A solvent trap was used in every test to prevent evaporation.

All the tests had a conditioning time for the bioinks, 5 minutes pre-shear (to remove the rheological history of the inks) and 5 minutes equilibrium time (to stabilise the ink after the pre-shear). The frequency and strain were 1 Hz and 1% respectively in every test unless specified, the shear rate

was 1 s^{-1} unless specified, and the temperature was 15ºC for the 0% gelatin bioink and 22ºC for the rest of the bioink, unless specified.

First, a temperature sweep was performed from 10ºC to 40ºC, at 1.5ºC/min. The aim was to examine the behaviour of different bioinks at different temperatures (if they behaved more than a liquid or more than a gel). Theoretically, an ink needs to behave like a gel to be suitable for bioprinting.

Second, a viscosity test was undertaken, in order to determine the behaviour of the bioink at different shear rates (0.01-1000 s^{-1}). Different shear rates are used to simulate the conditions where the ink is at rest and where it goes through the printing nozzle, and this test was used to determine the viscosity of the ink at both processes.

Apart from that, frequency and strain sweeps were performed. The frequency sweep had a frequency range from 0.1 to 20 Hz, and the strain sweep, a strain range from 0.01% to 1000%. A step-strain test was also done, where the recovery of the ink after different cycles of strain was assessed. This consisted of a time sweep at 1% strain for 3 minutes, then 30 seconds at 100% strain (cycle 1). This cycle was repeated four times. After the 100% strain step, the ink should recover its properties back to what it was at the beginning.

Finally, an in-situ crosslinking rheology was performed. This was performed using with a different geometry (20 mm parallel plate) which allowed the attachment of a light source for UV curing. Temperature could not be controlled in this case, therefore, for both inks (0% and 3.5% gelatin) were tested at room temperature. The crosslinking of the hydrogels in the printing process was done using a light source (Omnicure® LX505) at 405 nm wavelength. However, this lamp does not have the attachment for the rheometer, so the experiments were performed using another UV lamp, Omnicure® Series 1500 (Lumen Dynamics, Canada). It was fitted with a 365 nm UV wavelength filter (a commonly used wavelength, but cytotoxic). The lamp was set at 2 mW/cm^2 intensity.

The specifications of the different tests are summarised in Table 5.

Table 5. Conditions used for each rheological test. The temperature was set at 15°C for the ink without gelatin (0%), and at 22°C for the ink with gelatin.

Test	Pre-shear (s^{-1})	Equilibrium (min)	T (°C)	Strain (%)	Frequency (Hz)	Shear rate (s^{-1})	Time (min)	UV (365 nm)
Temperature sweep	5 min	5 min	**10 – 40 (1.5°C/min)**	1	1	-	-	-
Viscosity	5 min	5 min	15 / 22	1	1	**0.01 - 1000**	-	-
Frequency	5 min	5 min	15 / 22	1	**0.1 - 20**	-	-	-
Strain	5 min	5 min	15 / 22	**0.01 - 1000**	1	-	-	-
Step-strain	5 min	5 min	15 / 22	**1 for 3 min 100 for 30s Repeat cycle (x5)**	1	-	**21**	-
in situ UV crosslinking rheology	5 min	5 min	-	1	1	-	**10**	**2 mW/cm^2, for 1 min at min 2**

4.2.5 Characterisation of casted hydrogel discs

Hydrogel discs were casted by pipetting 100 µl of ink mixture in PBS into an 8 mm Ø (diameter) x 1 mm thick mould, or 200 µl of ink mixture into an 8 mm Ø x 3 mm thick mould. These were subjected to a double crosslinking process, which involves UV crosslinking for 1 minute, and then ionic crosslinking using 2% (w/v) $CaCl_2$ for 10 minutes. The UV crosslinking was performed with a visible light lamp (Omnicure® LX505) at 405 nm wavelength and 2 mW/cm^2 intensity. Before any experiment, the intensity of the UV lamp was measured with the CON-TROL-CURE® Silver line UV Radiometer. The distance of the light guide was adjusted to match 2 mW/cm^2 on the reading of the light meter. For the following tests, only samples for mechanical testing were prepared in 3 mm thick moulds, for the rest of the tests 1 mm thick samples were used.

4.2.5.1 Free polymer content and swelling ratio

Gels were casted in triplicate in water in the 1 mm thick moulds, and the initial weight of samples was recorded (w_0). They were freeze dried overnight and weighed (w_1). They were later incubated in PBS overnight at 37°C, washed twice with DI water and weighed again (w_2). Finally, they were freeze dried overnight again and the final weight was recorded (w_3). The sol-gel fractions and swelling ratio were calculated following the equations below:

$$Sol\ fraction\ (\%) = \frac{w_1 - w_3}{w_1} \cdot 100 \quad (7)$$

$$Gel\ fraction\ (\%) = 100 - Sol\ fraction \quad (8)$$

$$Swelling\ ratio\ (\%) = \frac{w_2}{w_1} \cdot 100 \quad (9)$$

4.2.5.2 Mechanical test

Hydrogel samples were prepared using the above method in 3 mm thick moulds. The discs were subjected to a compression test on the EZ-L Shimdazu mechanical tester, fitted with a 10 N load cell. Stress (y axis) vs strain (x axis) was measured, allowing the gels to compress until they were 0.5 mm thick. Results were collected from the Shimdazu TrapeziumX software. The compression modulus was calculated as the slope in the linear region of the stress-strain curve (10-15% strain).

4.2.5.3 Degradability of gels

Samples were prepared using the above method in 1 mm thick moulds. The discs were freeze dried and weighed (w_0). Afterwards, they were degraded in a solution of 2 U/ml type I collagenase (≥ 125 U/mg lyophilised powder, Sigma-Aldrich, USA) in PBS, at 37°C. Each day, the gels were collected, washed twice with DI water and freeze dried. The next day, the weight was recorded (w_1) and degradation medium was added to the gels. The process of collecting the gels, freeze drying and recording the weight (w_x) was done every day until the gels degraded completely. The degradation profile was calculated with the equation (6).

4.2.6 Microsphere distribution in ink

The dry GelMA microspheres (MPs) were first rehydrated overnight by adding 15 µl PBS per 5 mg MPs. Rehydrated GelMA microspheres were mixed with the bioink to 10 mg MPs/ml ink and transferred to a syringe for printing. 3 µl (1 mm of core ink, by setting the core:shell ratio at 1:0 so that only the core ink was extruded) were extruded in a flat bottom 96-well plate, in three regions of the syringe: beginning, middle and end. After the extrusion, the samples were imaged with the Axiovert 40 CFL microscope. The images were then analysed with ImageJ to count the number of microspheres per observation area. All were done in triplicate.

4.3 Release study

The release of the growth factor interleukin-2 (IL-2, BioLegend) from the GelMA microspheres was studied. First, a 0.45 mg/ml IL-2 solution was added to the microspheres in a non-saturating volume, by gently pipetting the IL-2 solution on top of the dry microspheres. This was left overnight at 4°C to be absorbed. The following day, the release started in 0.1% BSA and 2 U/ml collagenase I in PBS release medium. Samples were left on a shaking plate. At each timepoint the medium was collected, frozen at -20ºC and replaced with new medium. 3 different conditions were tested.

On the one hand, there were free microspheres. The MPs loaded with IL-2 were directly suspended in the release medium (in 1.5 ml Eppendorf tubes). The medium, where the IL-2 was released from the microspheres, was collected at the timepoints (day 1, 2, 5, 10, 12, 14, 21) by centrifugation, to settle the MPs at the bottom of the tube and avoid their collection. On the other hand, there were casted microspheres. The MPs loaded with IL-2 were added to the 3.5% bioink, were casted in 8 mm Ø x 1 mm thick moulds and crosslinked as in section 4.2.5. Hydrogel discs were located in release medium in 1.5 ml Eppendorf tubes. The medium was collected at the timepoints (day 1, 2, 4, 6, 8, 12, 14 21) by centrifugation to settle the hydrogels and MPs at the bottom of the tube and avoid their collection.

Finally, the third condition was printed microspheres. The MPs loaded with IL-2 were added to the 3.5% bioink and co-axially printed. This was done having the 3.5% ink with the MPs at the shell and a slightly different ink at the core (7.5% GelMA / 3.5% gelatin dissolved in 50 mM $CaCl_2$ intead of in PBS. In this way, when the alginate of the shell made contact with the core ink, it would start crosslinking). The core:shell ratio was 0.25:0.75. 10 mm x 10 mm x 2.4 mm (x, y, z) scaffolds of 4 layers were printed, with 7 strands on each layer. The printed constructs were incubated in small petri dishes with release medium, and the medium was collected at different timepoints (day 1, 2, 4, 6, 8, 10, 12, 14) with a pipette, avoiding the gels.

The amount of IL-2 in each sample was determined with an Enzyme-Linked ImmunoSorbent Assay (ELISA).

4.3.1 ELISA

An ELISA kit (human IL-2 ELISA MAX™ deluxe set, Biolegend®) was used for the analysis. The analyses were performed according to the instructions of the manufacturer. First, 96-well flat-

bottom plates were coated with 100 µl/well capture antibody (diluted 200x in coating buffer), for 16 h at room temperature. The plates were then washed 3 times with 200 µl wash buffer (0.5% Tween® in PBS) to remove the antibodies that did not bind to the plates. The plates were blocked for 2 h at room temperature with 200 µl/well assay diluent (1x), to remove any free surface in the plate where any proteins could bind unspecifically. The washing steps were repeated.

Then, 100 µl of standard solutions (with IL-2 concentrations of 1000, 500, 250, 125, 62.5, 31.5, 15.625 and 0 pg/ml in assay diluent 1x), and samples (diluted in 1x assay buffer) were added in duplicate to the plate. The plates were incubated for 2 h at room temperature. The washing steps were repeated to remove any unspecific proteins. Afterwards, 100 µl/well of detection antibody (diluted 200x in 1x assay diluent) were added and plates were incubated for 1 h. The plates were washed again, and 100 µl/well avidin-HRP in (diluted 1000x in 1x assay diluent) were added. Plates were incubated for 30 minutes in the dark, at room temperature. The plates were washed thoroughly 5 times in wash buffer (30 s – 1 min each time). 100 µl/well of substrate solution were added and the plates were incubated for 30 minutes in the dark at room temperature.

Finally, 100 µl/well stop solution (2N H_2SO_4) were added. The plate was immediately read in a FLUOstar Omega plate reader (BMG Labech). The optical density was measured at 450 nm with wavelength correction at 570 nm. The 570 nm reading was subtracted from the 450 nm reading to obtain the correct absorbances. The concentration of each sample was determined by comparing against a standard curve that was established using the series IL-2 standard solutions.

Chapter 5

5. Results

5.1 GelMA microspheres

5.1.1 Yield of the process

The yield of each step of the generation and crosslinking of the microspheres (preparation of uncrosslinked microspheres, chemical crosslinking of microspheres, and preparation of crosslinked microspheres, respectively) was calculated following the equations (1) – (5). Table 6 summarizes the results.

Table 6. Yield of the process of microsphere generation and crosslinking.

Part of the process	*Yield (%)*
Y_1 (preparation of uncrosslinked microspheres)	90.2
Y_2 (chemical crosslinking of microspheres)	94.8
Y_3 (preparation of crosslinked microspheres)	85.5
Y_4 (crosslinking efficiency)	**95.8**
Y_5 (total yield)	**81.9**

The values in bold refer to the two most important values of the process. Y_4 suggests the adequacy and efficiency of the crosslinking process, and Y_5 is the total yield of GelMA production, from adding it to the oil on the first step to obtaining the crosslinked spheres. Both values were high, suggesting that the entire process was highly efficient, especially the crosslinking step.

5.1.2 Particle size analysis

The microspheres were generated, crosslinked and dried as stated in the methods. Afterwards, a small amount was rehydrated in water and analysed for the particle size distribution. Figure 14 shows the results.

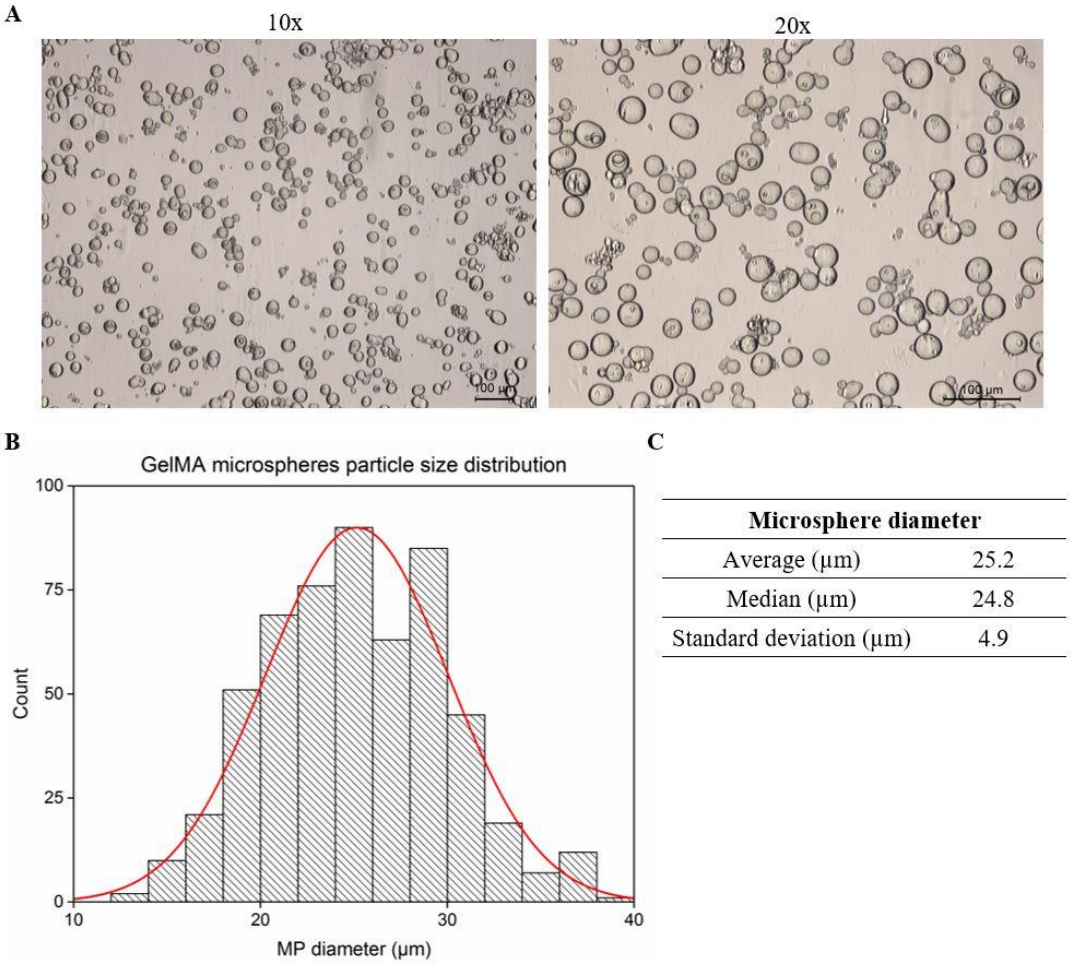

Figure 14. Microscopic images and particle size analysis of hydrated GelMA microspheres. A shows the images of the microspheres at different magnifications (scale bars: 100 µm), B shows the particle size analysis histogram, and C shows information about the diameters of the microspheres.

The particle size analysis showed a symmetric uniform distribution with almost the same average and median. 3316 microspheres were studied. They ranged from 10 to 40 µm in diameter, with the maximum peak at the 24 – 26 µm range. The average particle diameter was 25.2 µm, with a small standard deviation (4.9 µm).

5.1.3 Degradation of microspheres

The microspheres were subjected to a degradation study for 28 days, using 2 U/ml type I collagenase. Figure 15 illustrates the results.

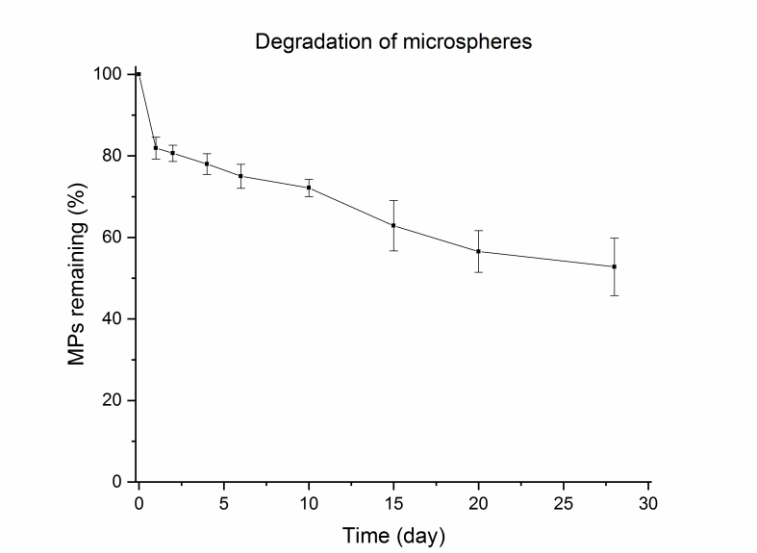

Figure 15. Degradation profile of GelMA microspheres. n = 3, error bars.

The degradation rate for the spheres was low, with less than 50% degraded by day 28. This low degradation profile might be due to the strong chemical crosslinking of the microspheres (with the ammonium persulfate and TEMED).

5.2 Bioink characterisation

As mentioned before in section 2 (preliminary work), previous students had characterised the bioink, consisting of 7.5% GelMA and 2% alginate. The GelMA used for the bioink had different characteristics compared to the one used for the microspheres. The GelMA for the bioink had a lower bloom (175 vs 300 of the microspheres), which is more adequate for cell attachment and growth. It was previously proven that GelMA prepared using a higher bloom gelatin (e.g. 300) led to phase separation in blends of two or more polymers (for example, in the case of alginate-GelMA) (118).

However, the previously used ink formulation (7.5% GelMA and 2% alginate) was printable at 15ºC. In this project, we aimed to make the ink printable at room temperature, as the custom-made printer had temperature control in the bioink cartridges, but not in the nozzle and printing platform. The previously established bioink did not have the optimal viscosity for extrusion printing at room temperature, therefore, the formulation was optimised in this study by adding gelatin. At the beginning, different gelatin concentrations were used, ranging from 2% to 5% (w/v). Various experiments were performed to identify the most optimal gelatin concentration. Afterwards, the bioink was characterised using the previous ink without gelatin as a control.

5.2.1 ^{1}H-NMR

Nuclear magnetic resonance spectroscopy was used to determine the degree of methacrylation of the synthesised GelMA. Both GelMA and gelatin were analysed, and the results were analysed and compared among them to obtain the methacrylation (or functionalisation) degree of GelMA. The results are shown in Figure 16.

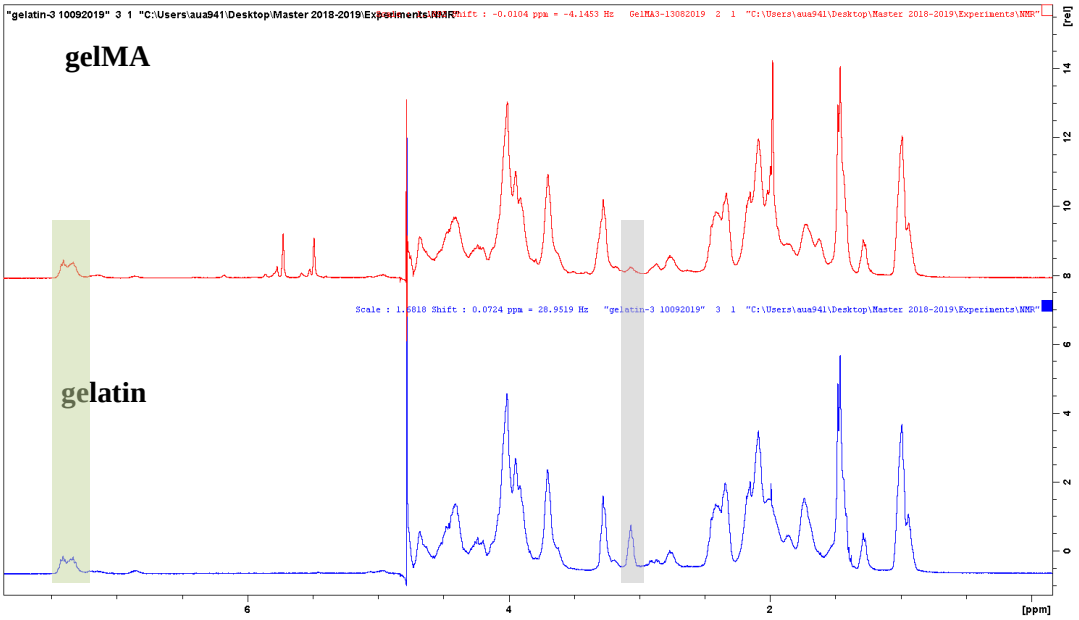

Figure 16. NMR spectra of GelMA and gelatin. The region in green corresponds to the phenylalanine (7.2-7.5 ppm) and the region in grey, to the lysine (2.95-3.2 ppm).

First, both spectra were normalised with the phenylalanine region (green). Afterwards, the lysine region (grey) was used to determine the degree of functionalisation (DoF) or methacrylation. This was done with the following equation:

$$DoF\ (\%) = 1 - \frac{A_{lys\ in\ gelMA}}{A_{lys\ in\ gelatin}} \cdot 100 \qquad (10)$$

The degree of methacrylation of the synthesised GelMA was 68.1%, which is a medium-high methacrylation degree.

5.2.2 Optimisation of the bioink for improved printability at room temperature

The effect of gelatin concentration on the printability of bioink at room temperature was investigated using three types of tests. These were filament test, filament fusion test and layer stacking test. The bioinks consisted of 7.5% GelMA, 2% alginate and a varying concentration of gelatin: 0%, 2%, 2.5%, 3%, 3.5%, 4% and 5%. Table 7 provides the designation of each ink with its respective ink composition.

Table 7. Summary of bioink composition of each ink tested.

Designation	*Ink composition*
0%	Alginate (2%) / GelMA (7.5%)
2%	Alginate (2%) / GelMA (7.5%) /gelatin (2%)
2.5%	Alginate (2%) / GelMA (7.5%) /gelatin (2.5%)
3%	Alginate (2%) / GelMA (7.5%) /gelatin (3%)
3.5%	Alginate (2%) / GelMA (7.5%) /gelatin (3.5%)
4%	Alginate (2%) / GelMA (7.5%) /gelatin (4%)
5%	Alginate (2%) / GelMA (7.5%) /gelatin (5%)

5.2.2.1 Filament test

In this test, the printing nozzle was positioned 5.5-6 cm above the printing platform. The ink (only in the core) was extruded for 5 seconds. This determined the extrudability of each ink formulation. If the ink was too rainy and generated droplets instead of an extruded line, it was discarded for the rest of tests. Figure 17 shows the results.

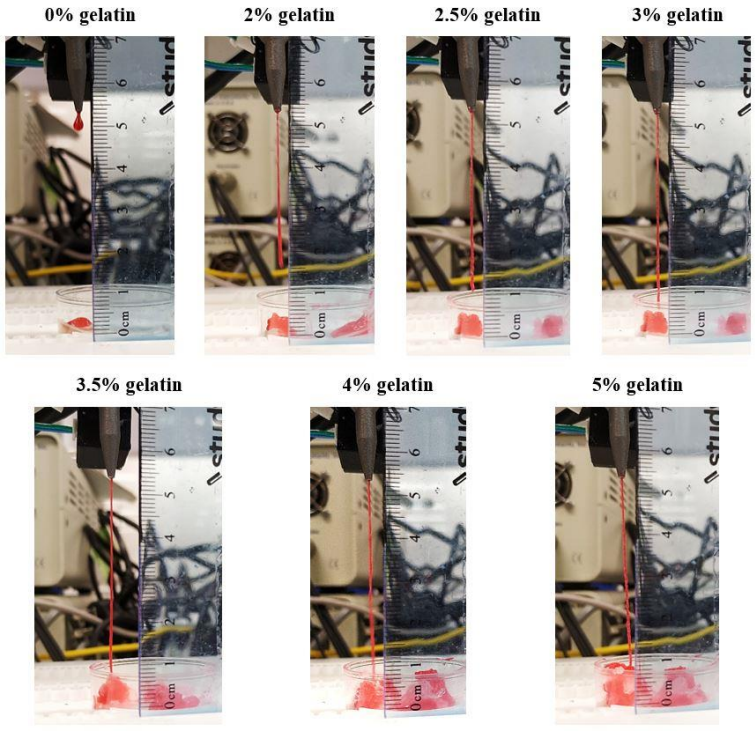

Figure 17. Photos of the filament test performed with bioinks containing different gelatin percentages. The ink without gelatin was also used for comparison. The ink was dyed red for better visibility. n = 3.

This test determined that, without adding gelatin, the ink was liquid and fell in droplets from the extruding nozzle. Thus, the formula was not extrudable at room temperature. The rest of the formulations passed the filament test and were subjected to the following experiments.

5.2.2.2 Filament fusion test

This test was performed to determine the shape fidelity of the extruded filaments. The distance between filaments increased after each strand. At lower separations, the filaments would be merged, and separated at higher distances. The number of merged filaments was used as an indicator for the shape fidelity. Figure 18 shows the results.

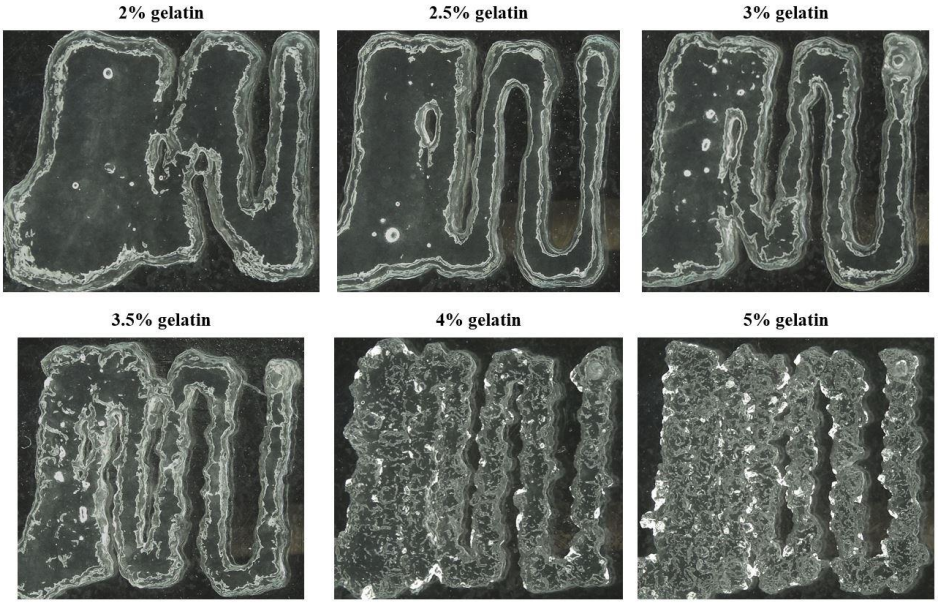

Figure 18. Printed scaffolds with different ink formulations, from 2% to 5% gelatin. The scaffolds had an increasing distance between layers, ranging from 1 to 2.5 mm. n = 3.

The visual examination of the samples determined that the 2% gelatin samples had a poor shape fidelity. Besides, 4% and 5% ink formulations were over-gelated, extruding thicker and irregular filaments. These parameters (filament diameter and distance between filaments) were measured with ImageJ and compared to the theoretical values. The results are in Table 8.

Table 8. Measurements of the filament diameter and spacing of the printed scaffolds. The theoretical values are shown on the first row for comparison. The values are displayed with their standard deviation. n = 3.

	Diameter	*d1*	*d2*	*d3*	*d4*	*d5*	*d6*
Theoretical	1	0	0.25	0.5	0.75	1	2
2%	1.13 ± 0.25	-	-	0.66 ± 0.05	0.72 ± 0.13	1.05 ± 0.1	1.34 ± 0.15
2.5%	1.08 ± 0.1	-	-	0.41 ± 0.05	0.74 ± 0.16	0.88 ± 0.07	1.3 ± 0.16
3%	1.07 ± 0.09	-	0.38 ± 0.04	0.57 ± 0.06	0.71 ± 0.08	0.98 ± 0.11	1.41 ± 0.08
3.5%	1.07 ± 0.08	-	-	0.53 ± 0.05	0.69 ± 0.04	0.93 ± 0.13	1.45 ± 0.13
4%	1.12 ± 0.11	-	-	0.29 ± 0.05	0.55 ± 0.09	0.72 ± 0.06	1.11 ± 0.06
5%	1.13 ± 0.1	-	-	0.31 ± 0.09	0.56 ± 0.1	0.8 ± 0.08	1.15 ± 0.21

The theoretical distances between filaments are schematically explained on Figure 19. The theoretical length of the filaments is shown on the left, which matches with the printing coordinates. The theoretical distance between filaments is shown on the right, where a filament thickness of 1 mm is considered.

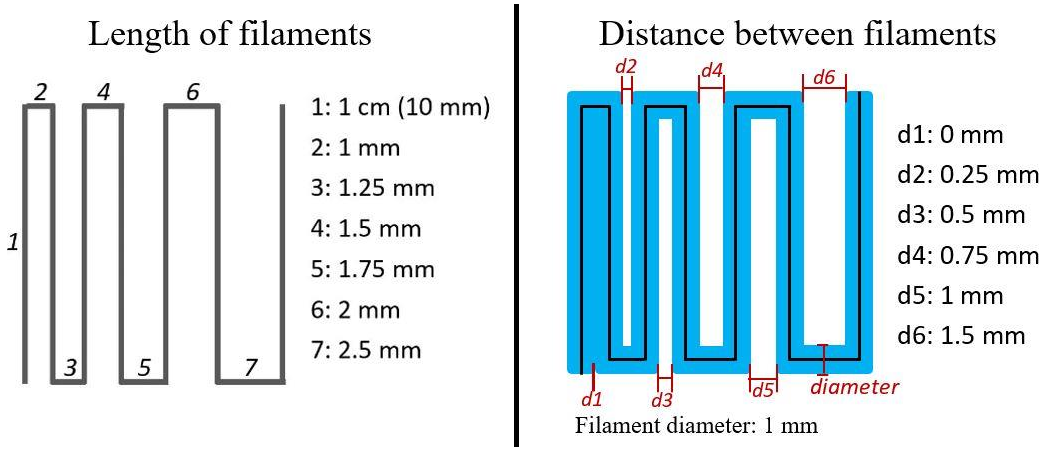

Figure 19. Theoretical length of filaments (left) and their theoretical distance (right) on the filament fusion test. The distance between filaments increased at every strand printed (printing direction from left to right). The ink would have the theoretical distances between filaments in case the shape fidelity was perfect. Even with an ink with perfect shape fidelity, the first two filaments would be fused (as d1 is 0 mm).

Looking into the filament diameter, those printed using the inks 2.5%, 3% and 3.5% appeared to be the closest to the theoretical value. However, there is no significant difference in the filament diameter across all testing groups. In the smallest distances (0.25, 0.5 and 0.75 mm spacing), those printed with the 2.5%, 3% and 3.5% formulations were closest to the theoretical values. Therefore,

it was concluded that these three inks were the ones with the better shape fidelity. Furthermore, observing the image of the 2% result (Figure 18), it was decided to not continue doing experiments on that ink.

5.2.2.3 Layer stacking test

This test was performed to complete the preliminary printing characterisation. 2.5% - 5% inks were tested. All the inks were printed at room temperature, with the same printing parameters: 0.23 ml/min flow and 140 mm/min speed. Lattices of 10 layers were intended to print, however, some bioinks did not achieve the 10 layers (2.5%, 4% and 5% gelatin inks achieved only 8 layers), because the strands merged or were brittle and the structure broke. The results are displayed in Figure 20.

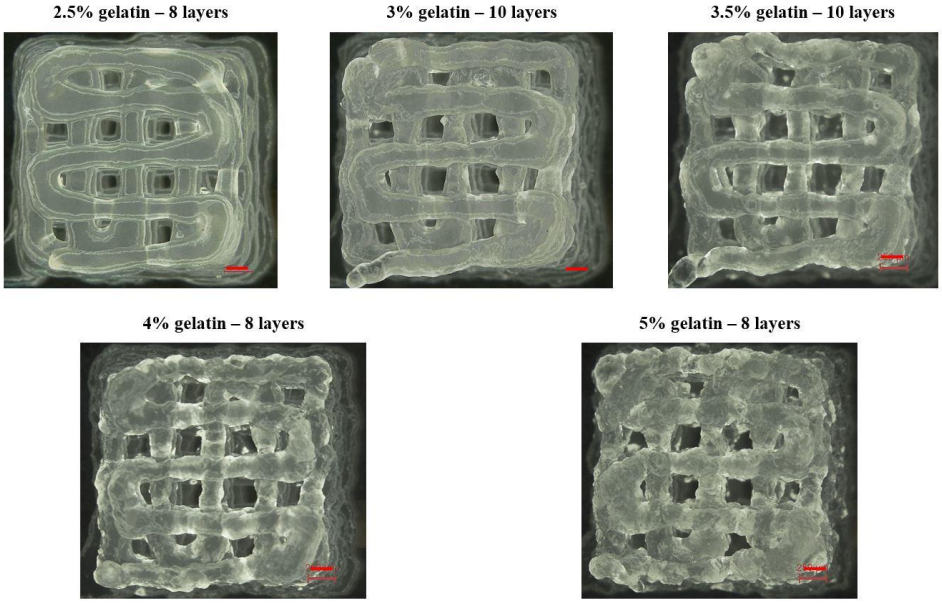

Figure 20. Layer stacking test. The printable scaffold with the highest number of layers was chosen as best result for each condition. Scale bar: 1 mm. n = 3.

The best results were obtained with 3% and 3.5% inks, as well-defined 10-layered structures could be printed. The scaffolds printed using 2.5% ink formulation were too rainy on the 10th layer, with the filaments merging. On the other hand, 4% and 5% gelatin scaffolds were over-gelled (as can already be seen on their 8th layer), and the 10th layer was rough and brittle, and so they were considered bad results. Figure 21 shows the 10-layered structures printed using the 2.5%, 4% and 5% gelatin inks respectively.

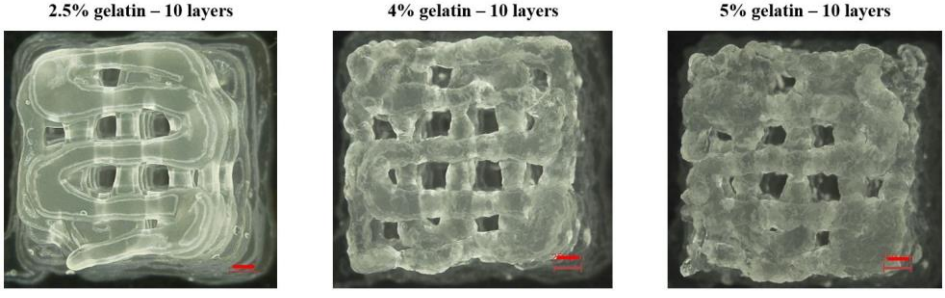

Figure 21. Images of the 10-layer results for 2.5%, 4% and 5% ink conditions. n = 3, scale bar: 1 mm.

Considering all the results obtained in the preliminary printing characterisation, 3% and 3.5% were selected to continue the studies.

5.2.3 Rheology

The different bioink formulations with 3% and 3.5% gelatin, as well as the ink without gelatin (0%), were subjected to rheological studies to determine its behaviour. Rheology measures the dynamic properties of fluids. The inks were subjected to rotation or oscillation, and their response was collected and analysed.

5.2.3.1 Temperature sweep

First, a temperature sweep was performed on the chosen ink formulations: 3% and 3.5% (and 0%). In this oscillation test, the frequency and strain remained constant (1 Hz and 1% respectively) and the temperature ranged from 10ºC to 40ºC, at a rate of 1.5ºC/min. Results are shown in Figure 22.

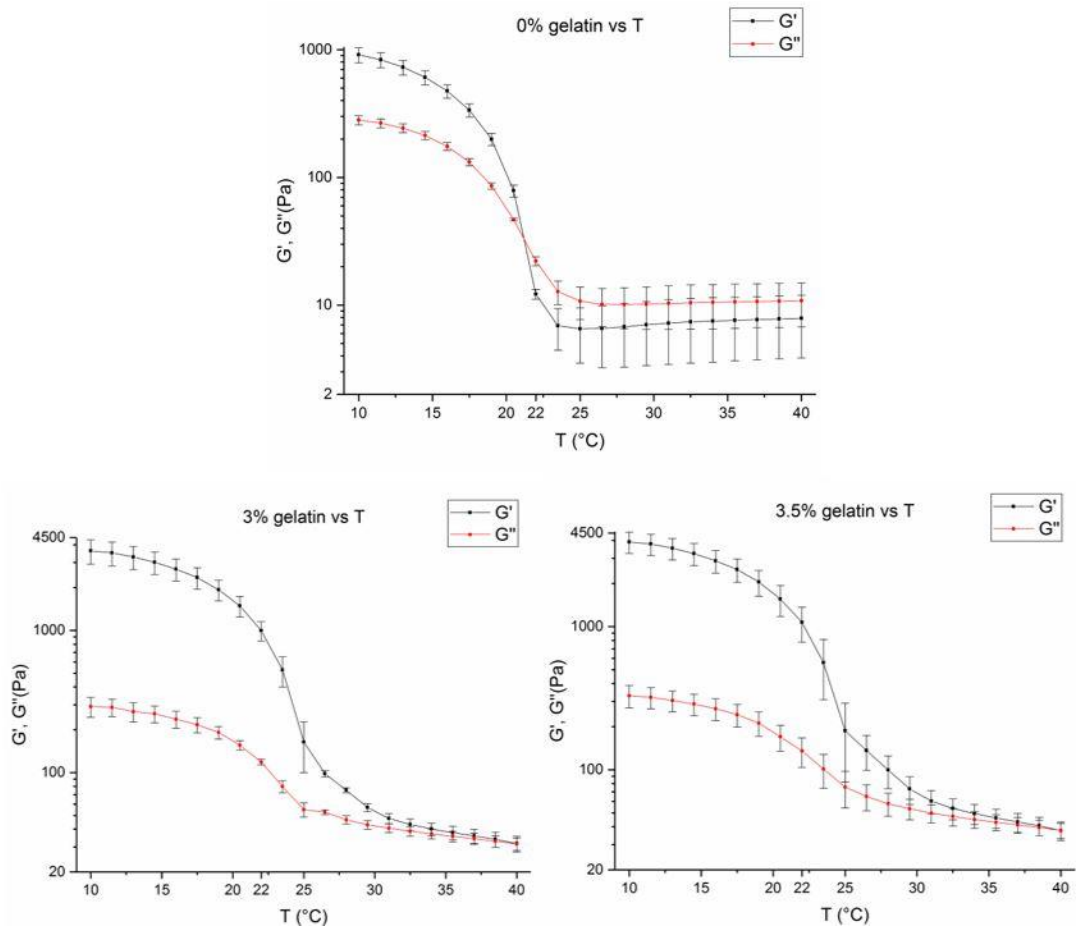

Figure 22. Results of the temperature sweep in the 3 conditions tested. G', storage modulus; G'', loss modulus. n = 3, error bars. The 0% gelatin ink (2% alginate/7.5% GelMA/0% gelatin) was gel-like (G' > G'') and it became a liquid-like (G'' > G') before reaching room temperature (22ºC). The 3% and 3.5% gelatin inks (2% alginate/7.5% GelMA/3% gelatin and 2% alginate/7.5% GelMA/3.5% gelatin respectively) were gel-like (G' > G'') and were close to become liquid-like from 30ºC to 40ºC, as G' and G'' had similar values.

The storage modulus (G') refers to the gel-like characteristics of a fluid, whereas the loss modulus (G'') refers to the liquid-like characteristics. When the storage modulus is higher than the loss modulus (G' > G''), the ink is elastically dominated and shows solid-like properties (meaning that it is gelled). On the contrary, when the loss modulus is higher than the storage modulus (G'' > G'), the ink is viscously dominated (meaning that it is liquid). For printing purposes, it is required for the inks to be elastically dominated.

Figure 23 shows that all the inks were elastically dominated with low temperatures (10-15ºC) and started decreasing in the storage modulus with the increase in temperature. The temperature where the two moduli crossed in the ink without gelatin is around 21ºC. Thus, the ink was viscously dominated (G'' > G') at the printing temperature (22ºC), therefore it was liquid and not suitable for extrusion printing. A close-up observation of these graphs is shown below for a better analysis of the ink behaviour at room temperature (15ºC – 25ºC).

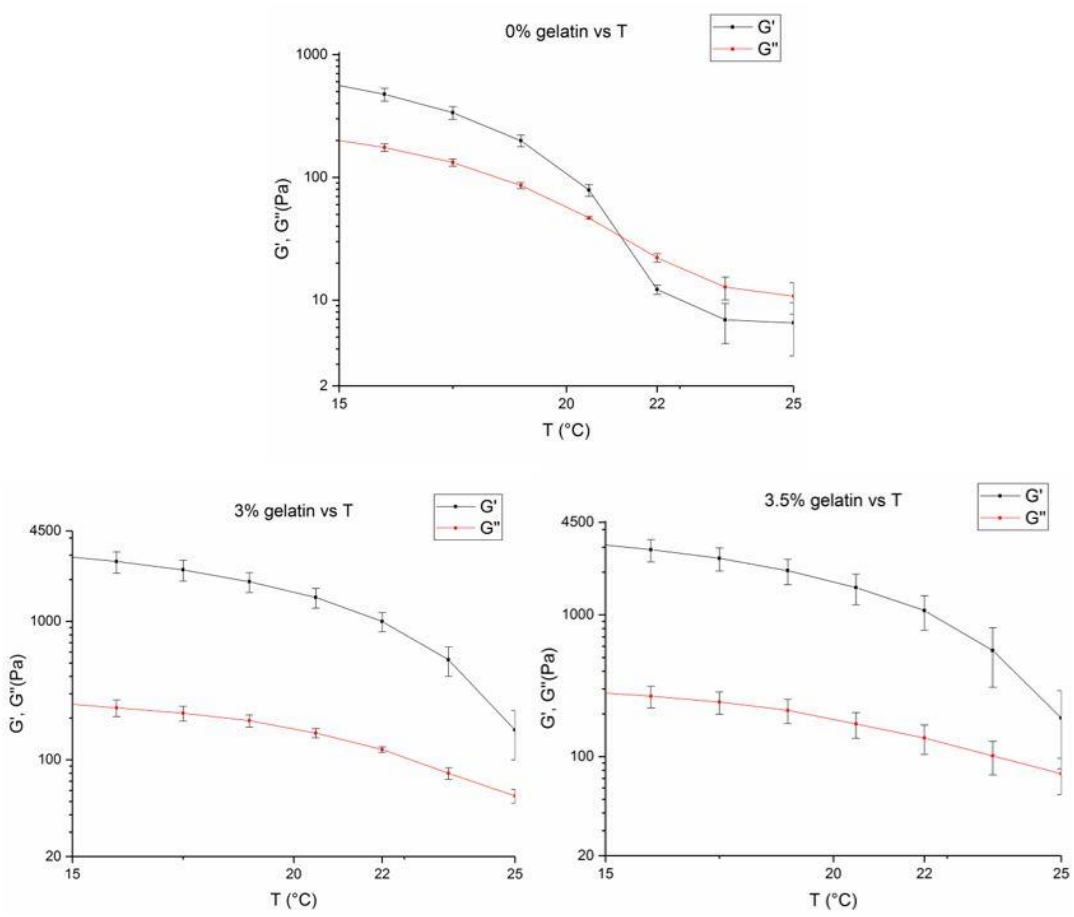

Figure 23. Close-up observation of Figure 22 in the temperature range, from 15ºC to 25ºC. n = 3, error bars. The ink without gelatin (2% alginate/7.5% GelMA/0% gelatin) changed from gel-like (G' > G'') to liquid-like (G'' > G') at 21ºC. The inks with gelatin inks (2% alginate/7.5% GelMA/3% gelatin and 2% alginate/7.5% GelMA/3.5% gelatin) had a similar behaviour among them, where G' > G'' was kept, although the difference between G' and G'' became smaller as the temperature increased. This means that the bioinks with gelatin retained gel-like properties from 15ºC to 25ºC.

The addition of gelatin (3% or 3.5%) increased the storage modulus of the 2% alginate 7.5% GelMA ink, making it elastically dominated at 22ºC. The two options (3% and 3.5%) were suitable for extrusion, as the storage modulus was higher than the loss modulus at this temperature. The graph below (Figure 24) compares the storage moduli (G') of all the inks.

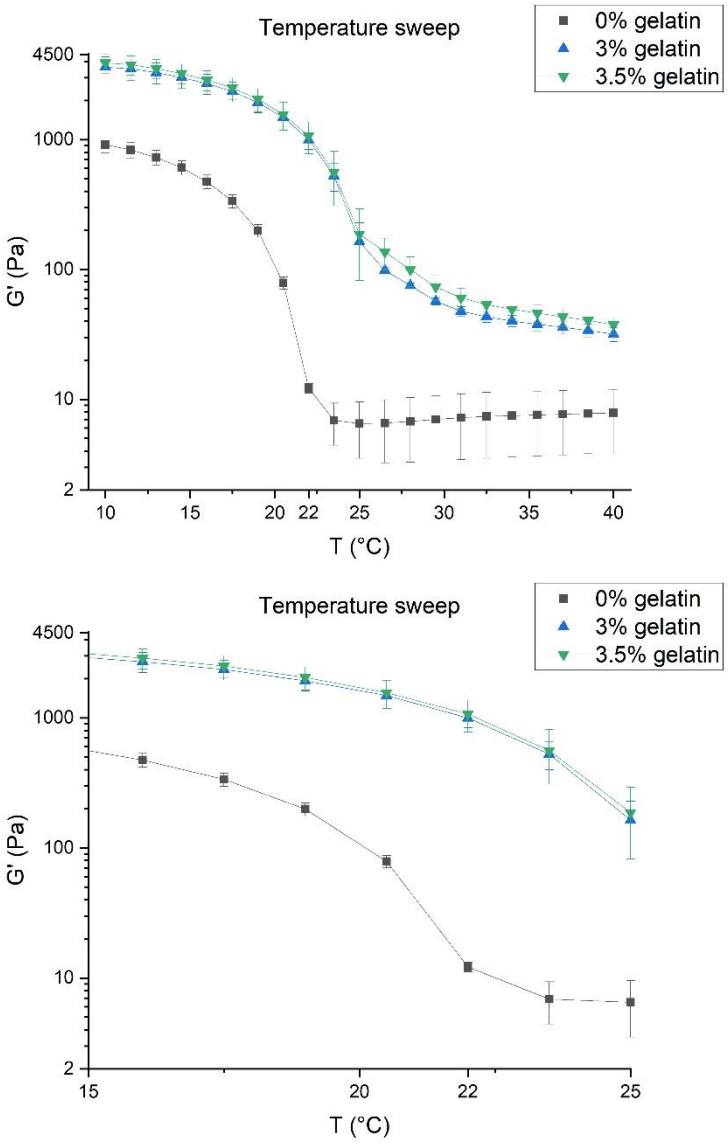

Figure 24. Storage moduli (G') of the different ink formulations (0%, 3%, 3.5%) at different temperature ranges: 10ºC – 40ºC (left), 15ºC – 25ºC (right). n = 3, error bars. The 0% ink (2% alginate/7.5% GelMA) had a different behaviour compared to the other two inks (3%, 3.5% gelatin), with a lower storage modulus, especially at temperatures above 20ºC.

This comparison shows that the storage modulus was significantly higher in the inks with gelatin (3% and 3.5%). Therefore, the two bioinks with gelatin were suitable for printing at room temperature. The following rheology tests were performed at 22ºC for the bioinks with gelatin (3% and 3.5% gelatin inks) and at 15ºC for the control bioink without gelatin (0% gelatin ink), unless otherwise specified. The control bioink is 2% alginate 7.5% GelMA, used and characterised

previously for printing at 15ºC, hence the comparison of the new bioinks with 3% and 3.5% gelatin at 22ºC with the one without gelatin at 15ºC.

5.2.3.2 Viscosity

In the rotation test, the viscosity of the ink was measured in a range of shear rate (0.01 – 1000 s^{-1}). The rest of the parameters remained stable: 1 Hz frequency, 1% strain, 22ºC (3%, 3.5% ink) or 15ºC (0% ink) temperature. Different forces and shear rates are applied in extrusion printing, changing the ink viscosity and consequently its behaviour. Therefore, making sure that the ink had a certain viscosity at a given shear rate was important. Figure 25 shows the results.

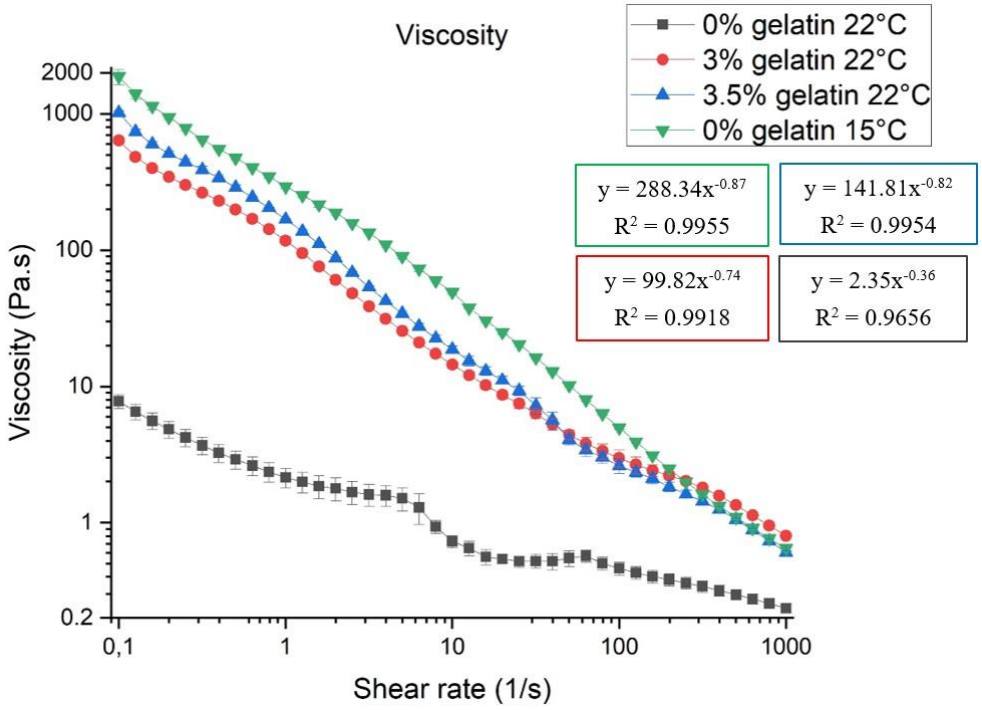

Figure 25. Graphical representation of ink viscosity at different shear rates (log scale). The two chosen inks, 3% and 3.5%, were compared to the 0% ink both at room temperature (22ºC) and at its optimal printing temperature (15ºC). Equations show power trendlines for each data set. n = 3, error bars.

The graph shows a significant drop in viscosity with the increase in temperature from 15 to 22ºC for the 0% ink (a 240-fold drop at 0.1 s^{-1} shear rate). On the other hand, the addition of gelatin significantly increases the ink viscosity at 22ºC, comparing 3% and 3.5% to 0% (82-fold increase for 3% and 130-fold increase for 3.5% when compared to 0% 22ºC ink at 0.1 s^{-1} shear rate). When comparing the inks with gelatin to the 0% ink, 3.5% is the most similar one (as there is a 1.7-fold drop from 0% 15ºC to 3.5% 22ºC, whereas from 0% 15ºC to 3% 22ºC there is a 2.95-fold drop). Table 9 shows the average viscosity of each bioink at different shear rates.

Table 9. Results of the viscosity (Pa·s) vs shear rate (s^{-1}) rheology. All the conditions tested were compared.

Shear rate (s^{-1})	*Viscosity (Pa·s)*			
	0% ink at 15ºC	*0% ink at 22ºC*	*3% ink at 22ºC*	*3.5% ink at 22ºC*
0.1	1880.33 ± 240.31	7.79 ± 0.91	638.60 ± 36.17	1018.70 ± 36.51
1	292.73 ± 10.18	2.15 ± 0.34	117.53 ± 7.11	168.40 ± 1.77
10	49.26 ± 10.18	0.73 ± 0.08	14.42 ± 0.63	18.72 ± 1.13
100	4.97 ± 0.14	0.46 ± 0.05	2.98 ± 0.42	2.61 ± 0.32
1000	0.65 ± 0.03	0.24 ± 0.02	0.80 ± 0.03	0.61 ± 0.02

The correlation between viscosity and shear rate determined their power law equations. These were then used to calculate the shear rate each ink suffered in the printing process. Finally, that shear rate was correlated to the viscosity (in the graph). This determined if the ink had an acceptable viscosity at the printing process. Two equations were used to resolve it.

$$\eta = K \cdot \gamma^{n-1} \tag{11}$$

η = viscosity

K = consistency factor

γ = shear rate

n = flow behaviour index

$$\gamma = \frac{4Q}{\pi R^3} \cdot \frac{3n+1}{4n} = \frac{8V}{D} \cdot \frac{3n+1}{4n} \tag{12}$$

Q = volumetric flow rate of printing

R = printhead/nozzle radius

V = speed of printing

D = printhead/nozzle diameter

Equation 11 is used to describe a power-law fluid behaviour, where K and n are part of the power trendlines (and the viscosity and the shear rate are y and x respectively). Furthermore, Equation 12 shows the Rabinowitsch–Mooney equation, which allows to estimate the shear rate during the extrusion of the bioink through the nozzle (119). The printing speed, flow and nozzle diameter were known values, and the flow behaviour index (n) was the exponent in the power-law fluid equation.

Table 10. Rheological parameters obtained by fitting the viscosity data with the power law model (Equation 11) and the Rabinowitsch-Mooney equation (Equation 12). The final goal was to determine the shear rate of the ink in the nozzle at the time of printing (γ), and the viscosity at that point (η_{nozzle}). For calculating the viscosity before and after printing (η_{rest}), a shear rate of 0.1 s^{-1} was assumed.

Ink	*Power law fitting*	*K*	*n-1*	*n*	*γ (s^{-1})*	*η_{nozzle} (Pa·s)*	*η_{rest} (Pa·s)*
0% 15ºC	$y = 288.34x^{-0.87}$	288.34	-0.87	0.13	**(Core) 125.44** **(Shell) 250.88**	**(Core) 4.29 ± 0.12** **(Shell) 2.34 ± 0.08**	**1880.33 ± 240.31**
0% 22ºC	$y = 2.3488x^{-0.36}$	2.35	-0.36	0.64	**(C) 53.23** **(S) 106.46**	**(C) 0.56 ± 0.07** **(S) 0.44 ± 0.05**	**7.79 ± 0.91**
3% 22ºC	$y = 99.82x^{-0.74}$	99.82	-0.74	0.20	**(C) 92.19** **(S) 184.38**	**(C) 3.57 ± 0.43** **(S) 2.15 ± 0.15**	**638.60 ± 36.17**
3.5% 22ºC	$y = 141.81x^{-0.82}$	141.81	-0.82	0.18	**(C) 101.29** **(S) 202.58**	**(C) 3.16 ± 0.28** **(S) 1.78 ± 0.14**	**1018.70 ± 36.51**

A bioink suitable for extrusion printing has two desirable features. First, it presents shear thinning while going through the printing nozzle. Second, a suitable bioink presents a fast recovery in viscosity after extrusion. When the shear stress is removed, the viscosity increases, and the ink behaves as a solid again, preserving the shape fidelity of the printed constructs.

K and n-1 were obtained by fitting the viscosity data with the power law model. The printing speed (V) was constant in all the cases, 140 mm/min, which is 2.3 mm/s. Finally, the diameter of the nozzle (D) was 400 µm in the core and 200 µm in the shell (0.4 and 0.2 mm). The shear rate in the nozzle can be calculated using Equation 12, based on which one can estimate the viscosity of ink during the process of printing (η_{nozzle}). The viscosity while going through the core of the printing nozzle for the ink with 0% gelatin was 4.29 ± 0.12 Pa·s at 15ºC and 0.56 ± 0.07 Pa.s at 22ºC. The bioinks with gelatin had a viscosity of 3.57 ± 0.43 Pa·s and 3.16 ± 0.28 Pa·s at 22ºC (for the 3% and 3.5% inks respectively). The results for the viscosity of the inks in the shell of the printing nozzle were similar: 2.34 ± 0.08 Pa·s and 0.44 ± 0.05 Pa·s for the ink with 0% gelatin at 15ºC and 22ºC respectively, and 2.15 ± 0.15 Pa·s and 1.78 ± 0.14 Pa·s for the 3% gelatin and 3.5% gelatin inks respectively. The 0% ink at 22ºC was less viscous (0.56 Pa·s), therefore, this confirmed that it became liquid while extruding through the nozzle. The bioink must behave like a liquid when going through the nozzle for it to be extrudable. When comparing the inks at 22ºC, the addition of gelatin slightly increased the viscosity, meaning that more force has to be applied for extruding the inks with 3% and 3.5% gelatin through the nozzle.

Moreover, the ink must behave like a solid once it is out of the nozzle, to retain its shape. The viscosity, among other factors, determines that. The shear rate "at rest", after printing, where no forces are applied, is considered 0.1 s^{-1}. The viscosities for that shear rate were calculated from the Equation 11 (η_{rest}). Considering that the 0% ink at 15ºC was a fluid while going through the core of the nozzle (4.29 ± 0.12 Pa·s), 0% ink could not retain its shape at 22ºC with 7.79 ± 0.91 Pa·s at rest. This was confirmed in earlier tests (filament test, filament fusion test), where the 0% bioink did not retain its shape after being extruded at 22ºC. The other two inks (with 3% and 3.5% gelatin) had a higher viscosity at rest (638.60 ± 36.17 Pa·s and 1018.70 ± 36.51 Pa·s respectively for 3% and 3.5%). The 0% gelatin ink presented a viscosity of 1880.33 ± 240.31 at 15ºC. All the bioinks presented a significant increase in viscosity between η_{nozzle} and η_{rest}, except the 0% gelatin ink at 22ºC. The differences among η_{core} and η_{rest} were 1876.04 ± 240.53 Pa·s for the 0% gelatin 15ºC ink, 7.23 ± 0.98 Pa·s for the 0% gelatin 22ºC ink, 635.03 ± 36.60 Pa·s for the 3% gelatin ink and 1015.54 ± 36.79 Pa·s for the 3.5% gelatin ink. Among these, 3.5% was chosen to continue with the rest of experiments, as its difference in viscosity between at rest and going through the nozzle at 22ºC was higher.

5.2.3.3 Effect of microsphere loading 2% alginate/7.5% GelMA/3.5% gelatin ink

Once the ink was chosen, microspheres were added to it to determine if they altered the ink composition and printability. More viscosity measurements were performed on the 3.5% ink to examine the effect of microspheres loading on the viscosity of bioinks (5 and 10 mg/ml microspheres). Figure 26 shows the effect of the microsphere addition on the 3.5% gelatin bioink. The ink without microspheres, with 5 mg/ml microspheres and with 10 mg/ml microspheres were compared.

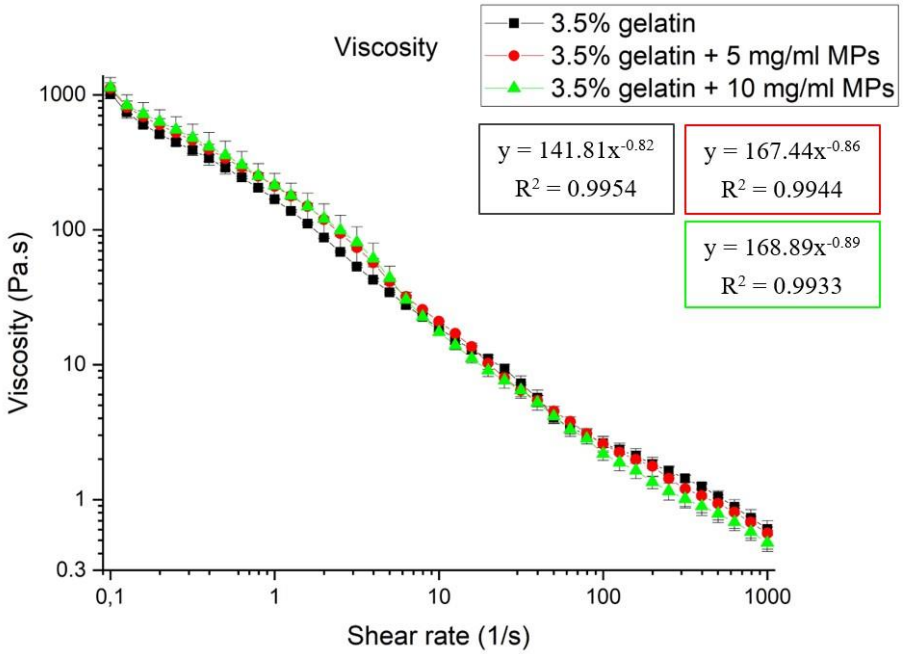

Figure 26. Graphical representation of ink viscosity at different shear rates (log scale). The chosen ink, 3.5%, was analysed without and with the inclusion of 5 mg/ml and 10 mg/ml GelMA microspheres. The experiment was held at room temperature (22ºC). Equations show power trendlines for each data set. n = 3, error bars.

The Equations 11 and 12 were used to calculate the shear rate in the nozzle and its viscosity, as well as the viscosity after the extrusion finished. Table 11 shows the results.

Table 11. Values extracted from the trendlines and equations 11 and 12. The final goal was to determine the shear rate of the ink in the nozzle at the time of printing (γ), and the viscosity at that point (η).

Ink	*Trendline*	*K*	*n-1*	*n*	*γ (s^{-1})*	*η_{nozzle} (Pa·s)*	*η_{rest} (Pa·s)*
3.5% gelatin	$y = 141.81x^{-0.82}$	141.81	-0.82	0.18	**(Core) 101.29** **(Shell) 202.58**	**(Core) 3.16 ±0.28** **(Shell) 1.78 ± 0.14**	**1018.7 ± 36.51**
3.5% gelatin + 5 mg/ml MP	$y = 167.44x^{-0.86}$	167.44	-0.86	0.14	**(C) 120.16** **(S) 240.32**	**(C) 2.69 ± 0.35** **(S) 1.48 ± 0.33**	**1115.67 ± 109.61**
3.5% gelatin + 10 mg/ml MPs	$y = 168.89x^{-0.89}$	168.89	-0.89	0.11	**(C) 145.06** **(S) 290.13**	**(C) 1.97 ± 0.25** **(S) 1.06 ± 0.15**	**1135 ± 205.66**

Typically, the smaller the n value, the more shear thinning the ink has. In this case, the bioink with 10 mg/ml MPs had the lowest n value (desirable for having less pressure applied for the ink to go through the nozzle) and the highest viscosity at rest (desirable for a better shape fidelity after printing). In this case, there was a slight difference in the viscosity at the nozzle between the 3 inks, but they all were low in general, suggesting liquid like properties in the nozzle for the ink with and

without microspheres. Moreover, increasing the microsphere loading resulted in an increase in the viscosity of the ink at rest, facilitating the shape retention of the prints. 10 mg/ml microspheres were chosen as the MP concentration for the ink, as it showed slightly better printing properties. However, the following rheological and hydrogel characterisation tests were performed in the 3.5% ink without microspheres in order to save material.

5.2.3.4 Other rheological measurements

Other oscillation tests were performed to determine the stability and optimal ink conditions: frequency, strain, and step-strain tests. In all of them, storage (G') and loss (G'') moduli of the 3.5% ink were measured at 22ºC and were compared to the control sample (0% gelatin) at 15ºC. In all the cases, all other parameters were kept constant (1 Hz frequency, 1% strain), except from the one that varied (see section 4.2.4 Rheology and Table 5 for more details).

Figure 27 gathers the graphs of these tests, where the G' of 3.5% ink was compared with the 0% ink measured at 15ºC.

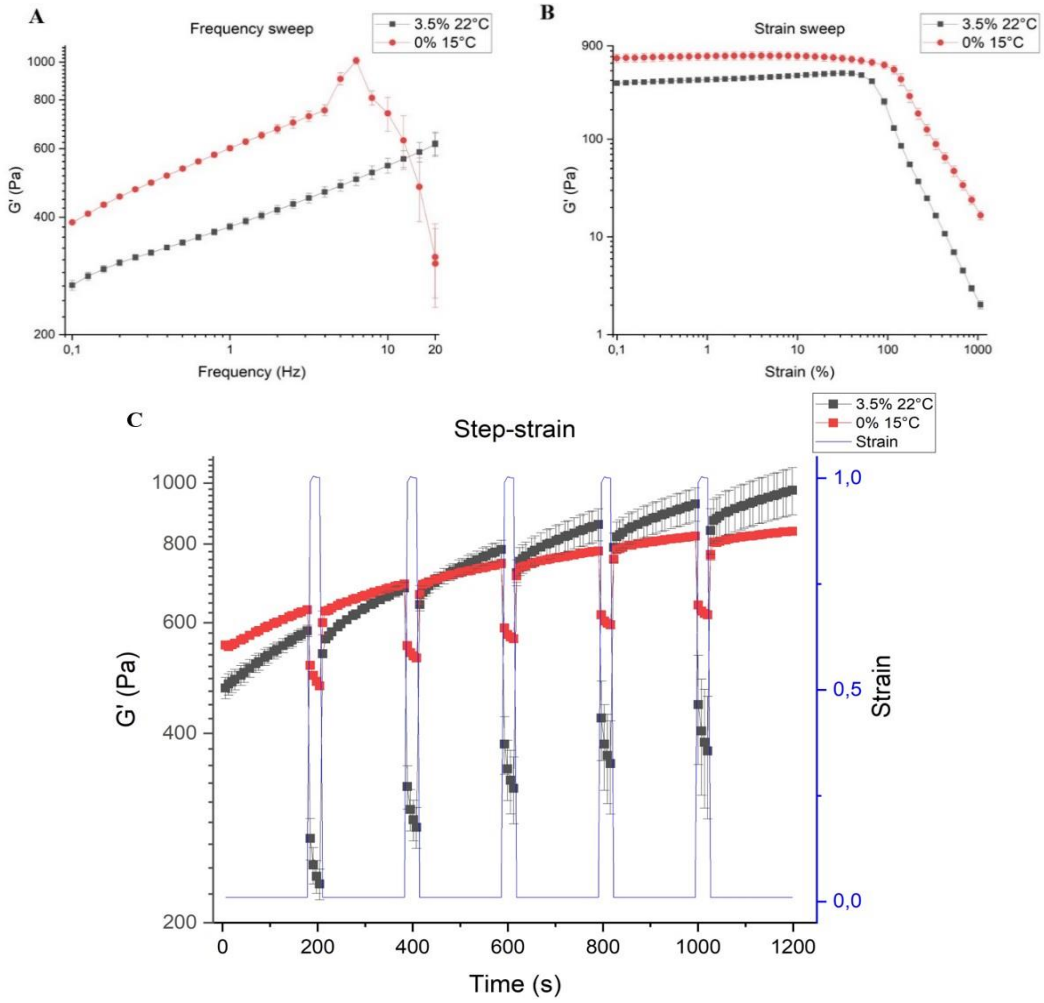

Figure 27. Results of the rheology tests, comparing the 2% alginate/7.5% GelMA/3.5% gelatin 22ºC bioink to the 2% alginate/7.5% GelMA 15ºC bioink. Frequency sweep at 0.1-20 Hz range (A), strain sweep at 0.1-1000% range (B) and step-strain test with 100% strain for the stress period and 1% strain for the recovery period (C). The storage modulus (G') is shown. Logarithmic scale was used in the x and y axes. n = 3, error bars.

In the frequency sweep, the behaviour of the ink was studied from 0.1 to 20 Hz. In the strain sweep, the ink behaviour was studied in the range of 0.1-1000% strain. These two tests were performed to ensure that the ink was stable at the frequency and strain at printing, 1 Hz and 1% respectively. Both ink types increased their storage modulus when the frequency increased, however, there is a significant drop in G' for the 0% sample measured at 15ºC, which might be due to the collapse of polymer network. Unlike the 0% sample measured at 15ºC, the G' of 3.5% ink, when measured at 22ºC, showed a linear trend in all the frequency region tested.

Regarding the strain sweep (Figure 27B), the G' of both bioinks was stable below certain percentage of strain (around 100% strain for the 0% gelatin ink at 15ºC, around 70-80% strain for the 3.5% gelatin ink at 22ºC). Above that strain percentage, the polymer network of both inks might have collapsed, resulting in a drop in storage modulus. The strain sweep was employed to calculate the yield point of the samples (Figure 28). The yield point occurs when a material deforms, due to a force. In this context, the material behaves as a solid (gel) in the syringe, and a force needs to be applied for it to behave as a liquid and get extruded through the syringe. Therefore, the strain at the yield point would be the one needed to apply at the syringe to start printing. This point was calculated where the storage modulus (G') dropped. Figure 28 explains it schematically.

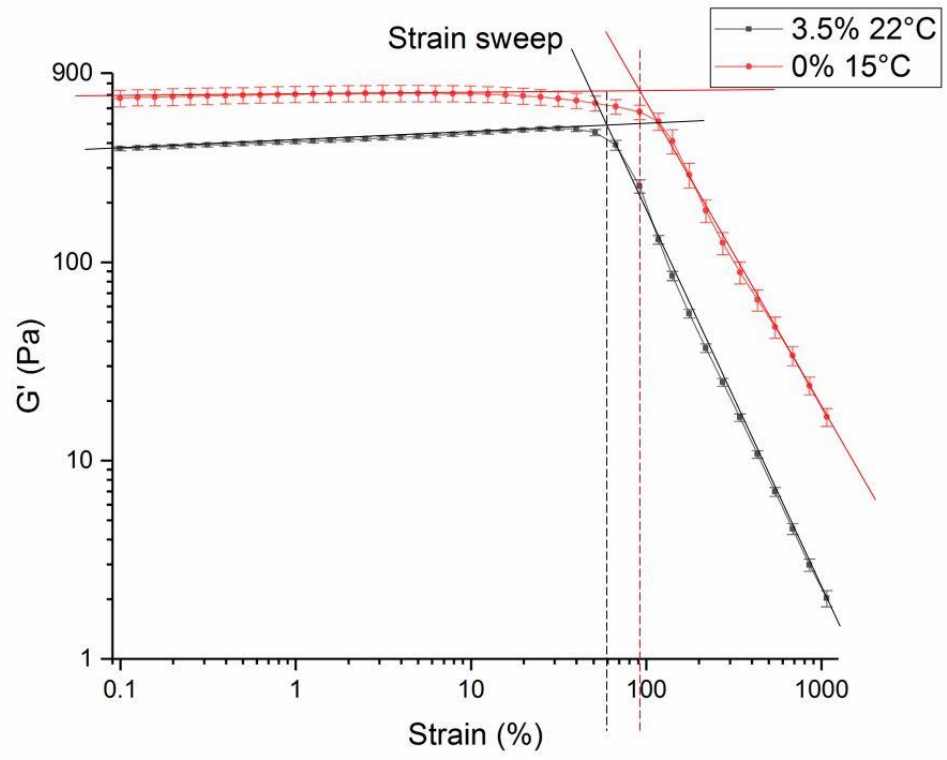

Figure 28. Yield points of the two ink types, at the cutting point of the line on the x axis. The yield strains were 60% and 90% for the 3.5% and 0% inks, respectively.

The yield point of the 3.5% bioink at 22ºC was an average of 61.7 ± 2.9%, and the yield point of the 0% bioink at 15ºC was an average of 93.3 ± 12.6%. According to these results, more force (or strain) would be required to squeeze the 0% ink at 15ºC. Therefore, the 3.5% ink would be more easily extruded.

Apart from that, the step-strain sweep was also analysed (Figure 27 C). The ability of the ink to recover after a stress was tested (for example, after the extrusion of the ink). This was a time sweep where the strain increased from 1% to 100% for 30 seconds. Afterwards, the samples were given 3 minutes to recover at 1% strain, before subjecting them to another stress period. The stress-recovery steps were repeated 5 times. When the ink was under stress (simulating the printing condition in the nozzle), the storage modulus decreased. When the stress came back to 1%, the ink was expected to recover to the initial storage modulus. The aim was to analyse the recovery time, and to see if the ink recovered to the initial storage modulus after the stress. In both ink types, a fast recovery was observed, obtaining the same storage modulus from before the stress in a short period of time (maximum 30 seconds for the 0% ink and 80 seconds for the 3.5% ink). Even if the trend of the storage modulus was slightly upwards, the ink recovered properly after every step. This phenomenon (G' slightly increasing over time) could not happen because of the evaporation of the ink, as a solvent trap was used to prevent it. Some molecular reorganisations could be responsible for it, where the polymer network would become stronger over time.

5.2.3.5 In-situ crosslinking rheology with UV or near-UV light

Finally, a last rheological test, a time sweep was performed with UV light, to monitor crosslinking kinetics of both inks. The UV lamp used was at 365 nm (the most efficient for the LAP photoinitiator), even if the hydrogels were casted with a 405 nm lamp. As it was mentioned in the methods section (4.2.4 Rheology), a special UV box had to be attached to the rheometer, and the only lamp available was the 365 nm one. The aim was to see the effect of the UV on the crosslinking and comparing both inks (the 2% alginate/7.5% GelMA and the 2% alginate/7.5% GelMA/3.5% gelatin). Results are in Figure 29.

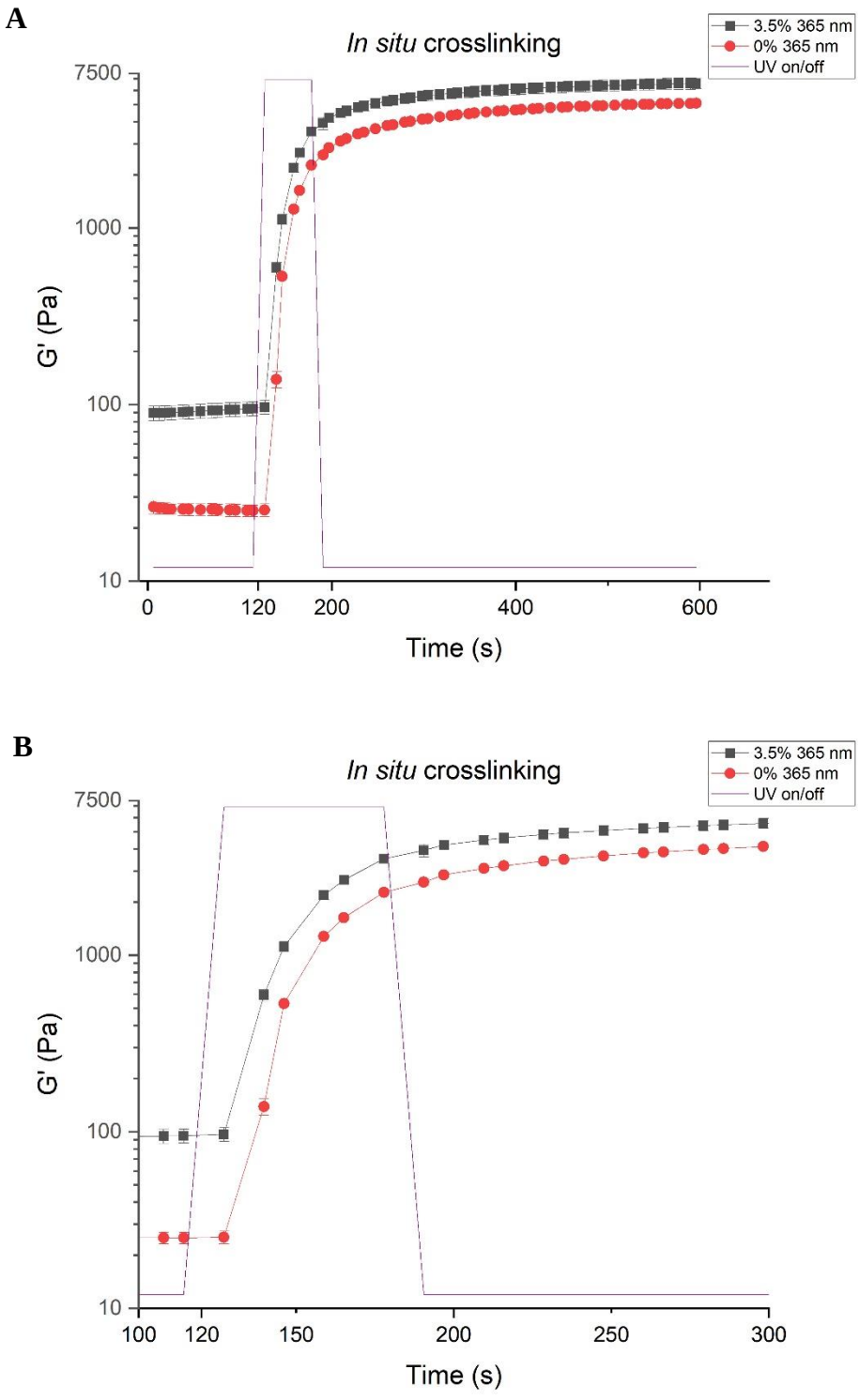

Figure 29. In-situ crosslinking trend of the 0% and 3.5% inks under UV light (365 nm wavelength). The full results (A) and a close-up on the UV on/off region (B) are shown. n = 3, error bars. The time sweep started with the UV light off. After 2 minutes, the UV light was turned on for 1 minute, and then off again. The 0% ink (2% alginate/7.5% GelMA) and the 3.5% ink (2% alginate/7.5% GelMA/3.5% gelatin) had an abrupt increase in G' after the UV light turned on (due to photocrosslinking), and the G' slightly increased even after the UV light turned off.

Figure 29 shows the increase in storage modulus of both bioinks, which occured when the UV light was turned on. After the UV light was turned off, the storage modulus of both bioinks became stable. Table 12 shows the storage modulus of the different conditions, at the beginning of the test and after 5 minutes (300 s).

Table 12. Summary of the results of the UV crosslinking rheology. The storage moduli and standard deviations are shown for the two bioinks, before and after crosslinking. The difference between them is also shown, to describe the increase in G' during the crosslinking.

	Storage modulus (G') (Pa)		
Condition	*Before crosslinking (0 s)*	*After crosslinking (300 s)*	*Difference*
0% ink 365 nm light	26.30 ± 2.26	4162.00 ± 68.00	4135.40 ± 70.26
3.5% ink 365 nm light	89.39 ± 8.38	5630.33 ± 383.76	5540.94 ± 392.14

The biggest difference was at the starting point of the samples (before the light was applied), where the 3.5% samples had a higher storage modulus than the 0% ones (89.39 ± 8.38 Pa·s for the 3.5% ink and 26.30 ± 2.26 Pa·s for the 0% ink). The reason behind that was the lack of temperature control at the rheology plate fitted for UV-light. All samples were tested at room temperature (22ºC), where the 0% ink had a liquid behaviour, presenting a lower storage modulus. After crosslinking, both inks increased in more than 4000 Pa·s their storage modulus. The increase of the 0% and 3.5% inks were 4135.40 ± 70.26 Pa·s and 5540.94 ± 392.14 Pa·s respectively. The higher storage modulus of the 3.5% ink was expected, as the samples contained more solid content (3.5% more gelatin than the 0% ink). This resulted in a more compact polymer network which was transated into a higher G' before and after crosslinking.

After the rheology tests were concluded, the crosslinked hydrogels were characterised to determine their swelling and mechanical properties as well as their degradation.

5.2.4 Characterisation of hydrogel discs

The swelling, mechanical and degradation properties of crosslinked hydrogels were determined. 3.5% bioink hydrogels were compared to 0% bioink hydrogels as a control. The hydrogel discs were obtained by pouring the ink mixtures with LAP in 8 mm diameter moulds and crosslinking them with 1 minute of UV light at 405 nm and 10 minutes of a 2% $CaCl_2$ solution, as specified in the methods (section 4.2.5). All the discs were 1 mm in height except in the mechanical test, where the height was 3 mm.

5.2.4.1 Free polymer content and swelling

The free polymer content and swelling fraction of 0% and 3.5% hydrogels were shown in Figure 30.

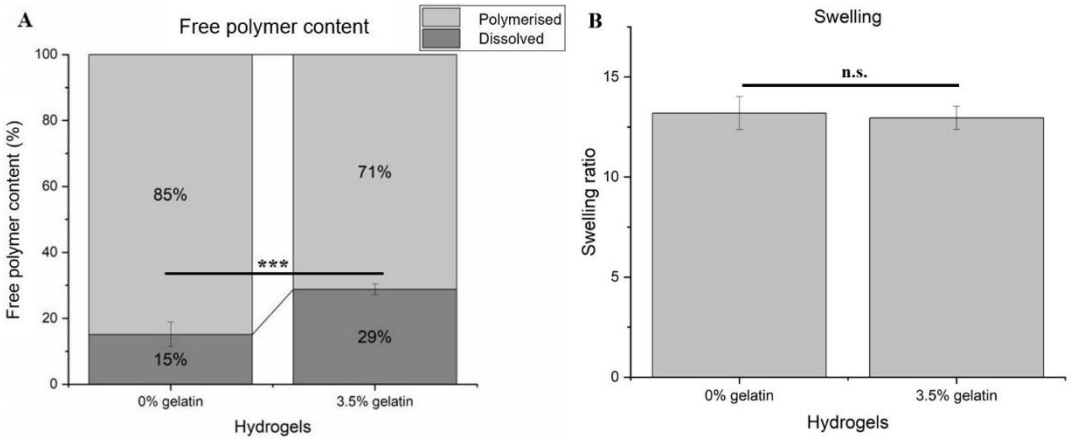

Figure 30. Results of the free polymer content (A) and swelling ratios (B) calculated on the 0% and 3.5% hydrogel discs. Crosslinking conditions: 1 minute under 405 nm light at 2 mW/cm^2 intensity and afterwards 10 minutes in a 2% $CaCl_2$ solution. n = 3, error bars. Significative differences are shown (p > 0.05: n.s., p 0.01-0.05: *, p 0.005-0.01 **, p 0.001-0.005: ***, p < 0.001 ****).

The free polymer content refers to the soluble fraction of the hydrogel, this is, the part that dissolves after being overnight in PBS. The polymerised fraction is the opposite of the soluble (dissolved) fraction (the remaining part of the hydrogel). Moreover, the swelling ratio of the gels describes how much water they absorb. In this case, the 3.5% hydrogels had a higher free polymer content and slightly lower but non-significative swelling. Gelatin is soluble at 37ºC, therefore, the 3.5% gelatin could have dissolved overnight at 37ºC, resulting in 29% ± 1.6% free polymer content (vs the 15% ± 3.7% of the 0% gelatin ink). The swelling ratios of the 0% ink and 3.5% ink were 13.20 ± 0.82% and 12.95 ± 0.58% respectively.

5.2.4.2 Mechanical test

A compression test was performed on 3 mm thick hydrogel discs. The compression modulus was calculated as the slope in the stress-strain curve at 10%-15% strain range. Four types of hydrogels were compared: 0% or 3.5% ink and directly after casting them or after leaving them overnight in PBS at 37ºC. The discs were left overnight at 37ºC to remove the unreactive polymers and the gelatin. In this way, the mechanical strength could be compared between the gels with and without the unreactive hydrogel and gelatin dissolved. Figure 31 shows the results.

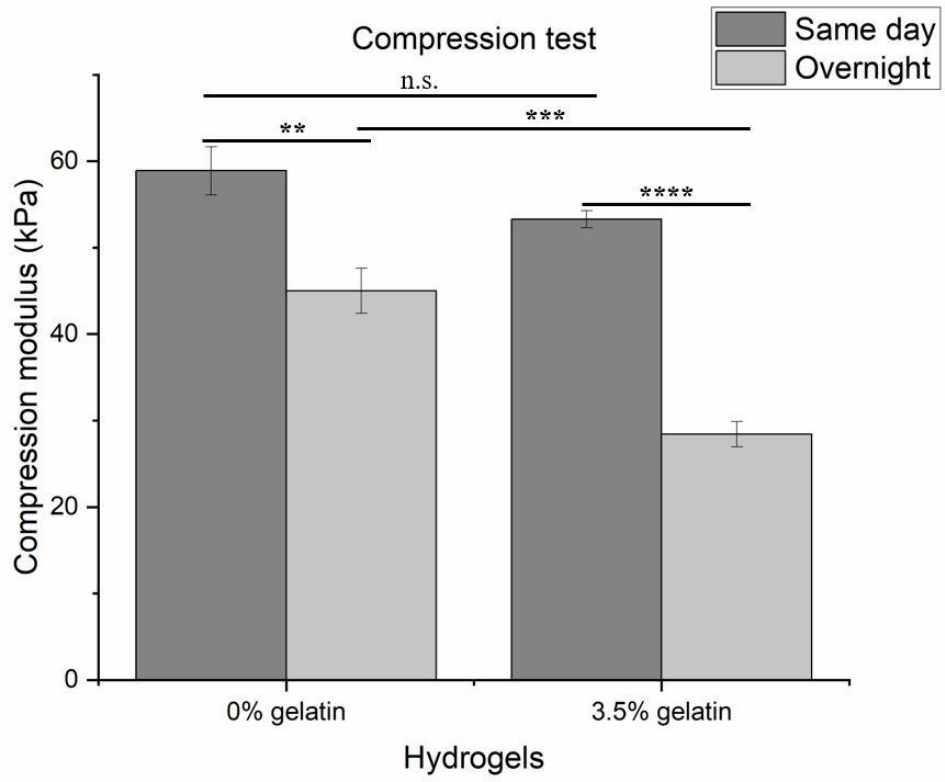

Figure 31. Compression modulus (kPa) in different gel conditions, showing the stiffness of each gel type. n = 3, error bars. Significative differences are shown (p > 0.05: n.s., p 0.01-0.05: *, p 0.005-0.01 **, p 0.001-0.005: ***, p < 0.001 ****).

These results showed some differences between conditions. There were no significant differences between the two ink types on the gels tested directly after UV crosslinking, meaning they had a similar stiffness. Besides, a decrease in the compression modulus was observed on the hydrogels that had been overnight in PBS at 37ºC (compared to the ones tested on the same day). These lower values correlated with the fraction dissolved overnight (free polymer content), therefore, the gels became more porous, mechanically weaker. However, this difference was bigger in the samples prepared using the 3.5% ink than the 0% ink, which was expected as the free polymer content was higher in the samples crosslinked using the 3.5% ink (referring to the gelatin fraction that dissolved overnight). The analysis was more focused on the results obtained after the removal of free polymers, as the condition is more consistent with the targeted application on in vitro cell culture. Observing the two gel types, the gels without gelatin were significantly stronger than the ones with 3.5% gelatin (45.01 ± 2.62 kPa of 0% vs 28.42 ± 1.46 kPa of 3.5%). In conclusion, both ink types provided similar mechanical properties before the removal of free polymers. Then, both gel types decreased their compression modulus compared to the "same day" studies, but the lack of crosslinking of the gelatin made the 3.5% gels significantly weaker than the 0% ones.

5.2.4.3 Degrdability of gels

The same degradation test done with the microspheres (5.1.3) was performed with the hydrogels prepared using 0% or 3.5% ink. The gels were subjected to a degradation study, using 2 U/ml type I collagenase. Figure 32 shows the results.

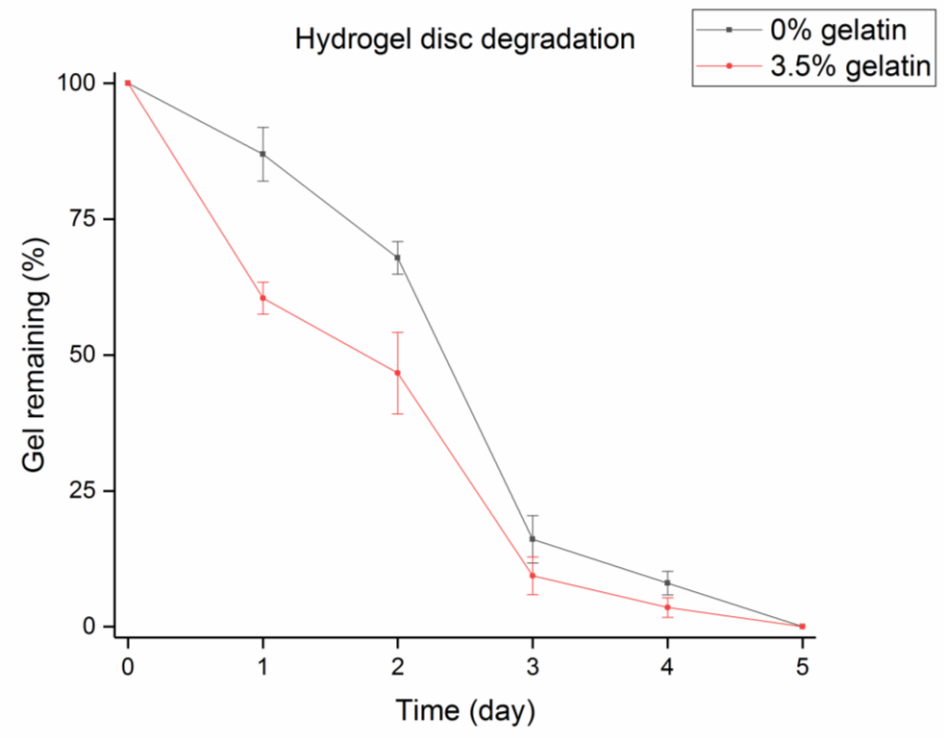

Figure 32. Degradation study of hydrogels. Measured with the dry weight of the discs. n = 6, error bars.

The hydrogel discs degraded fast, being completely degraded by day 5. 3.5% hydrogels degraded faster, especially in the first two days. This, together with the above mentioned mechanical testing, reflects the effect of the elution of unreactive polymers (and gelatin in the 3.5% gelatin condition), which results in a more porous structure that speeds up the degradation process when compared to the samples prepared using 0% gelatin ink.

5.2.5 Microsphere distribution in ink

It had to be ensured that the microspheres uniformly distributed in the ink before printing, and that they did not settle at the bottom of the syringe while printing. To assess the distribution of the GelMA microspheres in the ink, the microspheres, previously rehydrated with PBS, were mixed with the 3.5% ink and deposited in syringes for printing. 30 minutes later (time taken into account as the co-axial extrusion printing lasted no longer than 30 minutes), the ink was extruded in different regions of the syringe (bottom, first extruded; middle and top, last extruded). These regions were analysed under an optical microscope, and the count of microspheres was used to determine if their distribution was uniform throughout the syringe. This experiment was done only in the 3.5% ink. Results are displayed in Figure 33.

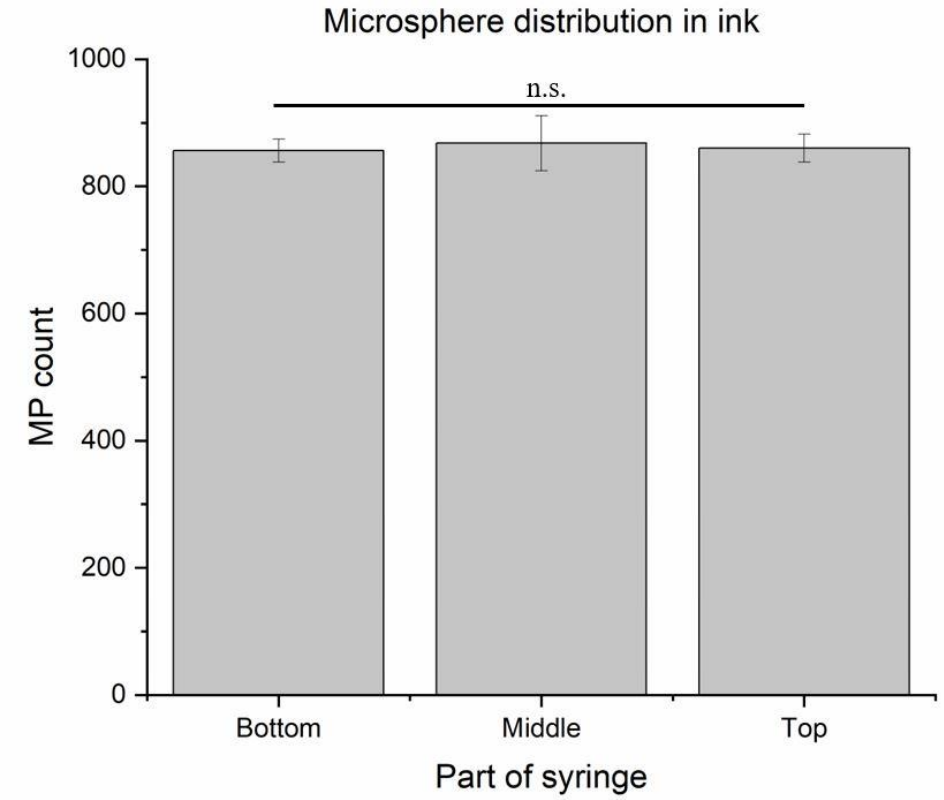

Figure 33. Microsphere distribution in the syringe, showing three different regions and the count of microparticles. n = 3, error bars. Significative differences are shown (p > 0.05: n.s., p 0.01-0.05: *, p 0.005-0.01 **, p 0.001-0.005: ***, p < 0.001 ****).

The count showed that the microsphere distribution was uniform throught the printing syringe, with no significant variation on the MP number in the different regions of the syringe. This proved that a uniform distribution of the microspheres in the ink, a critical factor to ensure the printed structure is reliable and replicable, was achieved.

5.3 Release study

A release study was performed from the GelMA microspheres to the medium. First, the IL-2 growth factor was adsorbed into the dry microspheres, and then the release started. 3 different conditions were analysed, including IL-2 loaded microspheres, casted hydrogels containing IL-2 loaded microspheres, co-axially printed hydrogels containing IL-2 loaded microspheres.

In all the cases, an added timepoint was taken at day 0, immediately after adding the release medium. This was measured to know what amount of the IL-2 was not adsorbed to the microspheres (and released immediately), and this quantity was subtracted from the total IL-2 added, in order to quantify the total IL-2 adsorbed to the spheres. Figure 34 shows the results.

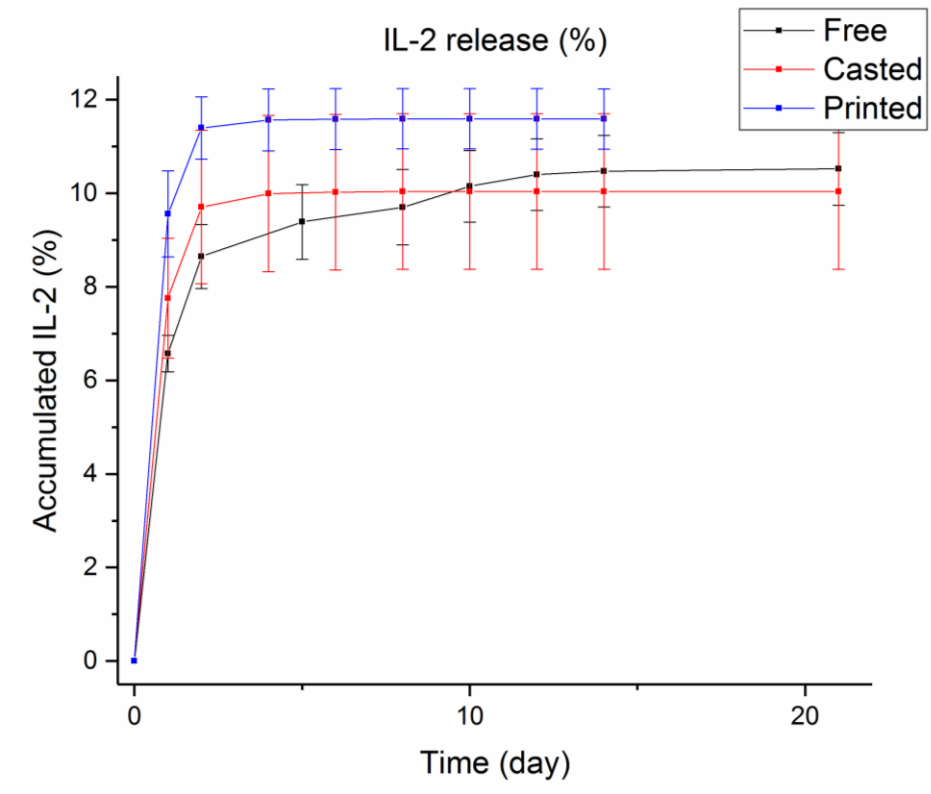

Figure 34. Accumulated release profile of the IL-2 in the three different conditions (free, casted and printed). n = 3, error bars.

The release profile was very similar in the three cases, with an initial burst release and reaching a plateau phase in the first 3-5 days. Initially it was expected that the casted and printed gels would have a more sustained release over time when compared to the free microspheres. However, in the three cases the profile was similar. One of the reasons why this could have happened was related to the fast degradability of the hydrogels, which after 2-4 days of release were completely degraded (section 5.2.4.3). Therefore, after day 4, the three conditions were the same (free microspheres). Besides, another factor that could have influenced on that release profile was the low degradability of the microspheres, and the strong interaction between the spheres and the IL-2. In this case, until the spheres degraded, the IL-2 would be attached to them. As a result of that, the maximum release obtained was 12% of the total inside the spheres.

On the first two days of the release, it is noticeable that the free microspheres were the ones releasing IL-2 slower, and that the spheres embedded into the gel (be it casted or printed) had a faster initial release. The free microspheres released 6.5% of the total 10.5% IL-2 released on the first day, compared to the 8% of the total 10% on casted gels and 9.5% of the total 11.5% on printed gels. Therefore, 62% of the total released IL-2 was released on the first day from the free microspheres, 80% from the casted gels and 82.6% from the printed gels. This might be due to the gels degrading and releasing some microspheres to the release medium. These released microspheres from the gels might have been collected with the release medium in day 1, resulting in a higher quantification of IL-2. Nevertheless, this was a preliminary study, which could not be repeated due to time constraints.

Chapter 6

6. Discussion

In this project the 2% alginate, 7.5% GelMA and 3.5% gelatin ink was identified and assessed against the ink previously developed, consisting of 2% alginate and 7.5% GelMA, with a focus on improving the printability at room temperature. GelMA microspheres were added to the ink formulation. These were also characterised and their effect on the bioink was assessed. Finally, the release of the growth factor from the microspheres was also analysed. The discussion is focused in three main points:

- Bioink. Comparison between the two main inks (gelatin vs no gelatin). Analysis of filament tests, rheology and hydrogel characteristics.
- Microspheres. Preparation, characterisation of GelMA microspheres and their distribution in the identified ink formulation.
- Release. Characterisation and comparison of IL-2 release from the GelMA microspheres, and casted and printed hydrogels where IL-2 preloaded microspheres were encapsulated.

6.1 Bioink

The bioink used was composed of 68% DoF 175 bloom GelMA (7.5%), medium viscosity alginate (2%) and gelatin (300 bloom). GelMA and alginate concentrations had previously been optimised, but this bioink was liquid at room temperature (22ºC), therefore, not printable. This project intended to develop a bioink printable at room temperature, as the custom-made bioprinter used did not have temperature control on the printing nozzle and base (as explained in section 1.3.3.1). The idea with this project was to add gelatin to the previously developed ink to make it printable at room temperature.

The first step of the bioink optimisation was to determine the gelatin concentration for printing at room temperature. The filament test (Figure 17) showed that without gelatin, the ink was too rainy and fell in droplets. Afterwards, the filament fusion test (Figure 18) and layer stacking tests (Figures 19-20) identified 2.5%, 3% and 3.5% as the best options. Lower gelatin concentrations provided bad shape fidelity, with filaments spreading and merging after being deposited by the printer. Higher gelatin concentrations generated rough constructs, where layer stacking was also compromised. Some of these tests were previously performed by other groups (120). The distance between filaments (Table 8) was a quantitative indicator of the shape fidelity in each ink formulation. In this case, the distances between filaments printed using the 2.5% - 3.5% gelatin inks were the closer to the theoretical distances. For this reason, these three were chosen for rheological characterisation.

Different rheological tests were performed: temperature sweep, viscosity test, strain sweep, frequency sweep, step-strain and in situ UV-crosslinking rheology. Temperature sweep was first done with the three chosen inks and the one without gelatin (Figure 21-23). When the storage modulus (G') is higher than the loss modulus (G''), the ink is elastically dominated, this is, its gel-

like properties are more dominant than its liquid-like properties. On the contrary, when G'' > G', the ink is viscously dominated and its liquid-like properties prevail (121). For extrusion printing, the ink was required to be elastically dominated (G' > G''). The ink without gelatin proved that it was liquid at room temperature. All the inks with gelatin were gel-like at room temperature (22ºC), however, 2.5% ink was almost on the verge of becoming liquid. Thus, it was discarded for the following tests.

The next rheological test was the viscosity test (Figure 24). This was important for the assessment of the printability. The viscosity of the ink plays a fundamental role for extrusion printing. Generally, hydrogels behave as non-Newtonian materials, with shear thinning characteristics (121). With shear thinning, the viscosity decreases when the shear stress increases. Before and after printing, the shear stress can be considered inexistent (0.1 s^{-1}). In these occasions, the ink is elastically dominated (gel). However, for printing, the ink suffers a stress (shear stress) when it is pushed through the nozzle. As mentioned before, hydrogels suffer from shear thinning, reducing their viscosity until they become extrudable. In the viscosity test performed at room temperature, all the inks exhibited shear thinning effects. The inks with gelatin were clearly more viscous than the one without it. In addition, these were also compared to the ink without gelatin measured at 15ºC, as it was the previous printing condition. It was determined that the viscosity was similar between 2% alginate/7.5% GelMA at 15ºC and 2% alginate/7.5% GelMA/3.5% gelatin. The power law model and Rabinowitsch–Mooney equation (Equations 11 and 12 respectively) were employed to calculate the shear rate exerted on the ink at the moment of printing, by taking into account the nozzle dimensions and the ink consistency (122). All the calculations are displayed in Table 9. The inks with 3% and 3.5% gelatin were determined as similar to the 0% ink measured at 15ºC, which was previously defined as printable. Therefore, both 3% and 3.5% inks were also printable at room temperature, and the gelatin concentration was chosen to be 3.5% as it showed a slightly higher viscosity at rest. Previous works also show that other types of hydrogels also present shear thinning, for instance, hyaluronic acid (123). Other viscosity rheologies of printable inks provided similar results (124,125).

Other rheological tests included frequency sweeps, strain sweeps and step-strain sweeps (Figure 26). On the frequency and strain sweeps, the ink should ideally be constant in the region of the frequency and strain for printing (which were 1 Hz and 1% strain). All the inks tested here showed a similar trend, with a rising G' with increasing frequency. Taking the 0.3 - 4 Hz interval into account, the 0% bioink increased its G' from 490.5 ± 5.7 Pa·s to 752.2 ± 24.6 Pa·s (a difference of 261.7 ± 30.3 Pa·s), and the 3.5% increased it from 324.5 ± 5.3 Pa·s to 464.5 ± 14.3 Pa·s (a difference of 140 ± 19.6 Pa·s). A similar trend was reported in hyaluronic acid (123). The 0% ink had a drop in storage modulus at high frequency (it went from 1007.87 ± 20.25 Pa at 6.3 Hz to 304.33 ± 69.53 Pa at 20 Hz), due to the collapse of the hydrogel ink. The strain sweep of all the inks demonstrate a similar trend, the G' values of these inks remain constant with the range of strain being tested. The yield point of each ink determined, being 61.7% ± 2.9 and 93.3% ± 12.6 strain for the 3.5% ink (22ºC) and the 0% ink (15ºC) respectively. Apart from those tests, a step-strain test was performed. The purpose of the test was to assess if the recovery of the ink was complete after a stress period,

and how long would that recovery take. Both ink types showed the ability to recover after the stress, but the G' was constantly increasing. This could be due to molecular reorganisation of the bioink. The increase in G' was 278 ± 17 Pa for the 0% ink and 546 ± 102.5 Pa for the 3.5% ink during the entire test, and an average of 60.2 ± 12 Pa and 117.2 ± 22 Pa during each step for 0% and 3.5% inks respectively (so the 0% ink increased less than the 3.5% ink). Importantly, the inks demonstrated a rapid recovery rate after the stress period, reaching the previous storage moduli within 8 seconds. Hence, both inks showed the ability to recover after printing to retain shape fidelity, and they were able to withstand at least 5 cycles of stress-relaxation.

The last rheological test was the in-situ crosslinking (Figure 28). The 0% and 3.5% bioinks had a similar strong crosslinking trend. This might have occurred due to the 7.5% GelMA of both inks being UV-crosslinked. The molar extinction coefficient of the photoinitiator, LAP is 225 $M^{-1}cm^{-1}$ at 365 nm (as shown in Figure 10). LAP absorbed energy with UV light, generating strong networks.

The hydrogel properties were also tested in the form of gel discs. Free polymer content, swelling ratio and Young's modulus of the hydrogels prepared using the 0% ink or 3.5% ink were calculated (Figure 29 and 30). The free polymer content was higher in the 3.5% gels (15.1% ± 3.7 free polymer content for 0% hydrogels and 28.8% ± 1.6 for 3.5% gels). However, the differnce in swelling was non significant (13.2 ± 0.8 ratio for 0% hydrogels and 13.0 ± 0.6 for 3.5% hydrogels).

Besides, the mechanical test was employed to test the stiffness of the gels (compression modulus). There were no significant differences in the Young's moduli between the hydrogel systems when tested immediately after UV crosslinking (58.9 kPa ± 2.8 and 53.3 kPa ± 1.0 for the hydrogels prepared using the 0% ink and 3.5% ink respectively). However, there was a marked difference on the hydrogels that had been overnight in PBS at 37ºC (the 0% gels had 45.0 kPa ± 2.6 of Young's modulus and 3.5% gels had 28.4 kPa ± 1.5). Gels were porous after the free polymer content had dissolved overnight, making them mechanically weaker. These results are consistent with the free polymer content study, and suggested that the hydrogels prepared using the 3.5% ink results in a less densely packed polymer network. Given that the difference in the free polymer content between the two hydrogels was 13.7%, much higher than the gelatin concentration in the 3.5% ink, the presence of gelatin may have some steric effect limiting the efficiency of the UV crosslinking and resulting in a more porous structure. The Young's modulus depends on many different factors: the type of material, the degree of methacrylation of the GelMA, the source of GelMA, the alginate viscosity and the alginate molecular weight, etc (103,126).

Finally, the hydrogel degradation studies showed that the discs degraded fast, being completely degraded by day 5. The first two days 3.5% hydrogels degraded faster, probably due to its more porous structure. Previous authors described 70% DoF GelMA hydrogel degradations with collagenase of 70% in 28 days (127). Other authors assessed 10%/1% GelMA/alginate degradation, obtaining a 6% degradation in 100 hours (4 days) (128). In that case, however, alginate lyase was used instead of collagenase. Anyway, getting the gels completely degraded in 5 days was not desirable, as they were expected to last in the implanted site for a minimum of a month. The experiment was repeated twice with the same outcome. The reason why such fast degradations were

obtained is unknown. Further validation experiments and optimisation of the ink systems may be required in the future.

6.2 Microspheres

GelMA microspheres were generated by a water-in-oil emulsion method, with post-crosslinking using APS and TEMED. Their diameter was analysed and plotted in a histogram (Figure 14). The spheres were 12-40 μm in diameter, with the average in 25 μm. These results were compared to GelMA microspheres from other authors (114). Their results showed much smaller microspheres. For 15% DoF GelMA, 60% of the spheres were below 5 μm in diameter and 40% between 5 and 15 μm. For 50% DoF GelMA, 65% of the spheres were below 5 μm in diameter and 35% between 5 and 15 μm. For 90% DoF GelMA, 80% of the spheres were below 5 μm in diameter and 20% between 5 and 15 μm. This showed a pattern where the higher the degree of functionalisation, the smaller the spheres. The GelMA on this islet project was 82% DoF, however, the spheres were on average 5 times bigger. This might be due to the method for MP generation (1500 rpm for homogenisation vs 5000 rpm used in this project, application of N_2) and crosslinking (glutaraldehyde) used, or the GelMA concentration used (10% vs the 15% used in this project). In our case, glutaraldehyde was discarded due to its cytotoxicity even in the smallest concentrations (129).

The efficiency of the process of generation of microspheres was remarkable. The total yield was 82%, meaning that only 18% of the total GelMA used was lost during the whole process of homogenisation to washing, drying and crosslinking. The crosslinking efficiency was determined to be 96%, therefore, only 4% were uncrosslinked. The post-loading mode of growth factor to the microspheres was also a key factor for minimising the loss of IL-2. By using the post-loading technique, only the required amount of IL-2 was added to the appropriate amount of microspheres for each experiment, which contributed positively to the efficiency and cost reduction of the process.

The degradability of the spheres (Figure 15) was low compared to other GelMA spheres reported in the literature that degraded completely after 2 days (15% DoF) or 5 days (50% and 90% DoF) in 2 mg/ml collagenase solution (114). In the current system, around 50% of our GelMA spheres were remaining after 30 days, despite the fact that a lower concentration of collagenase (2 U/ml, corresponding to 20 μg/ml) was used. This concentration was employed because it was reported that the degradation activity in the human body would be equivalent to 2 U/ml collagenase (130). The slow degradation profile might reflect a highly crosslinked structure of the GelMA microspheres, which may have resulted in a retarded released profile of IL-2 (131). Further experiments are required to test the effect of IL-2 release on the on the biological functions of Tregs.

Another important factor about the microspheres was to prove that their addition did not alter the ink characteristics significantly regarding printability. For this reason, rheology was employed to compare the ink viscosity with or without microspheres (Figure 25). The results were very similar with 0, 5 or 10 mg/ml MPs, proving that such loadings of microspheres did not alter the ink behaviour. Finally, the microsphere distribution in the ink was an important factor. If the spheres

sedimented at the bottom of the syringe before printing, the ink would become heterogeneous, and the growth factor concentration would be non-uniform. The prints would no longer be reproducible. In order to prove the homogeneous distribution, the microspheres were counted from different regions of the syringe; top, middle, bottom (Figure 32). The count was similar in the three regions, with no significant differences, indicating that the microspheres at 5 or 10 mg/ml can be uniformly distributed in the ink.

6.3 Release

The release profile from the GelMA microspheres was studied in three different conditions: MPs suspended in the release medium (free), MPs encapsulated in hydrogel discs (casted) and MPs encapsulated and co-axially printed in the shell of the structure (printed). The release was very similar in the three cases: initial burst release and plateau phase in the first 3-5 days. Initially it was expected that the casted and printed gels would have a more sustained release over time when compared to the free microspheres. However, the fast degradability of the hydrogels, which after 2-4 days of release were completely degraded, seemed to be the reason why there was no difference. The three conditions showed a low total release (10-12% of the loaded IL-2 was only released). This could have happened due to the low degradability of the microspheres, and the strong interaction between the spheres and the IL-2. Other authors reported 70% of IL-2 release by day 21 from dextran/PLGA-PLA microspheres (132). Anyway, the presence of growth factors has been shown to be positive for recruiting cells (133), so having the IL-2 trapped in the GelMA microspheres may have a positive effect in keeping the Tregs next to the islets and microspheres. To test this, future experiments are required.

Chapter 7

7. Future work and directions

First, some experiments should be repeated. Both hydrogel discs and printed scaffolds, included those prepared using the gelatin-free ink, degraded within days (4-5 days). The gel degradation, mechanical test and sol-gel experiments should be repeated using other GelMA, alginate and gelatin batches (in case the ones used were contaminated), or even new LAP could be used.

Once the previous problem is solved, the release experiments should be repeated to observe any possible differences between free and entrapped MPs. In vitro experiments will be critical and essential to examine the effects of IL-2 release on the biological behaviour of Tregs. This information will be utilised to further improve the release profile of IL-2.

After obtaining stable hydrogels, the scaffolds could be tested with cells. The viability and functions of Tregs should be assessed in vitro, with and without microspheres, to assess if the IL-2 released from the MPs have positive effects on their viability and function. Where feasible, future experiments will involve co-axial printing of 3D structures where islets are located in the cores and Tregs in the shells. The islet viability and functions would then be assessed. Finally, the work done by Narangerel, a master student focused on the core and the vascularisation of the structure, could be combined with this one. In this way, the core would consist of the ink developed by her, islets, EPCs and VEGF (growth factors for endothelial cells) in PLGA microspheres. The shell would consist of the ink developed in this work, Tregs and IL-2 in GelMA microspheres.

To finalise, the 3D printed constructs with the different core and shell, islets, endothelial cells and Tregs would be subjected to animal studies. They would be implanted subcutaneously in mice and the evolution of the mice and constructs would be monitored.

Chapter 8

8. Conclusions

To sum up, the protocol to generate GelMA microspheres was established and optimised. Strongly crosslinked microparticles were achieved, with a high yield and crosslinking efficiency. Their size ranged from 12 to 40 µm (average of 25 µm), suitable to be loaded with IL-2 and incorporated in the bioink. Furthermore, the bioink for the shell structure was optimised and characterised. Gelatin was added to the previously characterised ink containing 2% alginate and 7.5% GelMA. The gelatin concentration was narrowed down to 3.5%, and the characterisation determined similar properties compared to the ink without gelatin. The microspheres were also incorporated to the ink and 1 cm x 1 cm scaffolds were printed with high shape fidelity. Unfortunately, the scaffolds degraded in a short period of time, which is a problem that will have to be solved in the future. Finally, the release of IL-2 entrapped in the GelMA microspheres was monitored, showing an initial burst release but a plateau phase after the second day (with a 10% of total release).

In conclusion, a bioink consisting of alginate, GelMA and gelatin was developed, printable by co-axial extrusion printing at room temperature. GelMA micropsheres, generated by water-in-oil emulsion, were also incorporated to the bioink. The spheres with IL-2 entrapped provided a release which would recruit Tregs. The final goal of these experiments would be to print islets in the core, with Tregs in the ink we developed (and the microspheres) in the shell. Tregs could be determinant on the success in implanting these constructs without immune response, and in providing a solution for type 1 diabetes.

Bibliography or List of References

1. Ravnic DJ, Leberfinger AN, Ozbolat IT. Bioprinting and Cellular Therapies for Type 1 Diabetes. Trends Biotechnol. 2017;35(11):1025–34.
2. Of D, Mellitus D. Diagnosis and classification of diabetes mellitus. Diabetes Care. 2014;37(SUPPL.1):81–90.
3. Kim J, Kang K, Drogemuller CJ, Wallace GG, Coates PT. Bioprinting an Artificial Pancreas for Type 1 Diabetes. Curr Diab Rep. 2019;19(8).
4. Magliano DJ, Islam RM, Barr ELM, Gregg EW, Pavkov ME, Harding JL, et al. Trends in incidence of total or type 2 diabetes: Systematic review. BMJ. 2019;366:1–12.
5. Maahs DM, West NA, Lawrence JM, Mayer-Davis EJ. Epidemiology of type 1 diabetes. Endocrinol Metab Clin North Am. 2010;39(3):481–97.
6. Ojo O. Dietary intake and type 2 diabetes. Nutrients. 2019;11(9).
7. Journey 2 Health. Beating type 2 diabetes [Internet]. [cited 2019 Apr 5]. Available from: https://journey2health.com/articles/beating-type-2-diabetes-EbjpTE
8. Dolenšek J, Rupnik MS, Stožer A. Structural similarities and differences between the human and the mouse pancreas. Islets. 2015;7(1):2–9.
9. Javed S, Alam U, Malik RA. Burning through the pain: Treatments for diabetic neuropathy. Diabetes, Obes Metab. 2015;17(12):1115–25.
10. Kumar SA, Delgado M, Mendez VE, Joddar B. Applications of stem cells and bioprinting for potential treatment of diabetes. World J Stem Cells. 2019;11(1):13–32.
11. Olokoba AB, Obateru OA, Olokoba LB. Type 2 diabetes mellitus: A review of current trends. Oman Med J. 2012;27(4):269–73.
12. Liese AD. The burden of diabetes mellitus among US youth: Prevalence estimates from the SEARCH for Diabetes in Youth Study: SEARCH for Diabetes in Youth Study Group. Pediatrics. 2006;118(4):1510–8.
13. Bluestone JA, Herold K, Eisenbarth G. Genetics, pathogenesis and clinical interventions in type 1 diabetes. Nature. 2010;464(7293):1293–300.
14. Donath MY, Dinarello CA, Mandrup-Poulsen T. Targeting innate immune mediators in type 1 and type 2 diabetes. Nat Rev Immunol [Internet]. 2019;19(12):734–46. Available from: http://dx.doi.org/10.1038/s41577-019-0213-9
15. Didericksen KW, Das BM. Type 2 diabetes as a familial illness: Findings from a focus group study. Fam Syst Health. 2019;37(3):235–43.
16. Bai C, Gao Y, Li X, Wang K, Xiong H, Shan Z, et al. MicroRNAs can effectively induce formation of insulin-producing cells from mesenchymal stem cells. J Tissue Eng Regen

Med. 2017;11(12):3457–68.

17. Acharjee S, Ghosh B, Al-Dhubiab BE, Nair AB. Understanding type 1 diabetes: Etiology and models. Can J Diabetes [Internet]. 2013;37(4):269–76. Available from: http://dx.doi.org/10.1016/j.jcjd.2013.05.001

18. Dávila LA, Bermúdez V, Aparicio D, Céspedes V, Escobar MC, Durán-Agüero S, et al. Effect of oral nutritional supplements with sucromalt and isomaltulose versus standard formula on glycaemic index, entero-insular axis peptides and subjective appetite in patients with type 2 diabetes: A randomised cross-over study. Nutrients. 2019;11(7).

19. Billings LK, Florez JC. The genetics of type 2 diabetes: What have we learned from GWAS? Ann N Y Acad Sci. 2010;1212:59–77.

20. Rosen ED, Kaestner KH, Natarajan R, Patti ME, Sallari R, Sander M, et al. Epigenetics and epigenomics: Implications for diabetes and obesity. Diabetes. 2018;67(10):1923–31.

21. Ojo O, Weldon SM, Thompson T, Crockett R, Wang XH. The effect of diabetes-specific enteral nutrition formula on cardiometabolic parameters in patients with type 2 diabetes: A systematic review and meta–analysis of randomised controlled trials. Nutrients. 2019;11(8).

22. Dunlay SM, Givertz MM, Aguilar D, Allen LA, Chan M, Desai AS, et al. Type 2 Diabetes Mellitus and Heart Failure, A Scientific Statement From the American Heart Association and Heart Failure Society of America. J Card Fail. 2019;25(8):584–619.

23. Sarwar N, Gao P, Kondapally Seshasai SR, Gobin R, Kaptoge S, Di Angelantonio E, et al. Diabetes mellitus, fasting blood glucose concentration, and risk of vascular disease: A collaborative meta-analysis of 102 prospective studies. Lancet [Internet]. 2010;375(9733):2215–22. Available from: http://dx.doi.org/10.1016/S0140-6736(10)60484-9

24. Thomas MC, Cooper ME, Zimmet P. Changing epidemiology of type 2 diabetes mellitus and associated chronic kidney disease. Nat Rev Nephrol. 2016;12(2):73–81.

25. Richter L, Freisinger E, Lüders F, Gebauer K, Meyborg M, Malyar NM. Impact of diabetes type on treatment and outcome of patients with peripheral artery disease. Diabetes Vasc Dis Res. 2018;15(6):504–10.

26. M.J. F. Microvascular and macrovascular complications of diabetes. Clin Diabetes [Internet]. 2008;26(3):116–22. Available from: http://clinical.diabetesjournals.org/content/29/3/116.full.pdf+html%5Cnhttp://ovidsp.ovid.com/ovidweb.cgi?T=JS&PAGE=reference&D=emed10&NEWS=N&AN=2011441759

27. Atkinson MA, Eisenbarth GS, Michels AW. Type 1 diabetes. Lancet [Internet]. 2014;383(9911):69–82. Available from: http://dx.doi.org/10.1016/S0140-6736(13)60591-7

28. Zhou Q, Melton DA. Pancreas regeneration. Nature. 2018;557(7705):351–8.

29. Herold KC, Vignali DAA, Cooke A, Bluestone JA. Type I diabetes: Translating mechanistic observations into effective clinical outcomes. Nat Rev Immunol. 2013;13(4):243–56.

30. Rahier J, Guiot Y, Goebbels RM, Sempoux C, Henquin JC. Pancreatic beta-cell mass in European subjects with type 2 diabetes. Diabetes, Obes Metab. 2008;10(4):32–42.

31. Butler AE, Janson J, Bonner-Weir S, Ritzel R, Rizza RA, Butler PC. Beta-cell deficit and increased beta-cell apoptosis in humans with type 2 diabetes. Diabetes. 2003;52:102–10.

32. Cryer PE. The barrier of hypoglycemia in diabetes. Diabetes. 2008;57(12):3169–76.

33. Bellin MD, Barton FB, Heitman A, Alejandro R, Hering BJ. Potent induction immunotherapy promotes long-term insulin independence after islet transplanttion in type 1 diabetes. Am J Transpl. 2012;12(6):1576–83.

34. Dall T, Mann S, Zhang Y, Quick W, Seifert R, Martin J, et al. Distinguishing the economic costs associated with type 1 and type 2 diabetes. Popul Health Manag. 2009;12(2):103–10.

35. Troppmann C. Complications after pancreas transplantation. Curr Opin Organ Transplant. 2010;15(1):112–8.

36. Duin S, Schütz K, Ahlfeld T, Lehmann S, Lode A, Ludwig B, et al. 3D Bioprinting of Functional Islets of Langerhans in an Alginate/Methylcellulose Hydrogel Blend. Adv Healthc Mater. 2019;1801631:1–14.

37. Liu X, Carter SSD, Renes MJ, Kim J, Rojas-Canales DM, Penko D, et al. Development of a Coaxial 3D Printing Platform for Biofabrication of Implantable Islet-Containing Constructs. Adv Healthc Mater. 2019;1801181:1–12.

38. O'Connell PJ, Holmes-Walker DJ, Goodman D, Hawthorne WJ, Loudovaris T, Gunton JE, et al. Multicenter Australian trial of islet transplantation: Improving accessibility and outcomes. Am J Transplant. 2013;13(7):1850–8.

39. Groll J, Boland T, Blunk T, Burdick JA, Cho D-W, Dalton PD, et al. Biofabrication: reappraising the definition of an evolving field. Biofabrication [Internet]. 2016;8(1):013001. Available from: http://www.ncbi.nlm.nih.gov/pubmed/26744832

40. Mironov V, Reis N, Derby B. Bioprinting : A Beginning. Tissue Eng. 2006;12(4):631–4.

41. Wang Z, Tian Z, Menard F, Kim K. Comparative study of gelatin methacrylate hydrogels from different sources for biofabrication applications. Biofabrication. 2017;9(4).

42. Mandrycky C, Wang Z, Kim K, Kim D. 3D Bioprinting for Engineering Complex Tissues. Biotechnol Adv [Internet]. 2016;34(4):422–34. Available from: https://www.ncbi.nlm.nih.gov/pmc/articles/PMC4879088/pdf/nihms748887.pdf

43. Morimoto Y, Hsiao AY, Takeuchi S. Point-, line-, and plane-shaped cellular constructs for 3D tissue assembly. Adv Drug Deliv Rev [Internet]. 2015;95:29–39. Available from: http://dx.doi.org/10.1016/j.addr.2015.09.003

44. Merck. 3D Bioprinting: Bioink selection guide [Internet]. [cited 2020 Jan 30]. Available from: https://www.sigmaaldrich.com/technical-documents/articles/materials-science/3d-bioprinting-bioinks.html

45. Park JY, Shim JH, Choi SA, Jang J, Kim M, Lee SH, et al. 3D printing technology to control BMP-2 and VEGF delivery spatially and temporally to promote large-volume bone regeneration. J Mater Chem B. 2015;3(27):5415–25.

46. Park JH, Jang J, Lee JS, Cho DW. Three-Dimensional Printing of Tissue/Organ Analogues Containing Living Cells. Ann Biomed Eng. 2017;45(1):180–94.

47. Skardal A, Atala A. Biomaterials for Integration with 3-D Bioprinting. Ann Biomed Eng. 2015;43(3):730–46.

48. Zhu W, Ma X, Gou M, Mei D, Zhang K, Chen S. 3D printing of functional biomaterials for tissue engineering. Curr Opin Biotechnol [Internet]. 2016;40:103–12. Available from: http://dx.doi.org/10.1016/j.copbio.2016.03.014

49. Moroni L, Boland T, Burdick JA, De Maria C, Derby B, Forgacs G, et al. Biofabrication: A Guide to Technology and Terminology. Trends Biotechnol. 2018;36(4):384–402.

50. Do AV, Khorsand B, Geary SM, Salem AK. 3D Printing of Scaffolds for Tissue Regeneration Applications. Adv Healthc Mater. 2015;4(12):1742–62.

51. Cui H, Nowicki M, Fisher JP, Zhang LG. 3D Bioprinting for Organ Regeneration. Adv Healthc Mater. 2017;6(1):1–54.

52. Gu BK, Choi DJ, Park SJ, Kim MS, Kang CM, Kim CH. 3-Dimensional Bioprinting for Tissue Engineering Applications. Biomater Res [Internet]. 2016;20(1):1–8. Available from: http://dx.doi.org/10.1186/s40824-016-0058-2

53. Skoog SA, Goering PL, Narayan RJ. Stereolithography in tissue engineering. J Mater Sci Mater Med. 2014;25(3):845–56.

54. Ozbolat IT, Hospodiuk M. Current advances and future perspectives in extrusion-based bioprinting. Biomaterials [Internet]. 2016;76:321–43. Available from: http://dx.doi.org/10.1016/j.biomaterials.2015.10.076

55. Murphy S V., Atala A. 3D bioprinting of tissues and organs. Nat Biotechnol. 2014;32(8):773–85.

56. Donderwinkel I, Hest CM Van, Cameron NR. Bio-inks for 3D bioprinting: recent advances and future prospects. Polym Chem. 2017;8:4451–71.

57. Vardanyan M, Parkin E, Gruessner C, Rodriguez Rilo HL. Pancreas vs. islet transplantation: A call on the future. Curr Opin Organ Transplant. 2010;15(1):124–30.

58. Ryan EA, Paty BW, Senior PA, Bigam D, Alfadhli E, Kneteman NM, et al. Five-year follow-up after clinical islet transplantation. Diabetes. 2005;54(7):2060–9.

59. Bennet W, Sundberg B, Groth C, Brendel MD, Brandhorst D, Brandhorst H, et al. Incompatibility Between Human Blood and Isolated Islets of Langerhans. Diabetologia. 1999;48:1907–14.

60. Bennet W, Groth CG, Larsson R, Nilsson B, Korsgren O. Isolated human islets trigger an instant blood mediated inflammatory reaction: Implications for intraportal islet transplantation as a treatment for patients with type 1 diabetes. Ups J Med Sci. 2000;105(2):125–33.

61. Van Der Windt DJ, Bottino R, Casu A, Campanile N, Cooper DKC. Rapid loss of intraportally transplanted islets: An overview of pathophysiology and preventive strategies. Xenotransplantation. 2007;14(4):288–97.

62. Leitao CB, Cure P, Tharavanij T, Baidal DA, Alejandro R. Current Challenges in Islet Transplantation. Curr Diab Rep. 2008;(8):324–31.

63. Agarwal A, Brayman KL. Update on islet cell transplantation for type 1 diabetes. Semin Intervent Radiol. 2012;29(2):90–8.

64. Hyder A, Laue C, Schrezenmeir J. Effect of the immunosuppressive regime of Edmonton protocol on the long-term in vitro insulin secretion from islets of two different species and age categories. Toxicol Vitr. 2005;19(4):541–6.

65. Yasunami Y, Nakafusa Y, Nitta N, Nakamura M, Goto M, Ono J, et al. A Novel Subcutaneous Site of Islet Transplantation Superior to the Liver. Transplantation. 2018;102(6):945–52.

66. Wszola M, Berman A, Gorski L, Ostaszewska A, Serwanska-Swietek M, Krajewska M, et al. Endoscopic Islet Autotransplantation Into Gastric Submucosa—1000-Day Follow-up of Patients. Transplant Proc [Internet]. 2018;50(7):2119–23. Available from: https://doi.org/10.1016/j.transproceed.2018.02.138

67. Calafiore R. Alginate microcapsules for pancreatic islet cell graft immunoprotection: Struggle and progress towards the final cure for type 1 diabetes mellitus. Expert Opin Biol Ther. 2003;3(2):201–5.

68. Klöck G, Frank H, Houben R, Zekorn T, Horcher A, Siebers U, et al. Production of purified alginates suitable for use in immunoisolated transplantation. Appl Microbiol Biotechnol. 1994;40(5):638–43.

69. Draget KI, Taylor C. Chemical, physical and biological properties of alginates and their biomedical implications. Food Hydrocoll [Internet]. 2011;25(2):251–6. Available from: http://dx.doi.org/10.1016/j.foodhyd.2009.10.007

70. Lehmann R, Zuellig RA, Kugelmeier P, Baenninger PB, Moritz W, Perren A, et al.

Superiority of small islets in human islet transplantation. Diabetes. 2007;56(3):594–603.

71. Colton CK. Oxygen supply to encapsulated therapeutic cells. Adv Drug Deliv Rev [Internet]. 2014;67–68:93–110. Available from: http://dx.doi.org/10.1016/j.addr.2014.02.007

72. Liu W, Zhong Z, Hu N, Zhou Y, Maggio L, Miri AK, et al. Coaxial extrusion bioprinting of 3D microfibrous constructs with cell-favorable gelatin methacrylolyl microenvironments. Biofabrication. 2019;10(2).

73. Sakaguchi S, Sakaguchi N, Asano M, Itoh M, Toda M. Immunologic self-tolerance maintained by activated T cells expressing IL-2 receptor alpha-chains (CD25). Breakdown of a single mechanism of self-tolerance causes various autoimmune diseases. J Immunol. 1995;155:1151–64.

74. Sakaguchi S. Naturally arising CD4+ regulatory T cells for immunogenic self-tolerance and negative control of immune responses. Annu Rev Immunol. 2004;22(1):531–62.

75. Krzystyniak A, Gołąb K, Witkowski P, Trzonkowski P. Islet cell transplant and the incorporation of Tregs. Curr Opin Organ Transplant. 2014;19(6):610–5.

76. Tang Q, Bluestone JA. The Foxp3+ regulatory T cell: A jack of all trades, master of regulation. Nat Immunol. 2008;9(3):239–44.

77. Oh S, Rankin AL, Caton AJ. CD4+CD25+ regulatory T cells in autoimmune arthritis. Immunol Rev. 2010;233(1):97–111.

78. Schneider A, Rieck M, Sanda S, Pihoker C, Greenbaum C, Buckner JH. The Effector T Cells of Diabetic Subjects Are Resistant to Regulation via CD4 + FOXP3 + Regulatory T Cells . J Immunol. 2008;181(10):7350–5.

79. Zhang N, Schröppel B, Lal G, Jakubzick C, Mao X, Yin N, et al. Regulatory T cells sequentially migrate from the site of the tissue inflammation to the draining NL to suppress the alloimmune response. Immunity. 2009;30(3):458–69.

80. Vågesjö E, Christoffersson G, Waldén TB, Carlsson PO, Essand M, Korsgren O, et al. Immunological shielding by induced recruitment of regulatory T-Lymphocytes delays rejection of islets transplanted in muscle. Cell Transplant. 2015;24(2):263–76.

81. Abo H, Flannigan KL, Geem D, Ngo VL, Harusato A, Denning TL. Combined IL-2 Immunocomplex and Anti-IL-5 mAb Treatment Expands Foxp3+ Treg Cells in the Absence of Eosinophilia and Ameliorates Experimental Colitis. Front Immunol. 2019;10(March):1–9.

82. Fan MY, Low JS, Tanimine N, Finn KK, Priyadharshini B, Germana SK, et al. Differential roles of IL-2 signaling in developing versus mature Tregs. Cell Rep. 2018;25(5):1204–13.

83. Zhou X, Bailey-Bucktrout SL, Jeker LT, Penaranda C, Martínez-Llordella M, Ashby M, et

al. Instability of the transcription factor Foxp3 leads to the generation of pathogenic memory T cells in vivo. Nat Immunol. 2009;10(9):1000–7.

84. Huang Y, Zhang XF, Gao G, Yonezawa T, Cui X. 3D bioprinting and the current applications in tissue engineering. Biotechnol J. 2017;12(8).

85. Velasco D, Quílez C, Garcia M, del Cañizo JF, Jorcano JL. 3D human skin bioprinting: a view from the bio side. J 3D Print Med. 2018;2(3):141–62.

86. Klak M, Kowalska P, Dobrzanski T, Tymicki G, Cywoniuk P, Gomolka M, et al. Bionic organs: Shear forces reduce pancreatic islet and mammalian cell viability during the process of 3d bioprinting. Micromachines. 2021;12(3).

87. Yue Z, Liu X, Coates PT, Wallace GG. Advances in printing biomaterials and living cells: Implications for islet cell transplantation. Curr Opin Organ Transplant. 2016;21(5):467–75.

88. O'Connell CD, Konate S, Onofrillo C, Kapsa R, Baker C, Duchi S, et al. Free-form co-axial bioprinting of a gelatin methacryloyl bio-ink by direct in situ photo-crosslinking during extrusion. Bioprinting [Internet]. 2020;19(April):e00087. Available from: https://doi.org/10.1016/j.bprint.2020.e00087

89. Cornock R, Beirne S, Thompson B, Wallace GG. Coaxial additive manufacture of biomaterial composite scaffolds for tissue engineering. Biofabrication. 2014;6(2).

90. Gauvin R, Chen Y, Lee JW, Soman P, Zorlutuna P, Nichol JW, et al. Microfabrication of complex porous tissue engineering scaffolds using 3D projection stereolithography. Biomaterials. 2012;33(15):3824–34.

91. Noshadi I, Hong S, Sullivan KE, Sani ES, Portillo-lara R, Tamayol A, et al. In vitro and in vivo analysis of visible light crosslinkable gelatin methacrylolyl (GelMA) hydrogels. Biomater Sci. 2017;5(i):2093–105.

92. Wang Z, Kumar H, Tian Z, Jin X, Holzman JF, Menard F, et al. Visible Light Photoinitiation of Cell Adhesive Gelatin Methacryloyl Hydrogels for Stereolithography 3D Bioprinting. ACS Appl Mater Interfaces. 2018;

93. Fedorovich NE, Oudshoorn MH, van Geemen D, Hennink WE, Alblas J, Dhert WJA. The effect of photopolymerization on stem cells embedded in hydrogels. Biomaterials [Internet]. 2008;30(3):344–53. Available from: http://dx.doi.org/10.1016/j.biomaterials.2008.09.037

94. Gungor-Ozkerim PS, Inci I, Zhang YS, Khademhosseini A, Dokmeci MR. Bioinks for 3D bioprinting: an overview. Biomater Sci. 2018;6(5):915–46.

95. Bishop ES, Mostafa S, Pakvasa M, Luu HH, Lee MJ, Wolf M, et al. 3-D bioprinting technologies in tissue engineering and regenerative medicine: Current and future trends. Genes Dis. 2017;4(4):185–95.

96. Li J, Chen M, Fan X, Zhou H. Recent advances in bioprinting techniques : approaches , applications and future prospects. J Transl Med. 2016;1–15.

97. Panwar A, Tan LP. Current status of bioinks for micro-extrusion-based 3D bioprinting. Molecules. 2016;21(6):665–91.

98. Sorushanova A, Delgado LM, Wu Z, Shologu N, Kshirsagar A, Raghunath R, et al. The Collagen Suprafamily: From Biosynthesis to Advanced Biomaterial Development. Adv Mater. 2019;31(1):1–39.

99. Greene T, Lin CC. Modular Cross-Linking of Gelatin-Based Thiol-Norbornene Hydrogels for in Vitro 3D Culture of Hepatocellular Carcinoma Cells. ACS Biomater Sci Eng. 2015;1(12):1314–23.

100. Muñoz Z, Shih H, Lin C-C. Gelatin hydrogels formed by orthogonal thiol-norbornene photochemistry for cell encapsulation. Biomater Sci. 2014;2(8):1063–72.

101. Yoon HJ, Shin SR, Cha JM, Lee S, Kim J, Do T, et al. Cold Water Fish Gelatin Methacryloyl Hydrogel for Tissue Engineering Application. PLoS One. 2016;11(10):1–18.

102. Lin C-C, Ki CS, Shih H. Thiol-norbornene photo-click hydrogels for tissue engineering applications. J Appl Polym Sci. 2015;132(8).

103. Chen Y, Lin R, Qi H, Yang Y, Bae H, Melero-Martin JM, et al. Functional human vascular network generated in photocrosslinkable gelatin methacrylate hydrogels. Adv Funct Mater. 2012;22(10):2027–39.

104. Yue K, Santiago GT, Alvarez MM, Tamayol A, Annabi N, Khademhosseini A, et al. Synthesis, properties, and biomedical applications of gelatin methacrylolyl (GelMA) hydrogels. Biomaterials. 2015;73:254–71.

105. Monteiro N, Thrivikraman G, Athirasala A, Tahayeri A, Franca CM, Ferracane JL, et al. Photopolymerization of cell-laden methacrylolyl hydrogels using a dental curing light for regenerative dentistry. Dent Mater. 2018;34(3):389–99.

106. Fairbanks BD, Schwartz MP, Bowman CN, Anseth KS. Photoinitiated polymerization of PEG-diacrylate with lithium phenyl-2,4,6-trimethylbenzoylphosphinate: polymerization rate and cytocompatibility. Biomaterials [Internet]. 2009;30(35):6702–7. Available from: http://dx.doi.org/10.1016/j.biomaterials.2009.08.055

107. Lee KY, Mooney DJ. Alginate: Properties and biomedical applications. Prog Polym Sci [Internet]. 2012;37(1):106–26. Available from: http://dx.doi.org/10.1016/j.progpolymsci.2011.06.003

108. Smidsrod O, Skjak-Braek G. Alginate as immobilization matrix for cells. Trends Biotechnol. 1990;8:71–8.

109. Otterlei M, Østgaard K, Skjåk-Bræk G, Smidsr∅d O, Soon-Shiong P, Espevik T.

Induction of Cytokine Production from Human Monocytes Stimulated with Alginate. Vol. 10, Journal of Immunotherapy. 1991. p. 286–91.

110. Hiller T, Berg J, Elomaa L, Röhrs V, Ullah I, Schaar K, et al. Generation of a 3D Liver Model Comprising Human Extracellular Matrix in an Alginate/Gelatin-Based Bioink by Extrusion Bioprinting for Infection and Transduction Studies. Int J Mol Sci. 2018;19(3129):1–17.

111. Masaeli R, Jafarzadeh TS, Dinarvand R, Tahriri M, Rakhshan V, Ehfandyari-Manesh M. Preparation, characterization and evaluation of drug release properties of Simvastatin-loaded PLGA microspheres. Iran J Pharm Res. 2016;15(November 2015):205–11.

112. Nath SD, Son S, Sadiasa A, Min YK, Lee BT. Preparation and characterization of PLGA microspheres by the electrospraying method for delivering simvastatin for bone regeneration. Int J Pharm [Internet]. 2013;443(1–2):87–94. Available from: http://dx.doi.org/10.1016/j.ijpharm.2012.12.037

113. Matsumine H, Sasaki R, Tabata Y, Matsui M, Yamato M, Okano T, et al. Facial nerve regeneration using basic fibroblast growth factor-impregnated gelatin microspheres in a rat model. J Tissue Eng Regen Med. 2016;10:559–67.

114. Nguyen AH, McKinney J, Miller T, Bongiorno T, McDevitt TC. Gelatin methacrylate microspheres for growth factor controlled release. Acta Biomater. 2015;13:101–10.

115. Büyüköz M, Erdal E, Alsoy Altinkaya S. Nanofibrous gelatine scaffolds integrated with nerve growth factor-loaded alginate microspheres for brain tissue engineering. J Tissue Eng Regen Med. 2018;12(2):707–19.

116. Mathieu M, Vigier S, Labour MN, Jorgensen C, Belamie E, Noël D. Induction of mesenchymal stem cell differentiation and cartilage formation by cross-linker-free collagen microspheres. Eur Cells Mater. 2014;28:82–97.

117. Hoch E, Schuh C, Hirth T, Tovar GEM, Borchers K. Stiff gelatin hydrogels can be photo-chemically synthesized from low viscous gelatin solutions using molecularly functionalized gelatin with a high degree of methacrylation. J Mater Sci Mater Med. 2012;23(11):2607–17.

118. Panouillé M, Larreta-Garde V. Gelation behaviour of gelatin and alginate mixtures. Food Hydrocoll [Internet]. 2009;23(4):1074–80. Available from: http://dx.doi.org/10.1016/j.foodhyd.2008.06.011

119. Tian K, Bae J, Bakarich SE, Yang C, Gately RD, Spinks GM, et al. 3D Printing of Transparent and Conductive Heterogeneous Hydrogel–Elastomer Systems. Adv Mater. 2017;29(10).

120. Ribeiro A, Blokzijl MM, Levato R, Visser CW, Castilho M, Hennink WE, et al. Assessing bioink shape fidelity to aid material development in 3D bioprinting. Biofabrication. 2018;10(1).

121. Janmey PA, Georges PC, Hvidt S. Basic Rheology for Biologists. Methods Cell Biol. 2007;83.

122. Doran P. Bioprocess engineering principles: second edition. 2012;1–919.

123. von Lospichl B, Hemmati-Sadeghi S, Dey P, Dehne T, Haag R, Sittinger M, et al. Injectable hydrogels for treatment of osteoarthritis – A rheological study. Colloids Surfaces B Biointerfaces [Internet]. 2017;159:477–83. Available from: https://doi.org/10.1016/j.colsurfb.2017.07.073

124. Ozbolat V, Dey M, Ayan B, Ozbolat IT. Extrusion-based printing of sacrificial Carbopol ink for fabrication of microfluidic devices. Biofabrication. 2019;11(3).

125. Joas S, Tovar G, Celik O, Bonten C, Southan A. Extrusion-Based 3D Printing of Poly(ethylene glycol) Diacrylate Hydrogels Containing Positively and Negatively Charged Groups. Gels. 2018;4(3):69.

126. Li X, Chen S, Li J, Wang X, Zhang J, Kawazoe N, et al. 3D Culture of Chondrocytes in Gelatin Hydrogels with Different Stiffness. Polymers (Basel). 2016;8:269–84.

127. Zhao X, Sun X, Yildirimer L, Lang Q, Zhang Y, Cui W, et al. Cell infiltrative hydrogel fibrous scaffolds for accelerated wound healing. Acta Biomater. 2017;49:66–77.

128. Liu X, Zuo Y, Sun J, Guo Z, Fan H, Zhang X. Degradation regulated bioactive hydrogel as the bioink with desirable moldability for microfluidic biofabrication. Carbohydr Polym [Internet]. 2017;178(September):8–17. Available from: http://dx.doi.org/10.1016/j.carbpol.2017.09.014

129. Zeiger E, Gollapudi B, Spencer P. Genetic toxicity and carcinogenicity studies of glutaraldehyde - A review. Mutat Res - Rev Mutat Res. 2005;589(2):136–51.

130. Rizwan M, Peh GSL, Ang HP, Lwin NC, Adnan K, Mehta JS, et al. Sequentially-crosslinked bioactive hydrogels as nano-patterned substrates with customizable stiffness and degradation for corneal tissue engineering applications. Biomaterials [Internet]. 2017;120:139–54. Available from: http://dx.doi.org/10.1016/j.biomaterials.2016.12.026

131. Hirai T, Ramos TL, Lin PY, Simonetta F, Su LL, Picton LK, et al. Selective expansion of regulatory T cells using an orthogonal IL-2/IL-2 receptor system facilitates transplantation tolerance. J Clin Invest. 2021;131(8):1–14.

132. Zhao H, Wu F, Cai Y, Chen Y, Wei L, Liu Z, et al. Local antitumor effects of intratumoral delivery of rlL-2 loaded sustained-release dextran/PLGA-PLA core/shell microspheres. Int J Pharm [Internet]. 2013;450(1–2):235–40. Available from: http://dx.doi.org/10.1016/j.ijpharm.2013.04.051

133. Ratay ML, Glowacki AJ, Balmert SC, Acharya AP, Polat J, Andrews LP, et al. Treg-recruiting microspheres prevent inflammation in a murine model of dry eye disease. J Control Release [Internet]. 2017;258(September 2016):208–17. Available from:

http://dx.doi.org/10.1016/j.jconrel.2017.05.007

Appendices

Appendix 1. Bioresin development for 3D Lithography

1. Bioresin development for 3D lithography

Universiteit Utrecht

UMC Utrecht

Minor research project

Bioresin development for 3D lithography

Ane Urigoitia Asua

Examiner: Riccardo Levato

Second reviewer: Massimilliano Caiazzo

Utrecht, August 2018

Biofabrication Master programme, 2017-2018

Abstract

Bioprinting has arisen in the past years as a promising technology in tissue engineering. 3D printers are capable of manufacturing complex shapes mimicking tissues with high fidelity. However, 3D printing is not yet capable of solving one of the biggest problems in tissue engineering: the lack of vascularisation. Without blood vessels and capillaries, thick constructs become necrotic in their inner part, making their long-term culture inviable. 3D lithography is currently the bioprinting method with the highest accuracy available, printing layers of 20 µm. Therefore, digital light processing (DLP) printing (a light-based 3D lithography method) can be used to print a biocompatible material with perfusable channels that mimic vascularisation. Nevertheless, there are not many available biomaterials printable with DLP.

In this project, a new bioink formulation was developed for DLP printing, which supported cell viability, growth and differentiation into bone, endothelial cell attachment and monolayer formation for the creation of blood vessels, and with adequate mechanical properties. Two photocrosslinkable hydrogels were tested for the 3D printing and generating vascularised bone constructs: fish gelatin-methacrylate (f-GelMA) and fish gelatin-norbornene (f-gelNB). Besides, two different photoinitiators were used to induce the crosslinking: ruthenium and sodium persulfate (ru/SPS), a new promising visible-light initiator, and lithium phenyl-2,4,6-trimethylbenzoylphosphinate (LAP), a UV-light photoinitiator. All the hydrogels were first characterised regarding their crosslinking efficiency, mechanical properties, cell viability, proliferation and printability. Afterwards, the best ink formulation was chosen and printed with mesenchymal stem cells (MSCs) to check if osteogenesis and chondrogenesis were possible. Finally, the attachment of endothelial colony forming cells (ECFCs) to the surface of hydrogels and their capacity of forming monolayers was tested. Overall, f-GelMA 10% ru/SPS hydrogels were selected as the best condition for bioprinting and developing bone and cartilage, but ECFCs could not attach to their surface.

Laymen's summary

3D printing applied to biology, also known as bioprinting, has arisen in the past years as a promising technology in tissue engineering. Tissue engineering is the science that studies the combination of cells, materials and biological factors to replace tissues. 3D printers are capable of manufacturing complex shapes mimicking tissues with high fidelity, which is important for the correct function of these tissue models. However, 3D printing is not yet capable of solving one of the biggest problems in tissue engineering: the lack of vascularisation (generation of blood vessels and capillaries). Without it, thick constructs cannot obtain oxygen and nutrients in their inner part, and cells in this part die. 3D printers are able to print channels that mimic these blood vessels, but an extremely high resolution is required for this purpose, as some blood vessels are only a few µm thick. 3D lithography (or digital light processing (DLP)) is currently the bioprinting method with the highest accuracy available. These printers use a liquid resin, which reacts with light (either visible or UV light). When light hits a specific area of the resin, a thin layer of it reacts becoming solid, and complex 3D objects, designed digitally, are printed layer by layer with high resolution. Therefore, this technology can be used to print a biocompatible material (a material compatible with cells and not harmful to living tissues) with channels that mimic vascularisation. Nevertheless, there are not many available biomaterials that can be printed with the DLP printer.

In this project, a new bioink (biocompatible printable resin) formulation was developed for DLP printing, which supported cell living, growth and development of bone. Endothelial cells also needed to attach and form a monolayer. Endothelial cells are found on the walls of blood vessels, so if they are added to the inside of the printed channels, they need to cover the whole surface of the channel (what means generating a monolayer) to develop blood vessels. Two hydrogels were tested to check if they were adequate for 3D printing and generating bone constructs with blood vessels: fish gelatin-methacrylate (f-GelMA) and fish gelatin-norbornene (f-gelNB). Both are modified from fish skin gelatin and react and solidify in presence of light. Besides, these hydrogels need a molecule, called photoinitiator, which reacts and solidifies the hydrogels in presence of a given type of light (visible or UV). Two different photoinitiators were used to induce the gelation: ruthenium and sodium persulfate (ru/SPS), a new promising visible-light initiator, and lithium phenyl-2,4,6-trimethylbenzoylphosphinate (LAP), a UV-light photoinitiator. All gels were first characterised regarding their hydrogel properties, cell compatibility and capacity for DLP printing. Afterwards, the best bioink formulation was chosen and printed with mesenchymal stem cells (MSCs) to check if cartilage and bone could be developed. MSCs are pluripotent cells, which means that they can develop into many different cell types, including osteocytes (bone cells) or chondrocytes (cartilage cells). Finally, the attachment of endothelial colony forming cells (ECFCs, which are a type of endothelial cells) to the surface of hydrogels and their capacity of forming monolayers was tested. Overall, f-GelMA 10% ru/SPS hydrogels were selected as the best condition for bioprinting, but ECFCs could not attach to their surface.

Table of contents

List of Abbreviations

ALP: alkaline phosphate

AM: additive manufacturing

α-MEM: minimum essential medium α

ASAP: ascorbic acid

bFGF: basic fibroblast growth factor

BGP: β-glycerophosphate

CAD: computer-aided design

CS: chondroitin sulphate

DMA: dynamic mechanical analyser

DMD: digital micromirror device

DMEM: Dubeco's modified eagle medium

DMMB: dimethyl methylene blue

DLP: digital light processing

DoF: degree of functionalisation

EC: endothelial cell

ECFC: endothelial colony forming cell

ECM: extracellular matrix

FBS: fetal bovine serum

GAGs: glycosaminoglycans

gelNB: gelatin norbornene

f-gelNB: fish gelNB

p-gelNB: porcine gelNB

GelMA: gelatin methacrylate

f-GelMA: fish GelMA

p-GelMA: porcine GelMA

LAP: lithium phenyl-2,4,6-trimethylbenzoylphosphinate

MPER: mammalian protein extraction reagent

MSC: mesenchymal stem cell

eqMSC: equine mesenchymal stem cell

PBS: phosphate saline buffer

PEG4SH, P4A: polyethylene glycol-tetrathiol

P/S: penicillin/streptomycin

RGD: arginine-lysine-aspartate (arg-lys-asp)

ROS: reactive oxygen species

Ruthenium, Ru: tris (2,2'- bipyridyl) dichlororuthenium (II) hexahydrate

SLA: stereolithography

SPS: sodium persulfate

TFG-β: transforming growth factor β

UV: ultraviolet

List of Figures

List of Tables

1. Introduction

3D bioprinting has arisen in the past recent years as a promising method in various fields, especially in tissue engineering, because of its ability to generate biocompatible systems (1). It consists of the addition of biomaterials in a layer-by-layer fashion, achieving 3D constructs of various sizes, geometries and complexities (2). Using a combination of polymers (that act as scaffolds), living cells and growth factors, these constructs are able to mimic natural tissues *in vitro* (2). 3D bioprinting is currently being applied for various purposes: high throughput screening for drug testing or disease models, organ-on-a-chip models, personalised medicine, transplanting and tissue engineering (2,3). The last one has the biggest repercussion, as it is thought that the creation of artificial organs for transplanting could be possible in the future (4). The use of bioprinting has several advantages over the classical tissue engineering approaches. Until recently, tissues used to be studied *in vitro* in 2D monolayers, where the 3D environment of the natural tissue (cell-cell or cell-ECM interactions), crucial for its correct functioning, was poorly recreated (5,6). Besides, achieving complex shapes and structures with conventional 2D or 3D culturing is difficult, whereas they are easily manufactured with a 3D printer. Therefore, 3D bioprinting allows a better spatial relation of molecules than conventional methods do (1), and customised complex shapes can be generated.

3D bioprinting is one type of the additive manufacturing (AM) technology, used for printing biological or bioactive models (7). AM works as a computer-aided design and fabrication (CAD) technique. First, the desired construct is designed and the bioprinter's software slices it in thin layers. Afterwards, the biomaterials are deposited in the XYZ directions, using the digitally sliced layers as a reference. Finally, the bioprinted construct is cultured *in vitro* for the maturation of the tissue (1,6). There are different 3D bioprinting technologies, such as extrusion, inkjet, laser-induced or stereolithography. The choice of the technique depends on the aim of the printing and the type of tissue (2). Moreover, the materials used for bioprinting, also known as bioinks, must be suitable for the aim and the type of printing. They usually consist of scaffolds made of ceramic, polymeric, metallic, hydrogel or composite materials, and they provide cells with mechanical strength, as well as a niche where cells can attach, migrate and proliferate (7). These scaffolds are also generally porous, as it has been previously proven that they support better cell viabilities than purely solid ones (8). The bioinks need to be biocompatible for both cells and the host, printable, and structurally and mechanically stable in order to guarantee a long-term cell viability (9). Nevertheless, 3D bioprinting still has some drawbacks, being the lack of vascularisation in the bioprinted tissues and the lack of available bioinks the two most relevant ones. Blood vessels participate in the gas and nutrient exchange in tissues, a crucial function for the viability of tissues, but they cannot be bioprinted due to printing speed and resolution issues (1). On the other hand, the use of an optimal material that has an adequate biocompatibility, printability and mechanical strength remains a challenge (1,7). Extensive research is being performed to find a solution to these major problems in the field of biofabrication, testing methods for vascularization in tissues and new bioink formulations.

The vascular system, formed by blood vessels (macrovessels) that branch into small capillaries (microvessels), supplies tissues with oxygen and nutrients (10,11). The diameters of the vessels range from 2,5 cm in the aorta to 20 µm in the thinnest capillaries (12), and the maximum distance between two capillaries is 200 µm, which correlates with the maximum diffusion of oxygen in the body (13,14). The inner part of the blood vessels is coated with the endothelium, a monolayer of endothelial cells that acts as a barrier for controlling nutrient and molecule

exchange between the tissues and blood (11,12). Without vascularisation, nutrients and oxygen are unable to reach the centre of the tissues, which become necrotic (1,15). Hence, there are currently two possible approaches to achieve vascularised engineered tissues. The first one relies on the neoangiogenesis of the tissue, which occurs when the bioprinted construct develops *de novo* vasculature. Angiogenic factors and endothelial cells (ECs) are included in the bioink to obtain this type of vascularisation, the growth factors recruit the cells, encouraging capillary formation, and the ECs self-assemble creating vessels (12,16,17). However, the process is generally slow (18) and the complete vascularisation of the construct cannot be achieved, as blood vessels are generated randomly and they are not always interconnected (12). For this reason, this method is not recommendable for thick constructs (17). The second approach for achieving vascularised tissues relies on artificially generating tubular microchannels that resemble the vascular system, and attaching ECs to their inner walls (12,16,18). This often results in a need to manufacture complex shapes, which is possible using the 3D bioprinting technology (12). Some attempts bioprinting blood vessels have been made before, showing a serious limitation in the printing resolution, as only big vessels (with a minimum diameter of 5 mm) have been successfully printed (1,19). Therefore, both techniques could be combined, employing the bioprinting for generating macrovesselss, and the neoangiogenesis for microvessels (16). Even in this case, a 3D printing technique with the highest resolution possible should be used.

In summary, the most adequate bioprinting technology for the generation of tubular structures that resemble blood vessels is the one with the highest resolution. Table 1 summarises some features of each 3D printing technology, including their maximum resolution.

Table 1. Summary of features, advantages and disadvantages of the main four 3D bioprinting methods: inkjet printing, extrusion-based printing, laser-assisted printing and 3D lithography. Sources: Donderwinkel et al., Li et al. (2,7).

Characteristics	*Inkjet printing*	*Extrusion printing*	*Laser-assisted printing*	*3D lithography*
Cell viability	~ 90%	40-80%	> 95%	> 90%
Cell density	< 10^6 cells/ml	High, no limit	< 10^8 cells/ml	High, no limit
Ink viscosity	3,5-12 mPa/s	Up to $6 \cdot 10^7$ kPa/s	1-300 mPa/s	High, no limit
Cost	Low	Medium	High	Low
Printing speed	High	Low	Medium	High
Resolution	20-100 µm	200 µm	> 20 µm	20-200 µm
Biomaterials	Low viscosity liquids, cells, growth factors, biomolecules	Wide range of biocompatible materials, hydrogels, ceramics, cells, etc	Ceramics, hydrogels, cells, etc	Light-sensitive photocurable polymers
Advantages	Availability, concentration gradients of materials possible	Many materials available, homogeneous cell distribution	High precision, resolution	Highest resolution, increasing number of resins available
Disadvantages	Poor vertical structure, only liquid materials, thermal stress to cells	Low resolution and viability, poor stiffness	High cost and manufacturing time	Lack of biocompatible resins, use restricted to photopolymerisable materials

The table shows that all the methods have their limitations, but focusing on the resolution, inkjet printing, laser-assisted printing and 3D lithography are the most precise technologies. For bioprinting constructs with cells, the technology must also have a high printing speed, high viability and allow printing of high cell densities. The only technology which provides all these features is the 3D lithography.

3D lithography uses the principle of photopolymerization to turn liquid resins into solid (1). It can be laser-based (stereolithography or SLA) or light-based (digital light processing or DLP), being the latter the most biocompatible. Figure 1 shows the scheme of a DLP printer. DLP printers work with a digital micromirror device (DMD) projection system, where light is digitally directed to the micromirrors. These mirrors create a light pattern that is projected in the prepolymer (6,20,21). Thin layers are then polymerised in a layer-by-layer fashion, only where light is projected. Each layer attaches to the building plate, then, this plate automatically moves in the Z direction, and the next layer is projected and photopolymerized (6,22). The process continues until the 3D construct is printed. As in other 3D printing techniques, the CAD design is sliced in layers and each layer is projected on the bioink, matching each CAD layer with each printed layer (8). Finally, the light patterned by the DLP printer can either be visible or UV light (22).

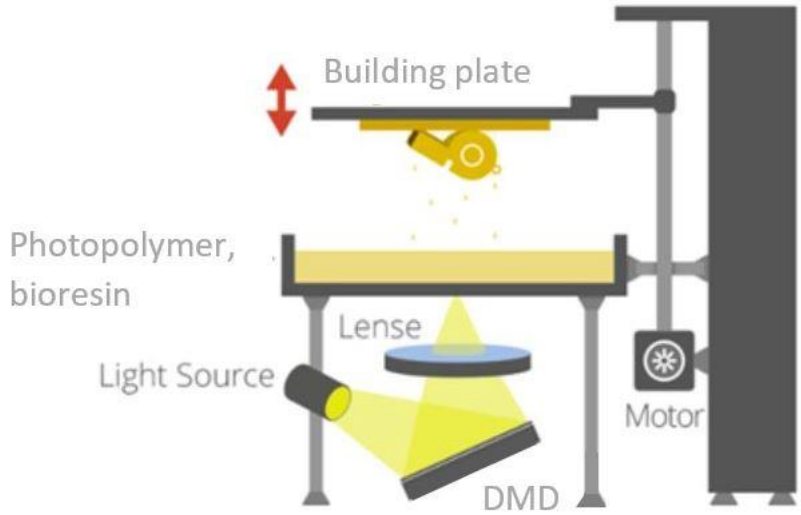

Figure 1. DLP printer's scheme (23), edited. The light comes from below, reaching the DMD where the light pattern is projected towards the bioresin. The bioresin or photopolymer is only crosslinked at the surface of the building plate, only where the light is projected. A motor pulls the building plate a few µm up, to receive another light pattern and obtain a second layer above the first one. The top layers of the constructs are printed last.

An entire layer is printed with a single projection, which results in a fast and reproducible printing process (3,6,20,21). Besides, it is a versatile method, able to print different materials with different mechanical properties, porosities or cells (6). Furthermore, an external force is not applied (as it occurs in extrusion-based printing, where the bioink is pushed through a nozzle), providing the DLP technology with a high cell viability of around 90% (9,21). Finally, DLP is well known for its high resolution, being possible to print 25-50 µm layers (3,7,8,21,22). The high accuracy of this bioprinting method allows to better mimic the complex microenvironment and structure of tissues (22). Therefore, given the high resolution and fast printing of the DLP, it should be possible to print a biomaterial with channels mimicking a vascular network, and then seed endothelial cells inside the channels to obtain vascularised tissues. Unfortunately, there are currently not many photopolymerisable materials that allow cell viability, because most photoinitiators (molecules used to induce the photopolymerisation) employed in DLP are soluble in organic solvents, which are cytotoxic (6,8,22). Therefore, a cytocompatible photopolymerisable bioink needs to be developed for its use in the DLP bioprinting.

Hydrogels are the most widely used bioinks in 3D bioprinting. They are porous hydrophilic polymers that resemble the extracellular matrix of tissues, with high biocompatibility and cytocompatibility (20). They can absorb up to 90-99% of their dry weight in water and their physical and chemical properties are tunable (24–26). They can also be 3D bioprinted to obtain complex shapes and morphologies (1,7,27). Natural polymers (collagen, laminin, gelatin, alginate, hyaluronic acid or fibrin), synthetic ones (polyethylene glycol (PEG) or polyvinyl alcohol (PVA)) or a combination of both can be used to generate hydrogels (24,25,28). Furthermore, some types of hydrogels are photopolymerisable, what is necessary for employing the hydrogel in the DLP printer. They polymerise in presence of light (visible or UV), generating covalent crosslinks that are more stable and stronger than other types of gelations such as thermal ones. Besides, their gelation is controllable, occurs in a short time, and there is no use of extreme temperatures or pH ranges that harm cells (21,29).

Gelatin is a commonly used polymer for hydrogel generation. It is derived from the hydrolysis of collagen and it presents a lower immunogenicity than its precursor (5,30). It is obtained inexpensively from various sources, included pork, calf or fish skin (4). Gelatin contains RGD (arginine-glycine-aspartate) sequences, which support cell attachment and growth (5,30–32). Currently, porcine or mammalian-derived gelatin is generally used, although it is thermally instable and it becomes gel at room temperature (33,34). Porcine gelatin is soluble in water above 40ºC (35). This is especially problematic for bioprinting, where a precise control of the gel viscosity is necessary (15). For example, the bioresin needs to be liquid for the DLP printing, which is not possible if the gelatin is solid at room temperature (and even if it was possible to keep the gel at 40ºC for the printing process, the viability of the encapsulated cells would decrease). As a solution, cold-water fish gelatin, liquid at room temperature (20-25ºC) can be used instead of the porcine one (32,33). Apart from being thermally more stable, it is more economic (32) and it has been proven to have similar physical and chemical properties to those of porcine GelMA, as well as a similar biocompatibility (33). Gelatin hydrogels are formed by thermorreversible crosslinking, as they are soluble in water (at >20-25ºC the fish gelatin) and they form gels when temperature drops (30,34,35). Unfortunately, these gels are mechanically weak and unstable, so they are not suitable for long-term cell culture (5,24). Hence, gelatin needs to be chemically modified to make it more stable and photopolymerisable.

Gelatin methacrylate, GelMA, is a modified gelatin widely employed for biomedical purposes. It is a photocrosslinkable hydrogel at room temperature (27,36), biocompatible, with tunable chemical and mechanical properties and applicable for long-term cell culture (17,33). It has been previously used in bioprinting, included 3D lithography or stereolithography (20,32), and it also shows properties for attaching endothelial cells, what is desired for creating vasculature (10). This polymer is obtained by adding methacrylate groups (methacrylic anhydride) to the amines of gelatin (35–37), in a process shown in Figure 2. The hydrogel is obtained from a mixture of the precursor (GelMA in this case), the photoinitiator and cells or biomolecules if they need to be encapsulated. When light of a given wavelength is directed to the mixture, the photoinitiator absorbs photons and excites or decomposes, initiating the polymerysation (24,31,37). The crosslinking of GelMA, shown in Figure 5A, occurs in a radical-mediated chain-growth reaction, which is fast and leads to the generation of heterogeneous crosslinks (24). However, the radical-mediated reactions present some limitations. First, they are oxygen inhibited, as oxygen reacts with the radicals, quenching them (31). As a consequence, a higher concentration of photoinitiators is required for the reaction, and even in this case, the crosslinking is incomplete (31). Second, due to the oxygen inhibition, the generated crosslinks are insufficient, conditioning the shape fidelity of the designs. This is especially undesirable in bioprinting, as the technology relies on the generation of precise and complex shapes (31). Third, the release of radicals that occurs in the process can affect cells, deriving in cell damage or death (5,30).

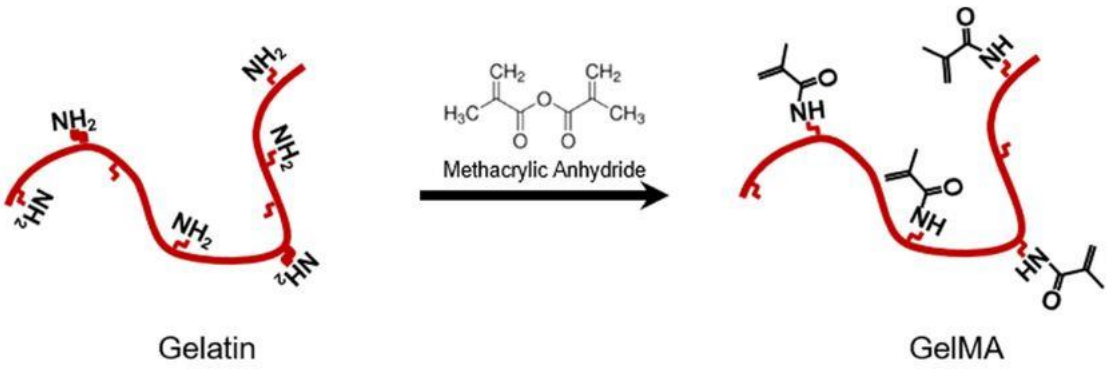

Figure 2. Scheme of the functionalisation of gelatin to GelMA (32). Methacrylate groups are added to the amine groups of gelatin. These methacrylic groups will react with other GelMA polymers to generate hydrogels.

As a solution to the problems that radical-mediated crosslinking presents, some hydrogels photocrosslink in orthogonal photoclick reactions, also called step-growth thiol-ene reactions (5,24,30). Gelatin norbornene, gelNB, is one of the hydrogels that photopolymerises in an orthogonal photoclick reaction (5,24,30). Modified from gelatin, it presents similar physical and chemical features to GelMA, with a higher cytocompatibility and similar ability to immobilise cells and proteins (5,24). This gel is obtained adding carbic anhydride molecules to gelatin (30), as is shown in Figure 3. The polymerisation of gelNB relies on a similar mechanism to that of GelMA, where light excites the photoinitiator and this reacts with the hydrogel, initiating the reaction. But in this case, a crosslinker with thiol groups is also needed to link different gelNB molecules (for example, polyethylene glycol-tetrathiol (PEG-4SH)), and the chemical reactions that occur are different. The photoinitiators react with sulfhydryl groups of the crosslinker, generating radicals that react the norbornene groups (24). In the resulting hydrogel, the gelNB molecules are linked together via the crosslinker (24). A scheme of the crosslinking of gelNB is shown in Figure 5B. This crosslinking method presents some advantages over the chain-growth photopolymerisation of GelMA. First, the generated chains are more organised and homogeneous (38). Second, the reaction is not oxygen inhibited (24,30,39), preserving the shape of the designs, hence, it is a are more suitable polymer for bioprinting. Third, the lack of oxygen inhibition allows the use of lower photoinitiator concentrations, reducing the toxicity (39). This results in a better cytocompatibility (5,24). Finally, the crosslinking of gelNB is extremely fast (30).

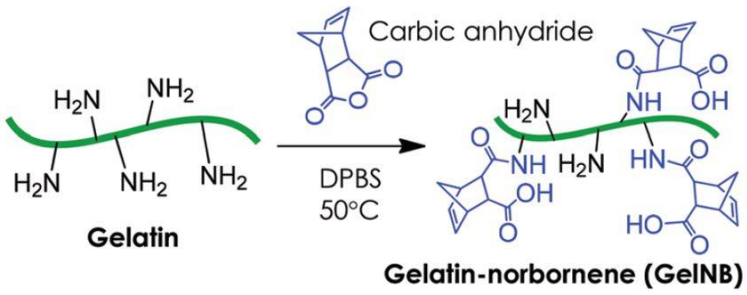

Figure 3. Scheme of the functionalisation of gelatin to gelNB (30). Norbornene groups are added to the amine groups of gelatin. These norbornene groups will react with other thiols used as crosslinkers to generate hydrogels.

Therefore, both GelMA and gelNB can form stable and cytocompatible hydrogels when they are crosslinked in presence of light and a photoinitiator. As mentioned above, the photoinitiators are molecules that, when they

receive light in a specific wavelength, they start the photopolymerisation (26,40). These also need to be biocompatible, cytocompatible and water soluble (26). Currently there are many photoinitiators that have been used with GelMA or gelNB, however, researchers are still searching for the optimal one to achieve stable gels without being toxic or harmful. The most commonly used ones work in the UV light range (250-400 nm wavelengths) (21). For example, Irgacure 2959 is the most widely used photoinitiator, as it is water soluble and there are no adverse effects in cell viability at the concentrations employed for gel crosslinking (40). Another commonly used photoinitiator, lithium phenyl-2,4,6-trimethylbenzoylphosphinate (LAP), also works under UV light exposure. It is more water-soluble and less cytotoxic than Irgacure 2959, and less initiator concentration is needed (40). However, the use of UV light (320-365 nm) for the crosslinking carries some limitations. UV irradiation can generate reactive oxygen species (ROS) that lead to DNA damage and possible cell toxicity (21,25,31). This damage is enhanced in long exposure times, which occurs in bioprinting. Besides, it has been shown that UV light has a low penetration depth, that may cause a poorer crosslinking in large constructs (31). For these reasons, the use of visible light is preferred for the bioprintng with encapsulated cells. LAP can be also used in near-UV visible light (405 nm) (40), but being close to UV wavelengths, it has also been reported as harmful to cells at long exposure times (21).

Using visible light-sensitive photoinitiators is safer (21,25) and it has also been demonstrated that visible light penetrates more than UV light does, facilitating the crosslinking efficiency on thick constructs (25). Nevertheless, most of the commercially available visible light photoinitiators have poor water solubility and toxicity (31,41). One of the most commonly used initiators is Eosin Y (500-600 nm), but it often requires coinitiators which are toxic (21,25,40). Apart from that, there is a relatively new visible-light photoinitiator that has not been extensively used yet: the tris(2,2′-bipyridyl)dichlororuthenium(II) hexahydrate (ruthenium or Ru) (31,42). It absorbs light at a peak of 452 mn, it is highly soluble in water and it requires of sodium persulfate (SPS) as a co-initiator (42). Furthermore, it is cytocompatible and it is not oxygen inhibited (31), so even with GelMA, the shape of the bioprinted constructs remain accurate. Figure 4 shows the molecular structure of both ruthenium and SPS. When ruthenium is in presence of light, it donates an electron to SPS, breaking both molecules and initiating the crosslinking reaction (42). This photoinitiation system can be used with both GelMA and gelNB.

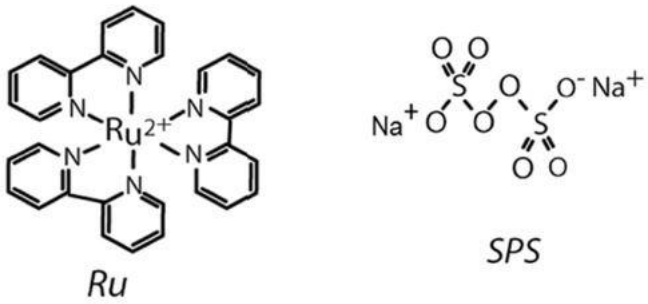

Figure 4. Structure of the photoinitiator (ruthenium) and its co-initiator (sodium persulfate) (22).

Once that the hydrogel and photoinitiators are selected, the photopolymerisation occurs mixing the hydrogel (either GelMA or gelNB), the photoinitiators (Ru/SPS), the crosslinker in the case of gelNB and the cells. This mixture is exposed to visible light and the gel crosslinks (as can be seen in Figure 5).

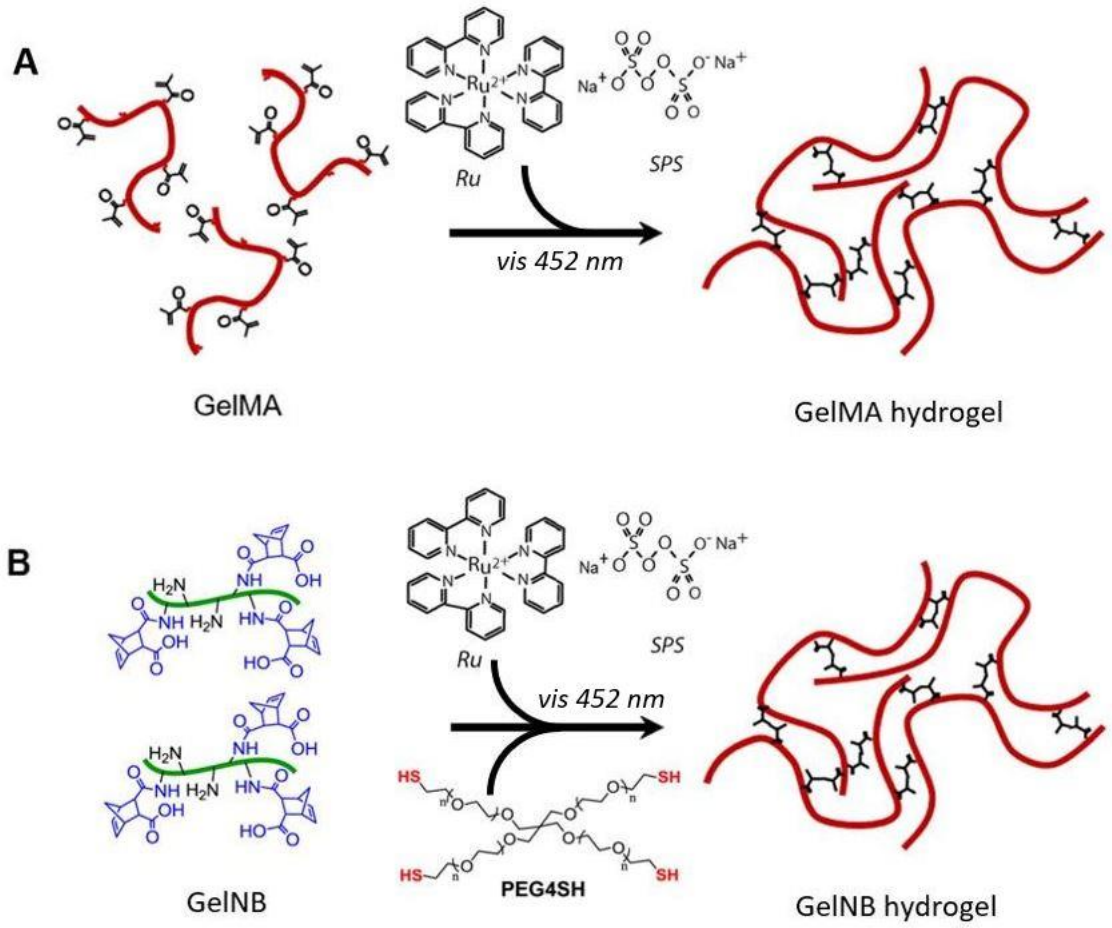

Figure 5. Photocrosslinking of GelMA (A) and gelNB (B) with visible light and the ruthenium/SPS photoinitiation system. Source: Yoon et al. (32), modified (5,22).

Unfortunately, the Ru/SPS system is only able to crosslink the hydrogel precursor for a maximum of 30 minutes, what results in a problem for DLP bioprinting, where only 2-3 mm thick constructs can be generated in this period of time. Nevertheless, there are no restrictions on the X and Y directions (as long as the designs fit in the building plate of the printer), so hydrogel models with channels that resemble vasculature can be bioprinted.

The aim of this project was to develop a bioresin able to differentiate towards bone and cartilage, and capable of creating channels that mimic vasculature where endothelial cells could attach and form monolayers.

For this purpose, first different hydrogel formulations were characterised to select the best gel composition regarding crosslinking efficiency, stiffness, cell viability and proliferation. Afterwards, printing parameters of the selected gels were optimised, to obtain constructs with as small as possible perfusable channels. Later, on the one hand constructs with cells were printed to assess the differentiation towards bone and cartilage, and on the other hand endothelial cells were seeded on the surface of gels, to check their attachment and monolayer formation. After all these experiments, the best gel and printing conditions were selected. Hydrogels varied on the gel concentration, the gel type (fish-GelMA and fish-gelNB) and the photoinitiator (ru/SPS and LAP). The more recently introduced gelNB and ru/SPS were compared to the more extended GelMA and LAP, to make a comparison and check if any improvements were achieved.

2. Methods

2.1 Hydrogel preparation

Hydrogels were made dissolving the hydrogel precursor in PBS and adding the photoinitiator. Freeze dried cold fish GelMA (f-GelMA) or cold fish gelNB (f-gelNB), both of 80% degree of functionalisation (DoF), were dissolved in PBS until obtaining a stock of 30% (w/v) concentration. These were warmed on the roller plate in the incubator to facilitate the dissolution. The two photoinitiators used, ru/SPS and LAP, were also dissolved, making the following stocks:

- Ruthenium (ru), tris(2,2′-bipyridyl)dichlororuthenium(II) hexahydrate (224758, Sigma-Aldrich, USA): 20 mM stock
- Sodium persulfate (SPS), (S6172, Sigma- Aldrich, USA): 200 mM stock
- Lithium phenyl-2,4,6-trimethylbenzoylphosphinate (LAP), (900889, Sigma-Aldrich, USA): 2% (w/v) stock

For f-gelNB gels, a crosslinker was also needed, polyethylene glycol 4 arms, also known as PEG4SH or P4A (JKA7002, Sigma-Aldrich, USA). A 50 mM stock was made. Once all the reactives were dissolved in PBS, they were mixed to obtain different gel conditions, shown in Table 2. Twelve conditions were tested in order to select the best one for the final goal, printing the hydrogels with the DLP.

Table 2. Reactives used for each condition. In the beginning, 12 conditions were tested using f-GelMA or f-gelNB, ru/SPS or LAP and different gel concentrations. The resting volume until reaching the final volume was filled with PBS. The mould used for casting the gels also differed in some conditions. n = 3.

Condition			*Final concentration in mixture*						*Mould*
			f-GelMA (% w/v)	*f-gelNB (% w/v)*	*Ru (mM)*	*SPS (mM)*	*LAP (% w/v)*	*P4A (mM)*	
f-GelMA	*5%*	*Ru/SPS*	5	-	2	20	-	-	Silicon
		LAP	5	-	-	-	0,05	-	Teflon
	10%	*Ru/SPS*	10	-	2	20	-	-	Silicon
		LAP	10	-	-	-	0,05	-	Teflon
	15%	*Ru/SPS*	15	-	2	20	-	-	Silicon
		LAP	15	-	-	-	0,05	-	Teflon
f-gelNB	*5%*	*Ru/SPS*	-	5	2	20	-	3,58	Silicon
		LAP	-	5	-	-	0,2	3,58	Silicon
	10%	*Ru/SPS*	-	10	2	20	-	7,16	Silicon
		LAP	-	10	-	-	0,2	7,16	Silicon
	15%	*Ru/SPS*	-	15	2	20	-	10,74	Silicon
		LAP	-	15	-	-	0,2	10,74	Silicon

Silicon moulds were used in almost all cases. However, f-GelMA suffers from oxygen inhibition with LAP, so Teflon moulds were used for these conditions to generate the hydrogels in an anoxic condition. All mixtures containing f-GelMA or f-gelNB were handled with gel pipettes.

Before mixing the reactives, all of them were kept in dark, covered with aluminium foil. Once mixed, they were added in the silicon mould or Teflon mould and exposed to visible light (ru/SPS gels) or UV light (LAP gels) to photocrosslink the hydrogels. Visible light was irradiated with a 20 W LED lamp (JMW20P-S, Jobmate, Australia) for 7,5 minutes, and UV light was irradiated in a UV oven, a UVP CL-1000L UV linker (UVP Cambridge, UK; 365 nm, 7 mW/cm²) for 5 minutes. Ø8 mm x 1 mm discs were obtained. 3 gels per condition were made.

2.2 Characterisation of hydrogels

Hydrogels were characterised to select the best conditions. Their crosslinking efficiency and mechanical properties were tested.

2.2.1 Crosslinking efficiency

The crosslinking efficiency of hydrogels was assessed calculating the sol fraction, gel content and swelling ratio. For this purpose, hydrogels underwent a set of freeze drying and swelling steps:

- Make gels → m_0
- Freeze drying overnight → $m_{dry,1}$
- Swelling overnight → $m_{swollen}$
- Freeze drying overnight → $m_{dry,2}$

Hydrogels were weighed inside eppendorfs and the weight of the empty eppendorfs was subtracted to obtain the hydrogel mass. When hydrogels were made, they were weighed (m_0) and freeze dried overnight. For this purpose, the eppendorfs were left open and wrapped with parafilm. A needle was used to make holes in the parafilm and let the liquid come out when freeze drying. The samples were frozen at -80ºC before placing them in the freeze dryer (Alpha 1-2 LD plus Freeze dryer, Salmenkipp, the Netherlands). The next day, the samples were removed from the freeze dryer and weighed ($m_{dry,1}$). 0,5 ml PBS was added to each sample and they were left overnight in the incubator at 37ºC to rehydrate. The following day, the gels were placed in other (previously weighed) eppendorfs and weighed ($m_{swollen}$), and they were freeze dried again, as explained above. The day after, they were weighed ($m_{dry,2}$).

The first dry weight involves both the crosslinked and the uncrosslinked part of the hydrogel. Then, gels were in PBS, where the uncrosslinked part of the gels dissolved, so the second dry weight is only of the crosslinked part. In this way it is possible to calculate how much of the total gel did not crosslink, which is known as the sol fraction. The higher it is, the poorer the crosslinking is, so ideally, low values are desired. The sol fraction of the hydrogels was calculated with the following equation (31):

$$Sol\ fraction\ (\%) = \frac{m_{dry,1} - m_{dry,2}}{m_{dry,1}} \cdot 100 \quad (1)$$

Apart from that, it is possible to calculate the amount of water that that the hydrogel absorbs and bounds to its molecules, which is known as the swelling ratio. Hydrogels generally have a high swelling capacity, but too high values are also not desirable, because they are related to a poorer crosslinking efficiency. Moreover, when microchannels are printed, as in the final goal of this project, high swelling ratios may lead to a constriction of the channels (18,36). The swelling ratio was calculated following the equation shown below (31):

$$Swelling\ ratio\ (q) = \frac{m_{swollen}}{m_{dry,2}} \quad (2)$$

Finally, the gel content, which refers to the macromer concentration in each hydrogel, was calculated as shown in the next equation:

$$Gel\ content\ (\%) = \frac{m_{dry,1}}{m_0} \cdot 100 \quad (3)$$

2.2.2 Mechanical testing

The twelve hydrogel conditions were also subjected to a compression testing with a Dynamic Mechanical Analyzer (Q800 DMA, TA Instruments, USA). Their elastic modulus was calculated by plotting their stress-strain curves. The diameter of hydrogels was measured with a digital calliper, and the software (TA Instrument Explorer) calculated their height. A strain ramp from -20% to -30% was applied, with an initial strain of -1%, and data was collected every 0.2 seconds. Once the stress-strain curves were plotted, the Young's modulus was calculated as the slope of the curve.

2.3 Cell culture

2.3.1 Mesenchymal stem cells

Equine mesenchymal stem cells (eqMSCs) were used for cell encapsulation experiments. All the materials (medium, cells, flasks, falcon tubes, …) were handled sterilely inside the laminar flow cabinet.

Cryopreserved vials stored in liquid nitrogen were obtained and defrosted until little ice was left in the vial. Then, all the liquid was transferred to a 50 ml falcon tube with 10 ml expansion medium. The MSCs expansion medium, described below, was previously prepared and prewarmed at 37ºC before its use. The 50 ml falcon was centrifuged (Centrifuge 5810R, Eppendorf, Germany) for 5 minutes at 1500 rpm in order to remove the medium used to cryopreserve the cells, which is toxic when it is warm and in long term. The supernatant was removed, cells were resuspended in 20 ml expansion medium and counted. To do so, 20 µl of the mixture were transferred to a sterile Eppendorf, 20 µl of trypan blue (TC10 trypan blue dye, 145-0013, Bio-Rad, USA) were added and 10 µl to the mixture were placed in a cell counting slide. This slide was placed in the cell counter (TC10 Automated Cell Counter, 145-0001, Bio-Rad, USA), which gave the cell concentration per ml. Once the cell quantity in the falcon tube (concentration * volume) was calculated, the falcon tube was centrifuged again, 1500 rpm, 5 minutes. In the meanwhile, the number of T175 flasks needed to contain $0{,}5*10^6$ cells in each one was calculated, and 20 ml expansion medium were added to each flask. The supernatant of the centrifuged tube was removed, 2 ml of expansion medium per flask were added to the tube, and the pellet was resuspended. 22 µl of basic fibroblast growth factor (bFGF) per ml flask were added to the falcon tube, and its content was split into all the T175 flasks,

adding 2 ml to each. The flasks were stored in the incubator at 37ºC and 5% CO_2 for them to grow and expand in optimal conditions.

MSCs expansion medium:

- Dubeco's Modified Eagle Medium (DMEM) (1X) + GlutaMAX, + 4,5 g/l d-glucose, + pyruvate (31966021, Thermo Fisher Scientific, USA): 500 ml (- 50 ml)
  - + Fetal bovine serum (FBS): 10% (50 ml)
  - + Penicillin/streptomycin (P/S): 1% (5 ml)
  - + Basic fibroblast growth factor (bFGF): fresh, 1 µl/ml

Medium was replaced every 3-4 days, by suctioning the medium and adding 20 ml medium + (2 ml medium + 22 µl bFGF) to each flask.

When the flasks were confluent, they were split into more flasks. Trypsin (25200, Thermo Fisher Scientific, USA) was used to detach the cells from the bottom of the flasks. First, medium was suctioned, and flasks were washed with 5 ml sterile PBS0. The PBS was also suctioned, and 2,5 ml trypsin/flask was added to each flask, spread at the bottom and incubated at 37ºC for 2 minutes. The trypsin was then inactivated by adding 5 ml expansion medium, cell clumps were broken by pipetting the liquid on the flask walls and the liquid was moved to a 50 ml falcon tube. The tube was centrifuged (1500 rpm, 5 minutes), cells were counted and split in 0,5 million cells per flask, as explained above.

2.3.2 Endothelial colony forming cells

Some experiments were also performed with endothelial colony forming ells (ECFCs). Both fluorescently labelled (GFP-ECFCs) and non-labelled cells were used. Cells were thawed, seeded and expanded as explained above, with the only difference that endothelial cell culture medium was used this time:

Endothelial cell expansion medium:

- Endothelial cell Growth Medium (EGM-2), (CC-3156, Lonza, USA): 500 ml (-50 ml)
  - + Fetal bovine serum (FBS): 10% (50 ml)
  - + Penicillin/streptomycin (P/S): 1% (5 ml)
  - + EGM-2 singlequots ((CC-3156, Lonza, USA):
    - Hydrocortisone (CC-4112A) 0,2 ml
    - hFGF-β (CC-4113A) 2 ml
    - VEGF (CC-4114A) 0,5 ml
    - R^3-IGF-1 (CC-4115A) 0,5 ml
    - Ascorbic acid (CC-4116A) 0,5 ml
    - hEGF (CC-4317A) 0,5 ml
    - GA-1000 (CC-4381A) 0,5 ml
    - Heparin (CC-4396A) 0,5 ml

Once medium was made, it was aliquoted in 50 ml falcon tubes, and the tubes were frozen at -20ºC until use.

Cells were seeded in T75 flasks at $0,5*10^6$ cells/flask, and medium was replaced every 2-3 days.

2.4 Cell encapsulation in hydrogels

Passage 6 equine MSCs were encapsulated in f-GelMA and f-gelNB hydrogels to test the cell viability and proliferation. Hydrogels were prepared as explained in the 2.1 section, with two differences: MSCs were also added to the hydrogel mixture, and all the reactives were handled sterilely.

The final cell concentration was 10^6 cells/ml hydrogel, so a stock of $80*10^6$ cells/ml was prepared first, by trypsinising, centrifuging and counting the cells as explained above. F-GelMA and f-gelNB were sterile, so they were added to previously weighed 50 ml falcon tubes in the flow cabinet, and tubes were weighed closed to keep sterility inside. The rest of reactives (ru, SPS, LAP, P4A) were not sterile, so they were weighed and dissolved non-sterilely and then sterile filtered in the flow cabinet with 0,22 µm filters. Stocks at the same concentration as in 2.1 section were made, with the final concentrations mentioned in Table 3. All the materials (spatula, tweezers, silicon and Teflon moulds, …) were either autoclaved or sterilized in ethanol. Crosslinking was performed inside the flow cabinet with the visible light lamp or a UV light lamp at 365 nm wavelength (6 mW/cm^2). 6 gels were made per condition, 3 for the day 1 analysis and 3 for the day 7 analysis.

Table 3. Hydrogel conditions and material concentrations used for embedding MSCs. n = 3.

Condition			*Final concentration in mixture*							*Mould*
			f-GelMA (% w/v)	*f-gelNB (% w/v)*	*Ru (mM)*	*SPS (mM)*	*LAP (% w/v)*	*P4A (mM)*	*MSCs (cells /ml)*	
f-GelMA	*10%*	*Ru/SPS*	10	-	2	20	-	-	$10*10^6$	Silicon
		LAP	10	-	-	-	0,05	-	$10*10^6$	Teflon
	15%	*Ru/SPS*	15	-	2	20	-	-	$10*10^6$	Silicon
		LAP	15	-	-	-	0,05	-	$10*10^6$	Teflon
f-gelNB	*5%*	*Ru/SPS*	-	5	2	20	-	3,58	$10*10^6$	Silicon
		LAP	-	5	-	-	0,2	3,58	$10*10^6$	Silicon
	10%	*Ru/SPS*	-	10	2	20	-	7,16	$10*10^6$	Silicon
		LAP	-	10	-	-	0,2	7,16	$10*10^6$	Silicon

Once the hydrogels were made, they were moved to a 48 well plate and cultured in 0,5 ml MSCs expansion medium/well for a week, in the incubator at 37ºC. Medium was refreshed every 2-3 days.

2.5 Cell viability

Cell viability of hydrogels was tested performing a live-dead assay, at day 1 and 7 of hydrogel culture with embedded MSCs. First, hydrogels were cut in half with a sterile scalpel blade (the test was performed in half gel only). Afterwards, they followed a set of washing and staining steps:

- 5 minutes PBS0-Ca-Mg (x2)
- 15 minutes calcein AM/ethidium homodimer-1 in PBS0-Ca-Mg (*)
- 5 minutes PBS0-Ca-Mg (x2)

(*) the calcein AM and ethidium homodimer-1 are part of the live-dead kit (LIVE/DEAD™ Viability/Cytotoxicity Kit for mammalian cells, L3224, Thermo Fisher Scientific, USA). 0,25 µl calcein AM and 0,5 µl ethidium homodimer-1 per ml PBS were used and kept in dark. The gels were incubated (for 15 minutes) in the incubator at 37ºC.

When the live-dead test was finished, the hydrogels (3 samples per day and condition) were observed at the fluorescence microscope (BX51, Olympus, Japan), showing living cells in green (where the calcein AM binds, with a 488/530 nm excitation/emission filter) and dead cells in red (where the ethidium homodimer-1 binds, with a 530/580 nm excitation/emission filter). Live and dead pictures of 5 sections per sample were taken, at 10x or 20x magnification of the microscope. The living and dead cells were counted with the ImageJ software. The cell count from all sections of the same hydrogel was summed, and the viability ratio was obtained:

$$Cell\ viability = \frac{living\ cells}{dead\ cells} \cdot 100 \quad (4)$$

After taking pictures of the live-dead assay, samples were freeze dried overnight (as explained in section 2.2.1).

2.6 DNA quantification

DNA of MSCs embedded in hydrogels was quantified by a PicoGreen assay. First, freeze dried samples were digested with papain. 1,57 mg/ml cysteine-HCL (DL-cysteine hydrochloride, C9768, Sigma-Aldrich, USA) and 250 µg/ml papain (Papain from papaya latex, P3125, Sigma-Aldrich, USA) were added to the 2X papain digestion buffer. 200 µl of the mixture were added to each sample (which were inside the Eppendorfs used for the freeze drying), and they were incubated overnight at 60C. The following day the samples were vortexed and incubated at 60ºC for one more hour.

Afterwards, the PicoGreen assay was performed (once the samples were at room temperature). First, a standard curve was made with a λDNA stock (QuantiT™ PicoGreen™ dsDNA assay kit, P11496, Thermo Fisher Scientific, USA). This stock was 100 µg/ml, and before making the standard curve, it was diluted 50 times in 1X TE buffer, obtaining a 2 µg/ml stock (A). The rest of the stocks for the standard curve, shown in Table 4, were made mixing a part of A in 1X TE buffer:

Table 4. Volumes of A (λDNA) and TE buffer added to each point of the working curve, with their final DNA concentrations. The final volume of each sample was 220 µl.

Standard curve	*λDNA (A) V (µl)*	*1x TE buffer V (µl)*	*[λDNA] (ng/ml)*
A	(already made)	(already made)	2000
B	176	44	1600
C	132	88	1200
D	88	132	800
E	44	176	400
F	22	198	200
G	11	209	100
H	0	220	0

Then, the samples from the papain digestion were diluted in 1X TE buffer so that they fit in the working curve, so if a high DNA amount is expected, a higher dilution should be applied. In the case of the hydrogels, they were diluted 5 times. 100 µl of both the standard curve and the samples, in duplo, were added to a flat bottom 96-well plate. Finally, the PicoGreen reagent was diluted 200 times in 1X TE buffer and kept in dark until use. 100 µl were added to each well with a multi-channel pipette, incubated for 5 minutes in dark and measured. The measurements were made in the Fluoroskan spectrofluorimeter (Fluoroskan Ascent FL, 5210450, Thermo Fisher Scientific, USA), with an excitation/emission filter at 485/520 nm. The emission intensity of each well was saved and transferred to an Excel file. The standard curve was made with the values of A-H samples, obtaining a linear regression equation. This was used to calculate the DNA concentration of the rest of the samples (ng/ml), where the 1:5 dilution was considered. The DNA amount was also calculated, using the 200 µl of the papain digestion as volume.

2.7 DLP printing of hydrogels

Hydrogels were printed at the digital light processing (DLP) printer. First, the desired constructs were designed in TinkerCAD (Autodesk, USA), modified (re-scaled in some cases) with Print Studio software (Autodesk, USA) and processed with the Perfactory software (EnvisionTEC, Germany), where the print jobs were built and sent to the Perfactory® 3 Mini (EnvisionTec, Gladbeck, Germany). The printer used a 60 mm lens, which allowed a resolution of 50 µm, and every time before using was calibrated to set the desired light intensity. The intensity varied until the optimal was found, and the irradiation time per layer was 10 seconds.

Hydrogels were 3D printed adding 2 ml of the precursor mixture to the centre of the baseplate, with care on not leaving bubbles. The baseplate used was a special one for hydrogels, empty and highly hydrophobic. In this way, the precursor liquid added did not spread through the plate and stayed where it was added. When hydrogels were printed, for a maximum of 30 minutes, they were removed from the building plate using a scalpel blade and washed in PBS for 15 minutes before analysing or using them. Both the building plate and the baseplate were washed first with PBS and later with ethanol. The baseplate was handled and washed smoothly.

The settings used for printing hydrogels had an error where the bottom layers of the design were not printed. In order to determine how thick was the unprinted part, a 4 x 4 x 4 mm^3 cube was printed using the same settings and the photocurable resin PIC100. The z axis of the cube was measured to determine the thickness of this unprinted part, and a layer this thick was added to the bottom of the hydrogel designs.

2.8 Characterisation of hydrogels

The hydrogel precursors were added to a glass slide, which was located at the printer. Different light energies were irradiated to print Ø4 mm discs, and discs with different thicknesses were obtained. Pictures of the resulting gels were taken, and their thicknesses, also known as the cure depth (C_d), were measured with ImageJ and plotted versus the irradiation energy to obtain the working curve. The slope of these curves is the light penetration depth (D_p), and the point where the working curves cut the x axis is the minimum irradiation energy required to crosslink the hydrogel (E_c). The working curve was plotted following the equation (5):

$$C_d = D_p \cdot \ln \frac{E}{E_c} \quad (5)$$

A photoabsorber, Ponceau 4R (food colorant E124), a red dye, was also added to decrease the light penetration depth. 0, 1 or 2% dye was added to each condition, Table 5 shows all the conditions that were tested.

Table 5. Summary of the hydrogel conditions tested for 3D printing.

Condition			*Final concentration in mixture*						
			Dye (% v/v))	*f-GelMA (% w/v)*	*f-gelNB (% w/v)*	*Ru (mM)*	*SPS (mM)*	*LAP (% w/v)*	*P4A (mM)*
f-GelMA	*10%*	*Ru/SPS*	0	10	-	2	20	-	-
			1	10	-	2	20	-	-
			2	10	-	2	20	-	-
		LAP	0	10	-	-	-	0,2	-
			1	10	-	-	-	0,2	-
			2	10	-	-	-	0,2	-
	15%	*Ru/SPS*	0	15	-	2	20	-	-
			1	15	-	2	20	-	-
			2	15	-	2	20	-	-
		LAP	0	15	-	-	-	0,2	-
			1	15	-	-	-	0,2	-
			2	15	-	-	-	0,2	-
f-gelNB	*5%*	*Ru/SPS*	0	-	5	2	20	-	3,58
			1	-	5	2	20	-	3,58
			2	-	5	2	20	-	3,58
		LAP	0	-	5	-	-	0,2	3,58
			1	-	5	-	-	0,2	3,58
			2	-	5	-	-	0,2	3,58
	10%	*Ru/SPS*	0	-	10	2	20	-	7,16
			1	-	10	2	20	-	7,16
			2	-	10	2	20	-	7,16
		LAP	0	-	10	-	-	0,2	7,16
			1	-	10	-	-	0,2	7,16
			2	-	10	-	-	0,2	7,16

In previous experiments 0,05% LAP was used for f-GelMA, but this time the concentration was increased to 0,2% to avoid oxygen inhibition. Ru/SPS hydrogels were printed at the Perfactory® 3 Mini, but the LAP hydrogels were printed at the Ember printer (Autodesk, USA) at 405 nm wavelength. 2 samples per condition were printed.

2.9 Positive and negative features, ECFC attachment discs

Some designs were printed at the Envisiontec printer to optimise the printing energy. Experiments were only performed with the ru/SPS, 2% dye hydrogels, as LAP gels showed poor results. The following designs were printed at 100, 80 and 65 mJ/cm^2 energies:

- Positive features (CAD design in Figure 6): 9,4 mm x 4 mm x 3,2 mm (x, y, z). In the z axis the printing error (1,2 mm) was considered, so the real height of the design was 2 mm. The protuberances were 0,7 mm tall and 1 mm, 0,75 mm, 0,5 mm 0,3 mm, 0,2 mm, 0,1 mm and 0,05 mm wide respectively.

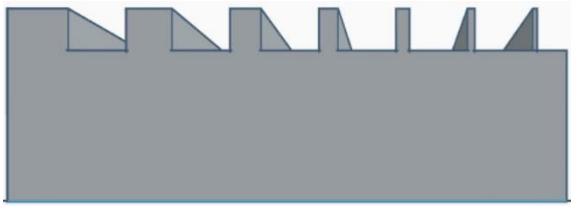

Figure 6. CAD design of positive features.

- Negative features (CAD design in Figure 7): 8,7 mm x 4 mm x 3,2 mm (x, y, z). In the z axis the printing error (1,2 mm) was considered, so the real height of the design was 2 mm. The channels had their first 0,5 mm (y) of 1 mm diameter to facilitate the perfusion, and the rest 3,5 mm varied: 1 mm, 0,75 mm, 0,5 mm 0,3 mm, 0,2 mm and 0,1 mm respectively.

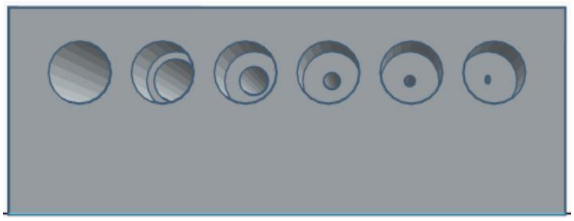

Figure 7. CAD design of negative features.

- Endothelial cell attachment discs (CAD design in Figure 8): Ø6 mm x 3,7 mm (z). In the z axis the printing error (1,2 mm) was considered, so the real height of the design was 2,5 mm. The discs had an inner empty disc of Ø4 mm x 1 mm (z), so that cells could be seeded without the cells falling from the discs.

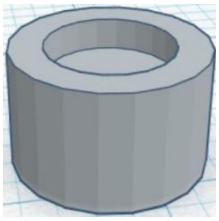

Figure 8. CAD design of ECFC attachment discs

The hydrogel conditions shown in Table 6 were tested.

Table 6. Hydrogel conditions used for positive and negative features, and ECFC attachment discs.

Condition		*Final concentration in mixture*					
		Dye (% v/v))	*f-GelMA (% w/v)*	*f-gelNB (% w/v)*	*Ru (mM)*	*SPS (mM)*	*P4A (mM)*
f-GelMA ru/SPS	*10%*	2	10	-	2	20	-
	15%	2	15	-	2	20	-
f-gelNB ru/SPS	*10%*	2	-	10	2	20	7,16

After printing, pictures were taken. Positive and negative features were measured (the thickness of positive features and the channel diameter of negative features) and compared to the theoretical size. In case of negative features, horizontal and vertical diameters were compared, because generally there is some overcrosslinking in the z axis, so the vertical diameter is smaller. The more similar both diameters were, the less overcrosslinking there was, and the better result. Negative features were also perfused with a needle and a syringe containing red dye.

Positive and negative features were kept in PBS at 5ºC, and ECFC attachment discs were kept in ethanol at 5ºC.

2.10 Printing of complex structures

Two designs were printed.

- Branching channels (CAD design in Figure 9): f-GelMA 10% and 15% ru/SPS 2% dye hydrogels were printed at 70 mJ/cm^2 energy. The design was 10,5 mm x 8 mm x 3,2 mm (x, y, z). In the z axis the printing error (1,2 mm) was considered, so the real height of the design was 2 mm. A Ø1 mm channel branched into Ø0,8 mm channels, which branched in Ø0,6 mm channels.

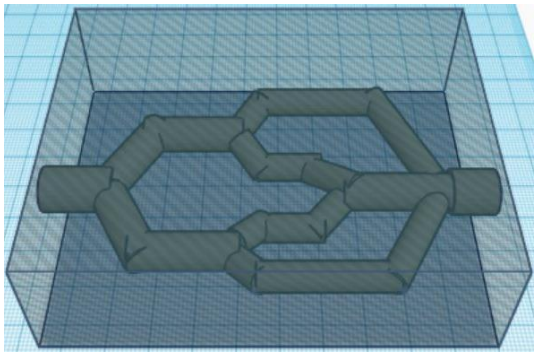

Figure 9. CAD design of the branching channels structure

- Spiral channel (CAD design in Figure 10): f-GelMA 8% + p-GelMA 2%, ru/SPS 2% dye hydrogels were printed at 70 mJ/cm^2 energy. The design was 7,5 mm x 2,4 mm x 3,2 mm (x, y, z). In the z axis the printing error (1,2 mm) was considered, so the real height of the design was 2 mm. A Ø0,55 mm straight channel crossed the structure, and a Ø0,55 mm spiral channel twisted around the straight channel.

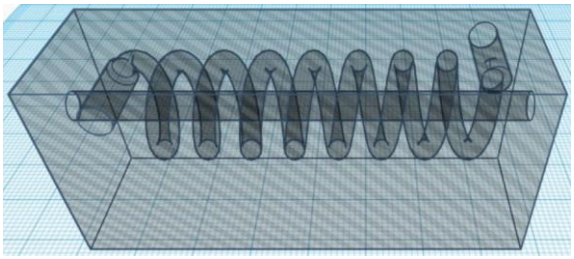

Figure 10. CAD design of the construct with the spiral channel

Pictures of both printed designs were taken, and they were perfused with the red dye.

2.11 DLP printing of cell-laden hydrogels

Ø6 mm x 3 mm designs (Ø6 mm x 1,8 mm with the error) of both 10% ru/SPS 2% red dye f-GelMA and f-gelNB were printed with MSCs. For this purpose, reactives were prepared as in section 2.4 (f-GelMA and f-gelNB were weighed in sterility and the rest -ru, SPS, P4A, dye- were sterile filtered) and equine MSCs passage 4 were cultured and trypsinised as in section 2.3.1. The final concentration of cells was $20*10^6$ MSCs/ml hydrogel, so a stock of $80*10^6$ MSCs/ml was prepared. The final concentrations of each reactive are shown in Table 7.

Table 7. Hydrogel conditions used for printing with MSCs.

Condition	*Final concentration in mixture*					
	f-GelMA (% w/v)	*f-gelNB (% w/v)*	*Ru (mM)*	*SPS (mM)*	*P4A (mM)*	*MSCs (cells/ml)*
f-GelMA 10% ru/SPS 2% dye	10	-	2	20	-	$20*10^6$
f-gelNB 10% ru/SPS 2% dye	-	10	2	20	7,16	$20*10^6$

As the printer was not in sterile conditioons, the baseplate was kept in ethanol for 20 minutes and the printer was thoroughly washed with ethanol (the inner walls, the building pate, etc). Before starting the print, the ethanol was removed from the baseplate and it was let dry. The hydrogel mixture was taken from the flow cabinet, added to the printer and the print was started. When the print was finished, the discs were transferred to a sterile 6-well plate and taken to the flow cabinet. Once there, they were washed in sterile PBS0 for 15 minutes, and then they were transferred to a 48-well plate, where 1/3 of the hydrogels were cultured in chondrogenic medium, 1/3 in hypertrophic medium and 1/3 in osteogenic medium for 28 days.

Chondrogenic differentiation medium:

- Dubeco's Modified Eagle Medium (DMEM) (1X) + GlutaMAX, + 4,5 g/l d-glucose, + pyruvate (31966021, Thermo Fisher Scientific, USA): 48,5 ml
  - + Fetal bovine serum (FBS): 10% (5 ml)
  - + Penicillin/streptomycin (P/S): 1% (0,5 ml)
  - + Ascorbic acid (ASAP): 1% (0,5 ml)
  - + B-glycerophosphate (BGP): 1% (0,5 ml)
  - + Dexamethosane: 0,1 µM (2 µl)

+ Transforming growth factor β (TGFβ): FRESH, 10 ng/ml (1 µl/ml)

Osteogenic differentiation medium:

- Minimum essential medium α (α-MEM) (1X), without ribonucleosides or deoxyribonucleosides (22561021, Thermo Fisher Scientific, USA): 43,5 ml
  + Penicillin/streptomycin (P/S): 1% (0,5 ml)
  + Ascorbic acid (ASAP): 1% (0,5 ml)
  + ITS premix: 1% (0,5 ml)
  + Dexamethosane: 0,1 µM (2 µl)

The hypertrophy was achieved by culturing the gels in chondrogenic medium for the first 14 days and then switching to osteogenic medium. Medium was refreshed every 2-3 days. At day 28 of culture, hydrogels were harvested, cut in 3 parts as shown in Figure 11, and one part was used for cartilage differentiation and DNA quantification assays (DMMB and PicoGreen), another part for bone differentiation and DNA quantification assays (ALP and PicoGreen), and the third part for histological analyses. 4 samples per condition were used.

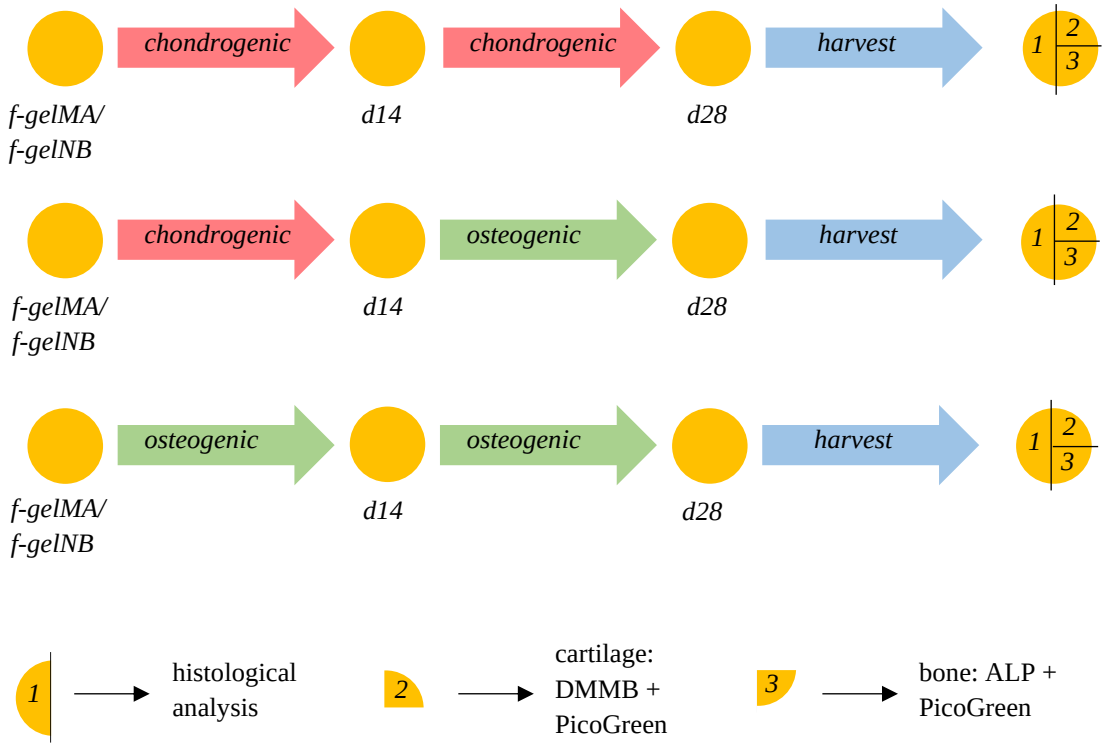

Figure 11. Schematic illustration of the culture of printed hydrogel discs and their treatment.

The histological analysis, DMMB and ALP are explained below, and the PicoGreen was performed as in section 2.6.

2.12 DMMB assay

The DMMB assay is the most commonly used technique to quantify glycosaminoglycans (GAGs), which are abundant in the cartilage tissue. The dimethylmethylene blue (DMMB) reagent reacts with sulphates on the GAGs.

Before the experiment, the hydrogels were freeze dried overnight and papain digested in PBS-EDTA overnight as in section 2.6.

The next day, the DMMB assay was performed. First, a standard curve was made with chondroitin sulphate (CS). A 0,5 mg/ml CS stock was diluted 50 times in PBS-EDTA buffer (A). The rest of the standard curve was obtained diluting the previous point 2 times, as shown in Table 8.

Table 8. Concentrations of each point of the standard curves, and volumes to add to obtain them.

Standard curve	*CS V (µl)*	*PBS-EDTA V (µl)*	*[CS] (µg/ml)*
A	500	0	10
B	250 of A	250	5
C	250 of B	250	2,5
D	250 of C	250	1,25
E	250 of D	250	0,625
F	250 of E	250	0,3125
G	250 of F	250	0,15625
H	250 of G	250	0,078125
I	250 of H	250	0,0390625
J	0	250	0

Afterwards, the samples were diluted. As 1/4 hydrogel was used this time, a 1/3 dilution was made. Then, 100 µl of the standard curve and samples were added in duplo to a flat bottom 96-well plate. Finally, 200 µl DMMB staining solution were added to each well with a multi-channel pipette and the absorbance was measured by the absorption microplate photometer (VersaMax ELISA, Molecular Devices, USA), at 525 and 595 nm. The results were transferred to an Excel file.

To calculate the quantity of GAGs in each sample, the 525 nm absorbance was divided by the 595 nm absorbance to extract the blank. Then, the standard curve was plotted with the polynomic formula ($y = ax^2 + bx + c$), and the GAG concentration of the samples was obtained using this formula. The GAG quantity was the concentration multiplied by the volume employed in the papain digestion (0,2 ml).

The chondrogenic differentiation was shown as GAGs/DNA, so the papain digested samples were also used for a DNA quantification assay, performed according to the 2.6 section.

2.13 ALP test

Alkaline phosphate (ALP) is an early osteogenic marker, so it is used to determine osteogenesis. 250 µl mammalian protein extraction reagent (MPER, 78503, Thermo Scientific Systems, USA) and frozen at -80ºC. Afterwards, they were defrosted and grinded. The grinder was washed twice in PBS-Tween and twice in PBS between samples. Once grinded, they were centrifuged for 5 minutes at 1500 rpm.

In the meanwhile, the ALP substrate solution and the standard curve were prepared. The first one was made adding a pNPP tablet and a Tris buffer tablet to 20 ml MPER buffer. The second one was prepared by adding the ALP

enzyme to the MPER buffer (A). The volumes used and the final ALP concentration on each tube is shown in Table 9.

Table 9. Volumes and final concentrations of the standard curve.

Standard curve	*ALP V (µl)*	*MPER V (µl)*	*[ALP] (U/ml)*
A	0,5	249,5	2
B	125 of A	125	1
C	125 of B	125	0,5
D	125 of C	125	0,25
E	125 of D	125	0,125
F	125 of E	125	0,0625
G	125 of F	125	0,03125
H	0	250	0

Then, samples' supernatant was collected, with care of not taking the pellet. The desired dilutions were made, in this case, no dilution, and 100 µl of the standard curve and samples were added in duplo to a flat bottom 96-well plate. Finally, 100 µl ALP substrate solution were added to each well with a multi-channel pipette and the absorbance was measured by the absorption microplate photometer (VersaMax ELISA, Molecular Devices, USA), at 405 and 655 nm, every minute for 30 minutes.

A standard curve of ALP activity/ml versus absorbance at 29 minutes was plotted to obtain a linear regression. The equation of this regression was to the activity/ml of the samples to calculate their ALP activity. The activity was calculated by multiplying the sample volume, 0,25 ml.

Moreover, the osteogenic differentiation was shown as GAGs/DNA, so the grinded and centrifuged samples were also used for a DNA quantification assay, performed according to the 2.6 section.

2.14 Processing of samples for histological analysis

Part of the hydrogels were processed for histology. These were located inside cassettes (the gels prom the same conditions in the same cassette) and left overnight in phosphate buffered 37% formaldehyde.

The following day, samples were dehydrated and prepared to embed in paraffin with the following steps:

1. 1h 70% ethanol
2. 1h 96% ethanol (x2)
3. 1h 100% ethanol (x2, the second was left overnight)
4. 1h xylene (x2)
5. Minimum 2h liquid paraffin (in the oven at 60ºC), refresh once

Finally, samples were embedded in paraffin, cooled down in an embedding station (Leica EG1150 modular tissue embedding center, Leica Biosystems, Germany) and stored for further analyses.

2.15 ECFC attachment to hydrogel surface

The ability of endothelial colony forming cells (ECFCs) to hydrogel surfaces was tested. Different trials were made:

1. Printed hydrogel discs (in section 2.9), stored in ethanol to keep sterility, were rehydrated in sterile PBS0 twice overnight before performing the experiment.
2. Hydrogels were casted in a 24-well plate, and many conditions were tested: f-GelMA 10% and 15%, f-GelMA 9% and 14% with 1% p-GelMA (10% and 15% gel in total), f-GelMA 8% and 13% with 2% p-GelMA (10% and 15% gel in total), p-GelMA 10% and 15%, f-GelMA 10% 0,5/5 mM/mM ru/SPS, f-GelMA 10% with MSCs seeded on top, f-GelMA 10% + fibrinogen, f-GelMA 8% with 2% porcine GelMA (10% gel in total) and non-fluorescent ECFCs. (*) The casted gels were washed overnight in PBS before the experiment.
3. Sterilely casted hydrogel discs in the silicon mould, washed thoroughly in sterile PBS to remove all uncrosslinked residues: f-GelMA 10% and 15%, f-GelMA 8% and 13% with 2% p-GelMA (10% and 15% gel in total), p-GelMA 10% and 15%, f-GelMA 10% + fibrinogen. In one case condition medium was used (**).

(*) Except from the case with 0,5/5 (mM/mM) ru/SPS, hydrogels had 2/20 mM/mM ru/SPS.

(**) Condition medium was used to check if cells did not attach to the gel surface because these released a toxic compound. Thus, cells were not seeded on top of the hydrogel, but in a separate well where there was not a hydrogel. When medium was changed, the medium that was in contact with the hydrogel was transferred to the well with cells. If cells died, it would mean that hydrogels release a toxic compound which detached or killed the cells.

The day of the experiment, ECFCs were trypsinised, counted (as in section 2.3) and added to the surface of the hydrogels in a concentration of $6{,}6*10^5$ cells/ml. The volume added corresponded to the one where 131,3 cells per mm^2 hydrogel were seeded.

After seeding the cells, they were left in the incubator for 30-45 minutes, so that the cells could attach to the hydrogel, and after this period of time, 0,4 ml endothelial cell medium was added. Medium was changed every 2-3 days.

Fluorescent (green) pictures were taken every 2-3 days to check the evolution of the attachment. The samples on the 24-well plate were observed at the inverted microscope, but the discs were observed at the upright fluorescence microscope.

2.16 Statistical analysis

A two-way ANOVA, with a subsequent Bonferroni test, was performed to find significant statistical differences between conditions. Different degrees of significance were taken into account: * for $p < 0{,}05$, ** for $p < 0{,}01$, *** for $p < 0{,}001$ and **** for $p < 0{,}0001$.

3. Results

3.1 Hydrogel characterisation

12 gel conditions were tested to select the best ones for further testing. First, the gels were characterised to determine their crosslinking efficiency and stiffness. 6 gels per condition were made, 3 for the sol fraction, swelling and gel content, and 3 for the compression testing.

3.1.1 Crosslinking efficiency and stiffness

The crosslinking efficiency was tested, by weighing the gels after a set of freeze drying and swelling steps. The results are shown in Figure 12.

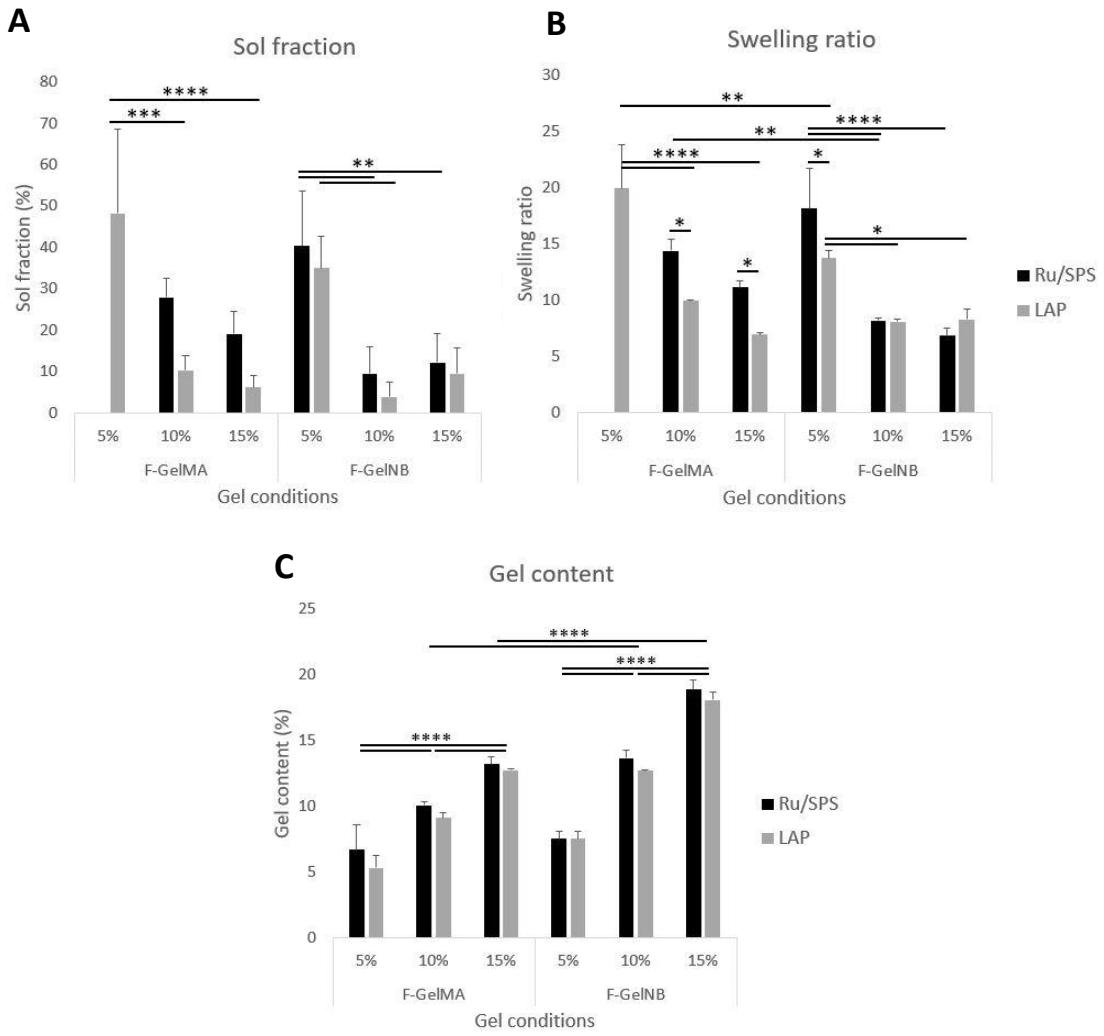

Figure 12. Crosslinking degree of different gel conditions, measured with different parameters: (A) sol fraction, (B) gel content and (C) swelling ratio. Standard deviations (n=3) and significative differences are shown.

Besides, the stiffness of the gels was tested by a compression testing on the Dynamic Mechanical Analysis machine. The results are shown in Figure 13.

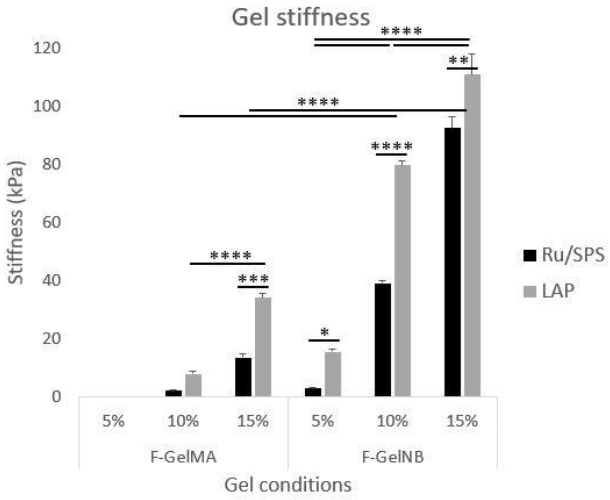

Figure 13. Stiffness of the 12 gel conditions, calculated from the compression test. Standard deviations (n=3) and significative differences are shown.

Significant differences can be observed among gels. F-GelMA 5% gels were weak, the Ru/SPS ones dissolved after being overnight in PBS, therefore, the sol fraction and swelling ratio could not be calculated. The LAP ones did not dissolve, so the crosslinking efficiency could be calculated, being too weak. For the rest of conditions, the f-gelNB 5% also have a poor crosslinking efficiency, as can be noted by the high sol fraction and low gel content (Figure 12A and C). F-gelNB gels had a higher crosslinking degree than the f-GelMA ones, comparing the same concentrations at the sol fraction and gel content. Comparing photoinitiators, there were no significant differences in the sol fraction and gel content, but there were in the swelling ratio (Figure 12B). The majority of the gels crosslinked with Ru/SPS absorbed more water than those crosslinked with LAP.

As for the stiffness (Figure 13), although f-GelMA 5% LAP gels could be used to obtain all the weights for the crosslinking efficiency, they were too weak to perform the compression test. Apart from that, LAP gels were clearly stiffer than Ru/SPS ones and the f-gelNB ones stiffer than those of the same concentration of f-GelMA. At higher gel concentration, stiffer gels.

Taking into account these results, 5% f-GelMA and 15% f-gelNB were removed for further testing, the first one because gels were too weak and they dissolved, and the last one because gels were too stiff.

3.1.2 Cell viability and proliferation

The conditions that were not discarded (f-GelMA 10-15% and f-gelNB 5-10%) were tested to check cell viability and proliferation. MSCs were encapsulated, and a live/dead assay was performed for viability (Figure 14) and a Picogreen assay and cell counting for proliferation (Figure 15).

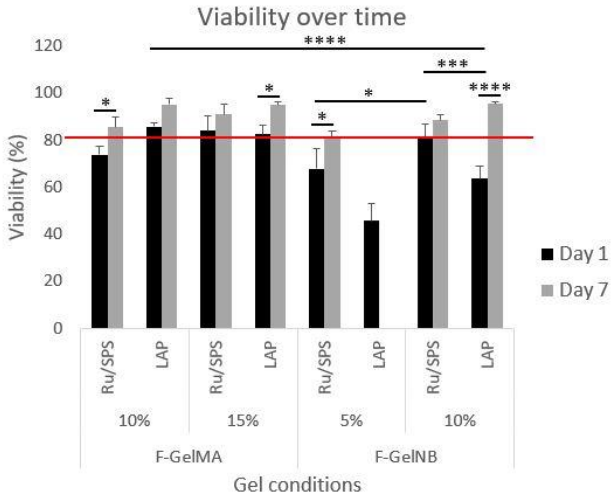

Figure 14. Cell viability over time, checked with a live/dead assay at day 1 and 7 after encapsulation. Minimum viability line is shown in red (80% living cells). Standard deviations (n=3) and significative differences are shown.

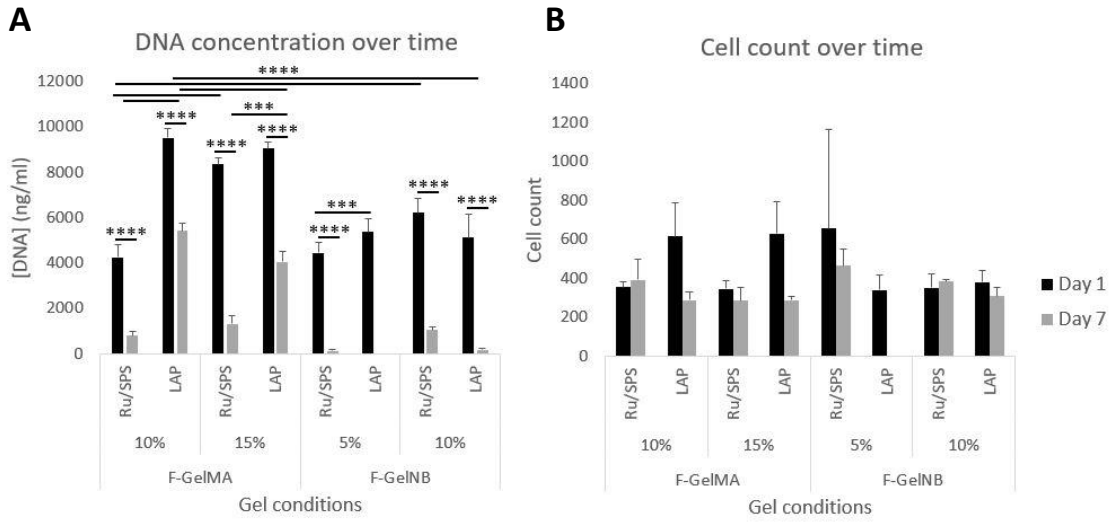

Figure 15. Cell proliferation over time, measured with a DNA quantification assay, PicoGreen (A) and the cell count from the live-dead images (B) at day 1 and 7. Standard deviations (n=3) and significative differences are shown.

Visually, f-gelNB gels were weaker than f-GelMA ones, and LAP gels similar or weaker than Ru/SPS gels, when in the previous tests the contrary was concluded (in Figure 13). F-gelNB 5% LAP gels dissolved by day 7, so tests could not be performed at that timepoint.

Regarding viability (Figure 14), most of the significant differences were at day 1, but by day 7 they were all at a similar level, being the living:dead cell ratio higher than before. In general, all of them present a similar viability ratio, higher than the minimum accepted one (80%), a week after cell encapsulation. The only exception was f-gelNB 5% LAP, where there was no gel.

As for proliferation, the DNA concentration was significantly reduced from day 1 to 7 in all cases. At day 7, differences could be observed among the f-GelMA group (Figure 15A), but not among the f-gelNB group. Besides, when comparing 10% f-GelMA vs f-gelNB gels, the first ones had a higher DNA amount than the second

ones, what correlates with higher living cell count. This decrease in DNA concentration was unusual, as it generally either increases (17) or stays similar (29,31). Thus, the cell count of the living cells from the live:dead assay at days 1 and 7 was plotted (Figure 15B). In this case, there were no significant differences, therefore, cell number maintained over a week. Anyway, the cell proliferation experiment should have been repeated. No conditions were discarded for the following experiments.

3.2 Bioprinting optimisation

Before printing complex structures and cells with the DLP stereolithography, the printing parameters were optimized.

3.2.1 Printing error

The Envisiontec DLP printer has an error when printing with the settings used for hydrogels. A 4 mm cube was printed with the hydrogels test and PIC100 (Figure 16) and the part that was not printed (error), was measured (Table 10).

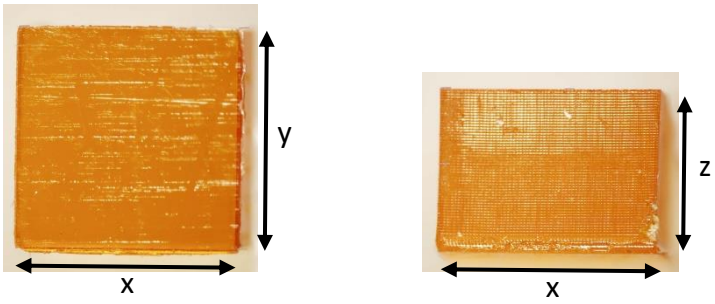

Figure 16. Cube printed with the DLP using PIC100 and the hydrogel settings from the software. Theoretically all sides had the same length, 4 mm. Pictures were taken at the microscope with 2.5x magnification.

Table 10. Measurements taken from all the sides of the cube. Each side was measured twice, using ImageJ and making the conversion to µm with the 2.5x scalebar. Standard deviation (sd) shown (n=2).

Axis	*Average length (µm)*	*sd*
x	4016,84	10,38
y	3998,60	26,95
Z	2848,76	25,83

The z side is smaller, as can be seen in both Figure 16 visually, and Table 10 checking the size of each. Both the x and y sides had the theoretical size, 4000 µm approximately (4 mm). However, the z side was smaller, with around 2,85 mm. The error was calculated:

$$4007{,}72\ (average\ between\ x\ and\ y) - 2848{,}76 = 1158{,}96\ \mu m\ \approx 1{,}16\ mm$$

Therefore, every time hydrogels were printed a 1,2 mm extra layer that would not be printed was added at the bottom part of the design.

3.2.2 Working curves

Working curves were made for both f-GelMA and f-gelNB, Ru/SPS (Figure 17) and LAP (data not shown). The Ru/SPS gels were made with the Envisiontec DLP and the LAP gels with the Atum DLP.

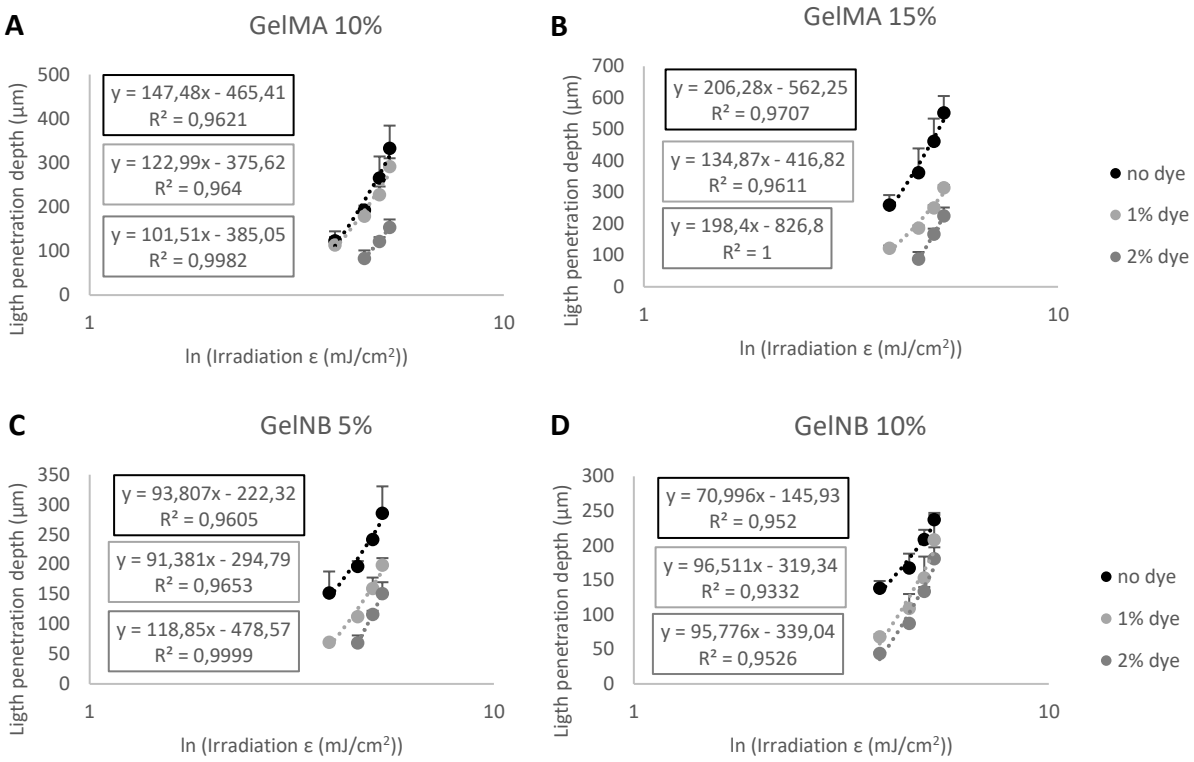

Figure 17. Working curves of gels with Ru/SPS, f-GelMA 10% (A), f-GelMA 15% (B), f-gelNB 5% (C) and f-gelNB 10% (D). The curves were calculated measuring the thickness of discs at different irradiated energies. Standard deviation is shown in the graphs (n=2).

The same experiment was performed using LAP. However, the results were not good. Using the lowest energy where gels could be crosslinked, the light penetration depth was too high (around 300 µm). As a result, it was decided to continue with the experiments only with the Envisiontec and Ru/SPS gels.

For the Ru/SPS group (Figure 17A and B), the trendlines with their equations were calculated in each graph. These equations are used to calculate the E_C, the minimum energy needed to crosslink the gel (in Table 11), with the following the equation 5 mentioned in the 2.8 section:

$$C_d = D_p \cdot \ln\frac{E}{E_C} \quad \rightarrow \quad E_C = e^{-b/slope} \tag{5}$$

Table 11. Minimum energy needed to crosslink the gel, obtained from the working curves. ln E_C was obtained by -b/slope.

Condition			*b*	*slope*	*ln E_C*	*E_C (mJ/cm^2)*
F-GelMA	*10%*	*no dye*	-465,41	147,48	3,16	23,47
		1% dye	-375,62	122,99	3,05	21,20
		2% dye	-385,05	101,51	3,79	44,40
	15%	*no dye*	-562,25	206,28	2,73	15,27
		1% dye	-416,82	134,87	3,09	21,99
		2% dye	-826,8	198,40	4,17	64,54
F-GelNB	*5%*	*no dye*	-222,20	93,81	2,37	10,68
		1% dye	-294,79	91,38	3,23	25,18
		2% dye	-478,57	118,85	4,03	56,07
	10%	*no dye*	-145,93	71,00	2,06	7,81
		1% dye	-319,34	96,51	3,31	27,35
		2% dye	-339,04	95,78	3,54	34,46

Once the minimum energy was calculated, the best condition for printing was selected, as well as the minimum printing intensity for each of them. The dye was used to increase the minimum energy, which is preferable. Thus, for all conditions the 2% dye was selected. As for the energy, all of them were between 35 and 65 mW/cm^2. Most of the following experiments and trials were performed with f-GelMA 10% 2% dye.

3.2.3 Positive and negative features

The resolution for printing hydrogels was tested, by printing positive and negative features, and perfusing the negative features (Figure 18).

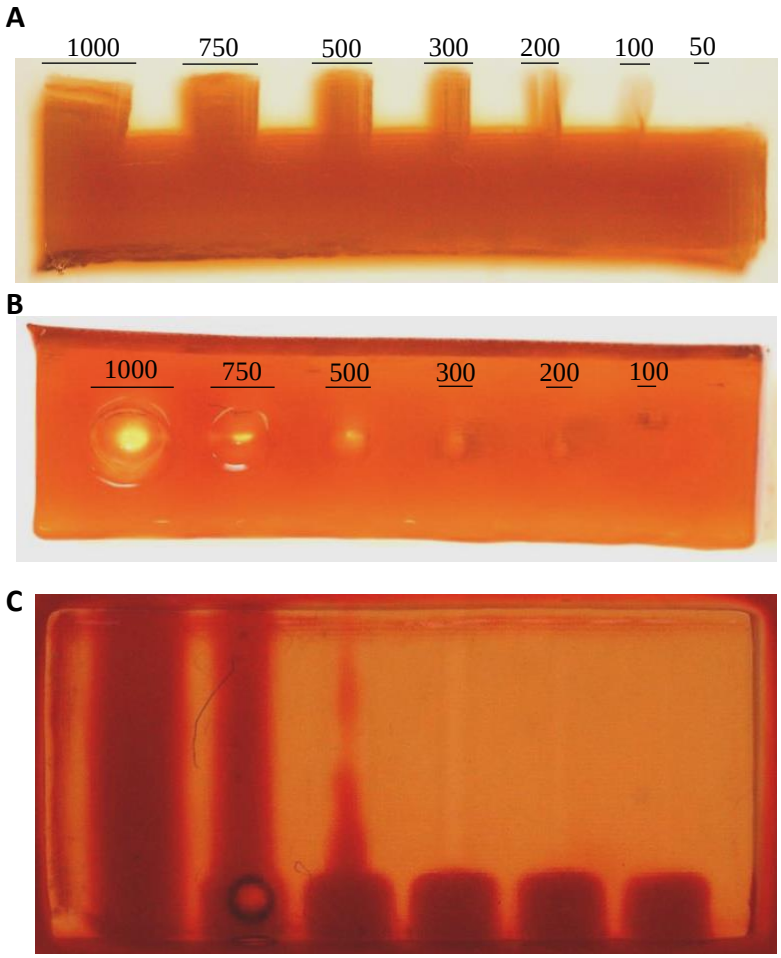

Figure 18. F-GelMA 10% 2% dye prints. Front view of positive features (A), bars with the theoretical width of each feature (µm). Back view of negative features (B), bars with the theoretical diameter of each channel (µm). Top view of negative features (C), perfused with red dye. Condition: f-GelMA 10% 2% dye 65 mJ/cm^2. Pictures were taken at the microscope with 1.5x magnification.

For f-GelMA, different conditions and intensities were tested, being 10% 2% dye 100 mJ/cm^2, 10% 2% dye 80 mJ/cm^2, 10% 2% dye 65 mJ/cm^2 and 15% 1,5% dye 100 mJ/cm^2 the best ones. The printed constructs were compared among them, by measuring the width of the positive and the diameter of the negative features on imageJ, and the channels were perfused. For the negative features, the horizontal and vertical diameters were calculated to detect the overcrosslinking (explained in section 2.9). By obtaining the ratio between the vertical and horizontal diameters, the circularity of the channels was calculated. In the following tables (Table 12 and 13), the comparison among these four conditions was made.

There were some difficulties printing 15% f-GelMA. The obtained constructs were brittle in the top layers, resulting in broken positive features or channels most of the times. For this reason, it was chosen to reduce the dye concentration from 2% to 1,5%.

Table 12. Comparison among the width of the positive features printed with f-GelMA. The closer to the theoretical, the better.

F-GELMA – POSITIVE FEATURES				
Column thickness (µm)	*Measured thickness (µm)*			
	10% 2% dye 100 mJ/cm^2	10% 2% dye 80 mJ/cm^2	10% 2% dye 65 mJ/cm^2	15% 1,5% dye 100 mJ/cm^2
1000	1318,96552	982,758621	1094,82759	1215,51724
750	1000	767,241379	844,827586	922,413793
500	714,285714	560,344828	593,406593	653,846154
300	500	494,505495	423,076923	445,054945
200	285,714286	230,769231	291,208791	274,725275
100	159,340659	-	153,846154	153,846154
50	-	-	-	-

Table 13. Comparison among the circularity of the negative features printed with f-GelMA. The closer to the 1, the better.

F-GELMA – NEGATIVE FEATURES				
Channel size (µm)	*Circularity*			
	10% 2% dye 100 mJ/cm^2	10% 2% dye 80 mJ/cm^2	10% 2% dye 65 mJ/cm^2	15% 1,5% dye 100 mJ/cm^2
1000	0,78854626	0,82524272	0,9009009	0,92741935
750	0,9005848	0,93333333	0,95930233	0,92307692
500	0,88888889	0,89473684	0,94915254	0,89830508
300	0,83333333	0,87179487	0,925	0,85294118
200	-	-	0,95652174	-
100	-	-	-	-

In both positive and negative features, the 10% 65 mJ/cm^2 was the best option. The positive features were closer to the theoretical size, and the negative features were the most circular ones. Besides, only the 65 mJ/cm^2 gel was perfusable until the third channel (500 µm), being the other 10% gels until the second (750 µm) and the 15% one only in the first (1 mm). The last one might have been because of the dye concentration used (1,5% instead of 2%), but as explained before, it was difficult to print full constructs at this gel concentration and 2% dye.

On the other hand, the same experiment was performed with f-gelNB. Trials with both 5% and 10% gel concentration (2% dye) were made, but the obtained prints were poor, as it is shown in Figure 19.

Figure 19. F-gelNB 10% 2% dye prints. Back view of positive features (A) and back view of negative features (B). Condition: f-gelNB 10% 2% dye 65 mJ/cm^2. Pictures were taken at the microscope with 1.5x magnification.

The figure shows the best results obtained with gelNB. Generally, the prints were broken, as part stayed crosslinked on the baseplate (where the resin was located) instead of remaining on the building plate. Hence, most of the printing experiments were performed with GelMA.

3.3 Osteogenesis and chondrogenesis of bioprinted hydrogels

Both f-GelMA and f-gelNB 10% were printed with 2% dye and at 70 mJ/cm^2 energy with MSCs embedded. These were cultured in chondrogenic, hypertrophic and osteogenic medium for 28 days. At day 28, gels were harvested to perform DMMB, ALP and PicoGreen tests. Results for chondrogenesis and osteogenesis are shown in Figure 20.

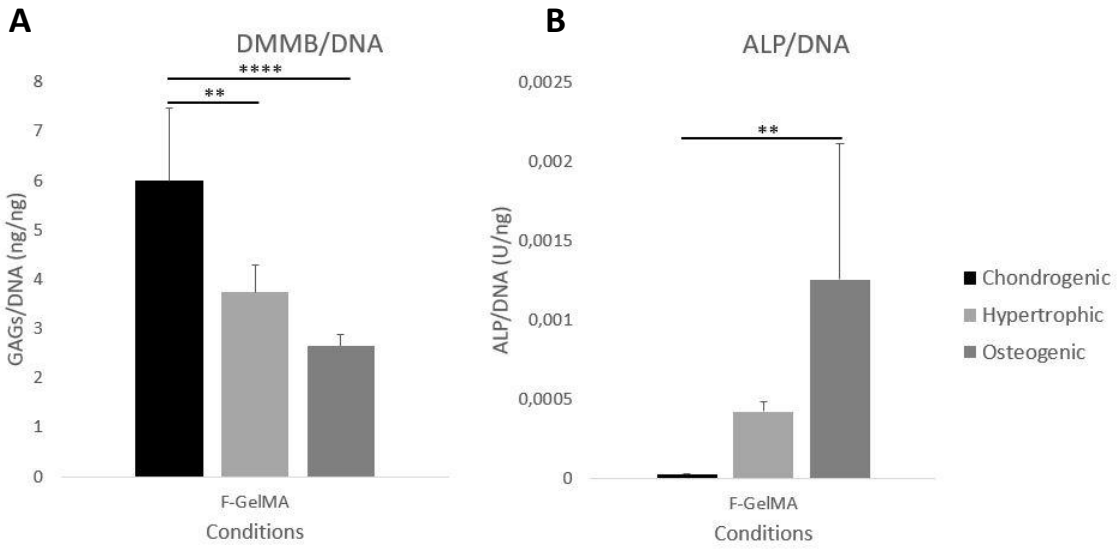

Figure 20. DMMB quantification (A) and ALP quantification (B) at day 28 of culture. DMMB was used to quantify GAGs (cartilage formation) and ALP for bone formation. Values were normalised for DNA quantity. Standard deviations (n=4) and significative differences are shown.

Although f-gelNB gels were also printed, they had the same problem as when positive and negative features were printed. As a result, the gels were thinner than the f-GelMA ones, most of them dissolved over the 28 days, and the ones that did not dissolve were extremely small and had undetectable GAG, ALP and DNA amounts. Therefore, they were discarded. Regarding GelMA hydrogels, cartilage production was significantly higher in the gels with chondrogenic medium (Figure 20A). For bone production, f-GelMA gels cultured in osteogenic medium had significantly higher ALP values than those cultured in chondrogenic medium. Thus, MSCs printed in f-GelMA gels could differentiate into cartilage and bone, whereas more testing should be done with f-gelNB to reach to a conclusion.

The harvested gels were also processed for histology, but these assays still need to be performed.

3.4 Printing of complex structures

Complex channels were printed to ensure that a vascular model could be printed in hydrogels with DLP lithograpy. Multiple channels that branched at different levels and spiral channels were printed.

3.4.1 Branching channels

The model shown below was printed (Figure 21) with f-GelMA 10% and 15%, 2% dye and 70 mJ/cm^2 energy. The constructs were perfused with red dye.

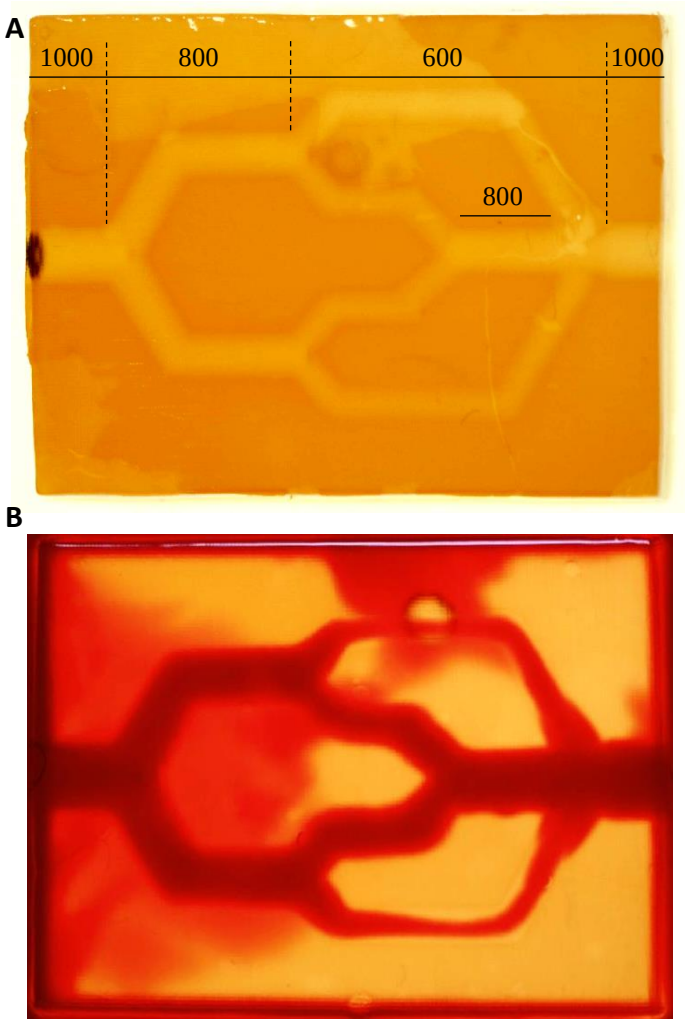

Figure 21. Printed structure with branching channels, f-GelMA 10% 2% dye 70 mJ/cm^2 energy. The bars (A) show the theoretical diameter of the channels. The channels with 600 µm diameter were designed at different levels, being the external ones slightly upper and the internal ones slightly lower than the rest. The channels were perfused (B). 3 gels per condition were printed. Pictures were taken at the microscope with 1,2x magnification.

Perfusing 10% gels was easier than 15% gels. Moreover, it has been previously mentioned that printing 15% gels carried some difficulties. Thus, it was determined that 10% gels had a better printing resolution. The 2 best gels were fixed in formalin to further perform a microCT.

3.4.2 Spiral channel

Apart from the branched channels, a structure with a straight channel at the centre and a spiral channel surrounding it was printed (Figure 22), with GelMA 10% (mixing 8% fish and 2% porcine), 2% dye and 70 mJ/cm^2. It was perfused with red dye.

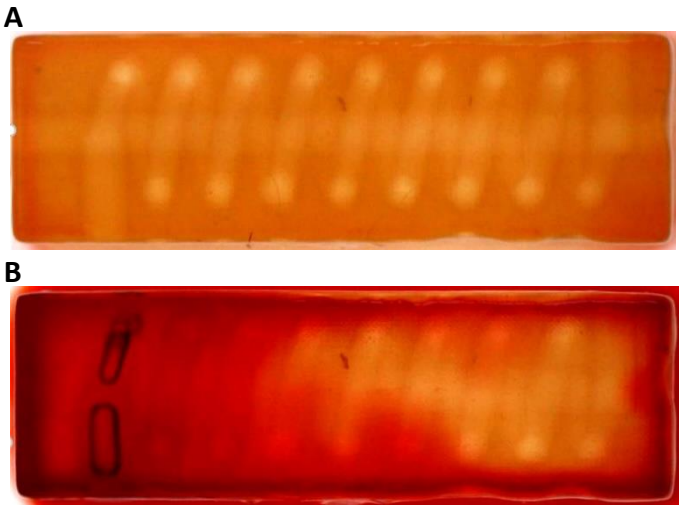

Figure 22. Printed structure with spiral channel, f-GelMA 8% - p-GelMA 2%, 2% dye 70 mJ/cm^2 energy. The theoretical diameter of the channels is 550 µm. The gel after being printed (A) and after being perfused (B). 6 gels were printed. Pictures taken at the microscope with 2.0x magnification.

In this case, only the first two-three twists could be perfused. A possible reason might be the fact of adding the 2% porcine GelMA, or the difficulty of the dye going from the lower part to the upper part of the twists. Anyway, the printing energy should be optimized again. The 2 best gels were fixed in formalin to further perform a microCT.

3.4 ECFC attachment to hydrogel surface

The attachment of the endothelial cells to the surface of gels was tested. To ensure that endothelial cells would attach to the walls of channels, a preliminary test was performed printing discs with a wall surrounding them (Figure 23). 4 conditions were printed, f-GelMA 10% 2% dye 100, 80 and 65 mJ/cm^2, and f-GelMA 15% 1,5% dye 100 mJ/cm^2.

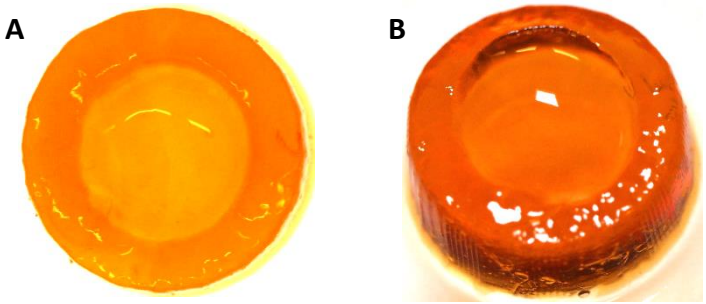

Figure 23. Pictures of the discs used to seed endothelial cells on top, top view (A) and 3/4 view (B). Images were taken at the microscope with 1.5x magnification. 10% f-GelMA 2% dye, 65 mJ/cm^2 is shown in the figure.

These gels were used to seed fluorescent endothelial cells on top, and their attachment and ability to generate a monolayer and cover the surface of the gels was tested (Figure 24).

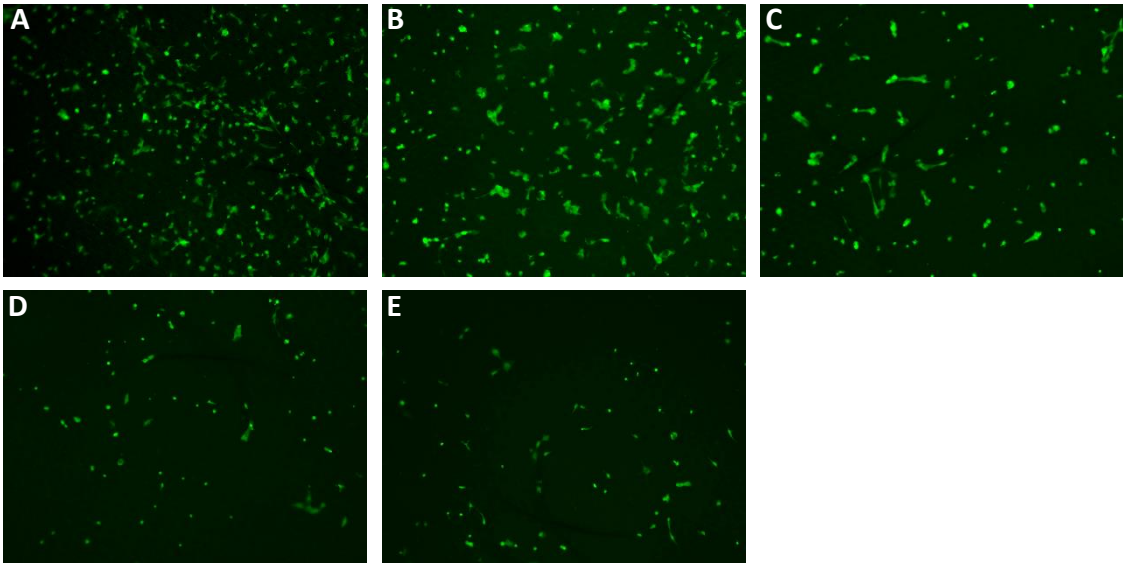

Figure 24. Evolution of the endothelial cell attachment to the surface of gels. 10% f-GelMA 2% dye 65 mJ/cm^2 is shown in the figure, at day 0, 1, 3, 6 and 7 (A-E, respectively). Pictures were taken at the upright fluorescence microscope, 4x magnification. 4 gels per condition were used.

Only pictures of the best condition are shown, because all had a similar trend. Cells seemed to grow on the first two days, but they did not attach and form monolayers, and they died over time.

The same experiment was performed with the gels casted in a 24 well plate. Many different conditions were tested (shown in the 2.15 section), obtaining slightly better results with the gels containing 1% or 2% porcine GelMA. The results are shown in Figure 25 and 26.

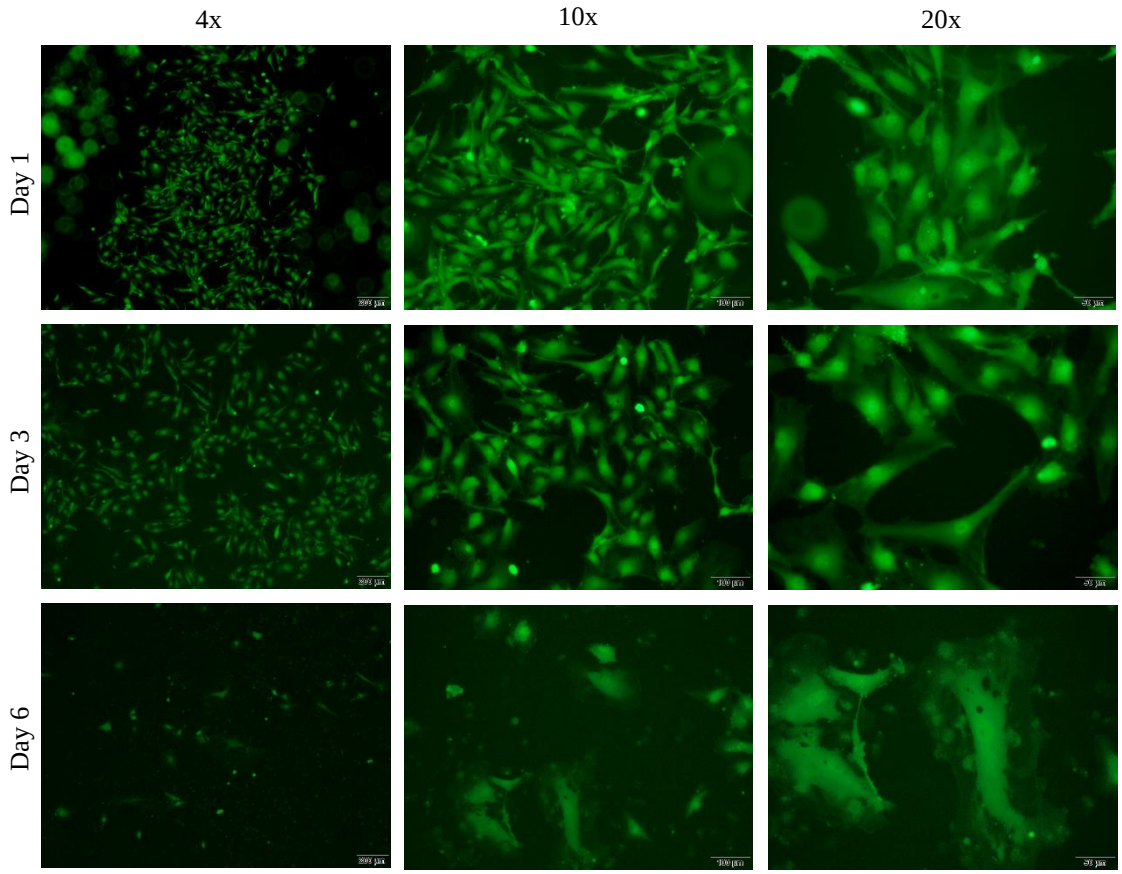

Figure 25. 9% f-GelMA + 1% p-GelMA gels. Pictures were taken at the inverted microscope at different magnifications, at day 1, 3 and 6 after adding the cells. 2 gels were made per condition.

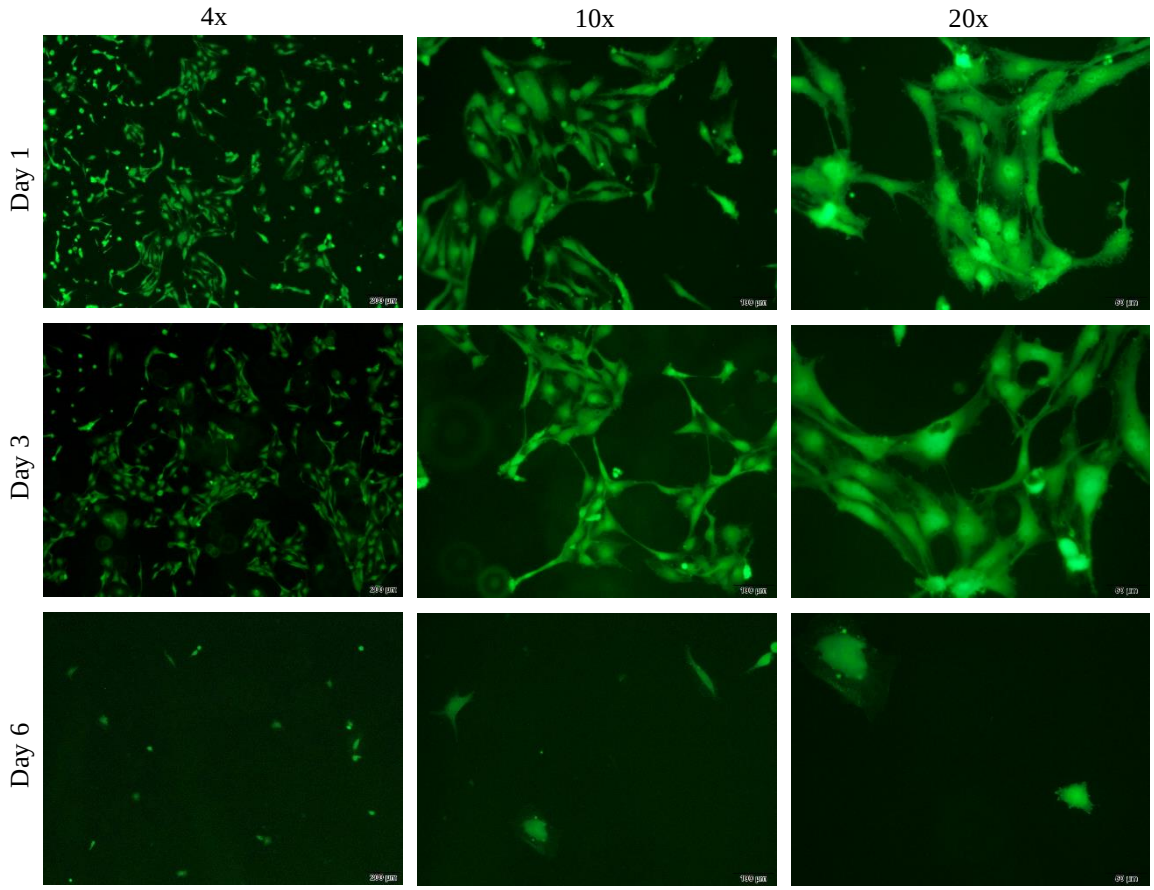

Figure 26. 14% f-GelMA + 1% p-GelMA gels. Pictures were taken at the inverted microscope at different magnifications, at day 1, 3 and 6 after adding the cells. 2 gels were made per condition.

In both cases (Figures 25 and 26), cells seemed to be forming monolayers at day 1. However, no proliferation was observed at day 3, and most of the cells were not attached by day 6. Furthermore, the attached cells did not look like normal endothelial cells when they form a monolayer, where cells have a more polygonal shape rather than being stretched (an example is shown on Figure 27). The day 6 10% gel picture at 20x magnification is not the shape or size endothelial cells have, probably some cells were converged because they were dying.

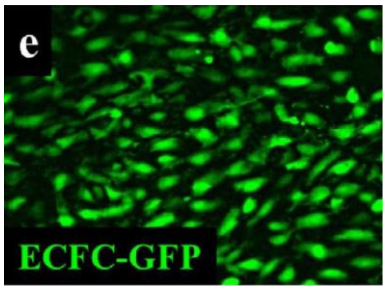

Figure 27. ECFCs attached to GelMA hydrogels, forming a monolayer (10). Picture taken at day 5 with 10x magnification.

None of the tested conditions worked, and it was speculated that it could have been due to the toxic molecules the gels released when they were not washed properly.

To determine if the last point was a problem, 6 mm diameter gels were casted and washed thoroughly during days. When they stopped releasing orange dye (due to the ruthenium), endothelial cells were attached on top. In one of

the conditions (f-GelMA 15%) condition medium was used in cells seeded wells without hydrogels (explained in the 2.15 section). In this way it could be proved if gels released a toxic compound that kills the cells. Results are shown in Figure 28.

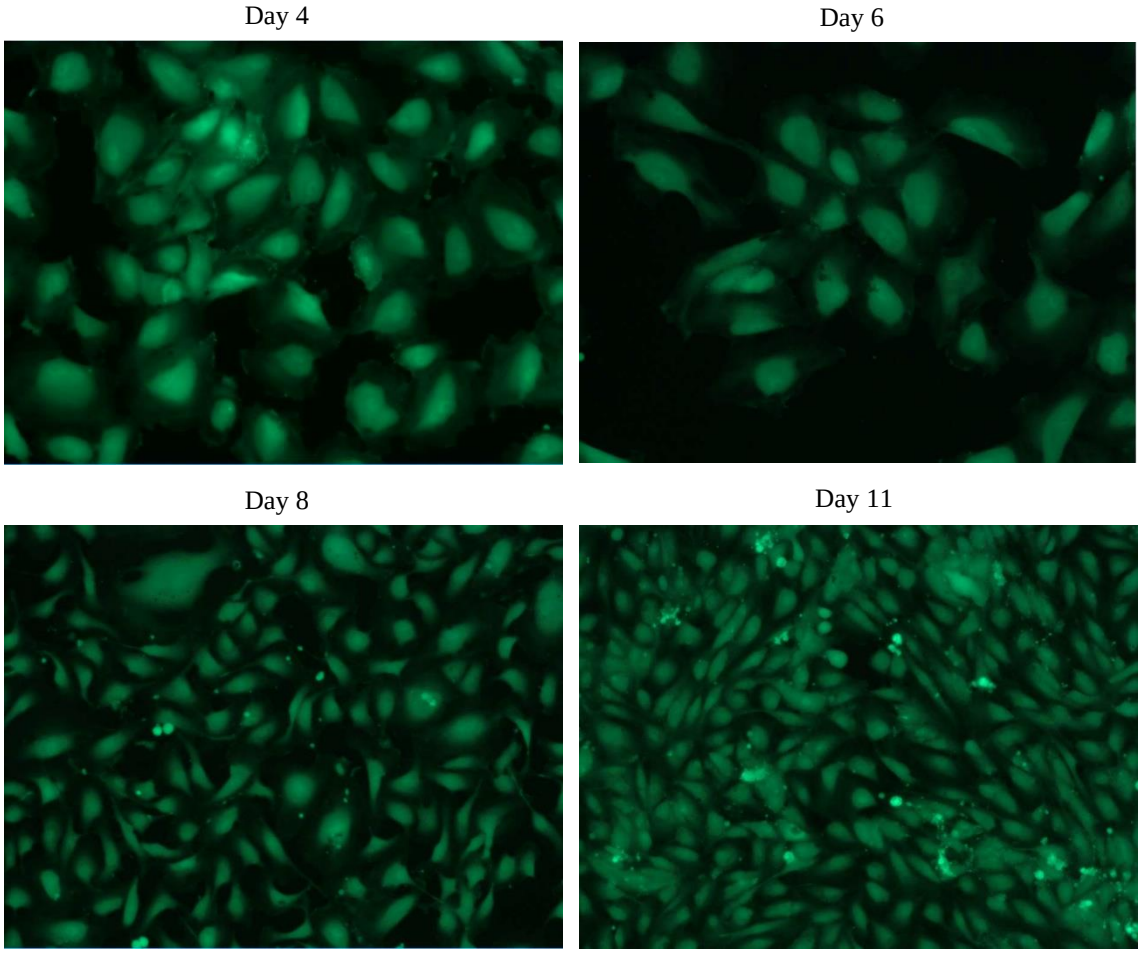

Figure 28. Fluorescent endothelial cells attached to the bottom of the 48-well plate. Images taken at the inverted fluorescence microscope at 10x magnification. Medium in contact with gels without cells was added at day 4 and 7.

The pictures show that not only cells did not die, but they proliferated when they were seeded in plastic (coated with collagen). The medium that had previously been in contact with gels did not cause any damage to cells in attachment or proliferation. Therefore, toxicity of hydrogels was not the reason why cells did not attach and died.

4. Discussion

Photocrosslinkable hydrogels are highly used for tissue engineering applications, because their properties (sol fraction, swelling, stiffness) are tunable and they allow high cell viability (36). Getalin methacrylate (GelMA) is one of the most commonly used hydrogels (33). However, hydrogels functionalised with methacrylate polymerise in a chain-growth reaction that may not be suitable for some cell types (30). For this reason, hydrogels that are polymerised via thiol-ene photoclick reactions, such as gelatin norbornene (gelNB) are preferred (5,24,28,30), but gelNB has not been well explored yet. Besides, UV light has been more widely used for the light-induced crosslinking, but long UV exposure results in DNA damage (21). Hence, new strategies are being explored using visible light, such as the ru/SPS system (22,31,42).

Theoretically, gelNB hydrogels crosslinked with ru/SPS would be the most suitable for tissue engineering applications, due to the previously mentioned advantages that both the gel precursor and the photoinitiators present. Nevertheless, the use of this combination has not been reported yet, therefore, different hydrogel combinations of GelMA, gelNB, ru/SPS and LAP were characterised and compared. Apart from that, cold fish gelatin was used instead of the regularly used porcine gelatin, due to its lower gelling point (33), which facilitates its applicability to DLP printing.

When the crosslinking efficiency and stiffness of gels was analysed, f-gelNB hydrogels had a higher gel content than their f-GelMA equivalents, which means that their crosslinking efficiency was higher on f-gelNB gels. Besides, swelling ratio of gels was analysed because it is related to mechanical properties of gels (36). This parameter is inversely proportional to the gel content, as the gel content increases with the density of the networks generated, and the swelling capacity of the gel is lower when these networks increase (43). In general, ru/SPS gels swelled more than LAP gels. According, to Lim et al. (31), GelMA 10% Ru/SPS gels had a sol fraction of around 10% and a swelling ratio of 9-10, whereas in this case, the sol fraction was 28% and the swelling ratio 14. However, it must be underlined that they used porcine GelMA, not fish GelMA, so the differences may lie in the source of the gelatin. When compared to p-GelMA, f-GelMA gels showed a higher swelling ratio (32).

Apart from that, the Young's modulus obtained by the compression test were also compared. This parameter is related to the swelling ratio, increasing when the swelling decreases and vice-versa (44). F-gelNB and LAP hydrogels were stiffer when compared to f-GelMA and Ru/SPS respectively. Besides, Yoon et al. and Wang et al. (32,33) compared, among other factors, the stiffness of fish and porcine GelMA, showing that gelatin from cold-water fish had a lower elastic modulus than the porcine one. It has been also shown that the degree of methacrylation of the hydrogel affects the stiffness, increasing with the methacrylation (10,17,32,36,45). In our case, highly methacrylated (80%) fish hydrogels were used, as Yoon et al. did (32), obtaining a result of around 5 kPa, 13 kPa and 47 kPa for 5%, 10% and 15% f-GelMA respectively. These are slightly higher than the LAP f-GelMA results, 8 kPa and 35 kPa for 10% and 15% f-GelMA, probably because of the different photoinitiator used by Yoon et al., Irgacure 2959. Too weak hydrogels degrade easily and do not provide cells with mechanical support, and too stiff hydrogels do not allow cells to migrate into it and the ECM they release stays confined around the cells instead of spreading all over the gel. For this reason, too weak (f-GelMA 5%) and too stiff hydrogels (f-gelNB 15%) were discarded.

Hydrogels are known to support cell growth with high viability (36). This could be observed in the results, where cell viability was over 80% by day 7 in all the conditions (except from 5% f-gelNB LAP gels, which degraded over time). Many authors have encapsulated different cell types in different hydrogels before. For example, Nichol et al. and Wang et al. encapsulated fibroblasts in different GelMA concentrations (21,33,36), Muñoz et al. and Lim et al. used MSCs (30,31). Lim et al. compared the use of the visible light (ru/SPS) to the UV light (Irgacure 2959), determining that the visible light provided a higher cell viability (of around 85%, similar to the results of f-GelMA ru/SPS day 7). Muñoz et al. compared MSCs viability encapsulated in GelMA and gelNB, where they determined that gelNB gels showed higher cell viability than GelMA ones. However, the differences in both visible and UV light-induced crosslinking, and f-GelMA and f-gelNB are not significant for these experiments, therefore, these premises cannot be confirmed. Finally, Lin et al. (8) reported that 0,125% or higher LAP

concentrations were toxic for cells. For f-GelMA gels, 0,05% LAP was used, but for f-gelNB gels, 0,2% LAP was used. This might be the reason why in Figure 14 cell viability is poor in f-gelNB LAP gels at day 1.

On the other hand, cell concentration in gels decreased in more than two-fold in almost all cases, meaning that cells did not proliferate and died over time. These results are supported by Celikkin et al. (27), who observed a decrease in DNA content over time when MSCs were encapsulated in GelMA. However, they contrast with the results obtained by other authors (9,21,31,32), where cells embedded in hydrogels proliferate over time. Despite the use of other photoinitiators or cells, in all cases they grow two to three times when embedded in GelMA, even when UV light is used. Lim et al. (31) proved that the use of ru/SPS photoinitiators improves cell proliferation over Irgacure 2959. Besides, according to Yoon et al. (32), there are no significant differences in cell proliferation among porcine and fish GelMA. Unfortunately, gelNB hydrogels are not comparable to previous literature. As the results obtained show the opposite of what has been previously stated, microscopy pictures from the live-dead assay were used to compare the cell count from day 1 to 7. Figure 15B shows that the number of cells remains stable in all cases except from f-GelMA LAP gels, where there is not even a significant decrease. Therefore, although literature already shows that ru/SPS gels outperform Irgacure or LAP gels, the proliferation test should be repeated in order to obtain a reliable conclusion and decide if there are significant differences among f-GelMA and f-gelNB.

Printability of hydrogels was tested by the generation of working curves in the DLP for all conditions (f-GelMA, f-gelNB, ru/SPS and LAP). The use of the photoabsorber (Ponceau red) was intended to decrease the light penetration depth of hydrogels, and thus, make the printing porcess more tunable and controllable. The working curves provide an approximate information of the irradiation light energy required to obtain a high resolution on the prints, contributed by the thickness of the layers printed, the thinner the better. Working curves were correct and linear for ru/SPS gels, however, with LAP hydrogels, they were not linear, being the light penetration depth too high for printing gels with small channels (the thinnest layers were 300 µm, whereas with ru/SPS 50-70 µm layers could be obtained). In any case, it has been previously reported that long UV or near-UV light exposure, decreases cell viability and is mutagenic (4,31). Moreover, in order to reduce oxygen inhibition with GelMA, LAP concentration was increased to 0,2%, which has been previously mentioned to be toxic (8). Thus, even if LAP hydrogels were printable, cells would have a poor viability. Apart from that, it has been proven that oxygen inhibition deteriorates the final result of the print, what occurs using photoinitiators such as LAP or Irgacure 2959, but not with ru/SPS (22). For this reason, all experiments were continued using only ru/SPS and visible light, with 2% photoabsorber.

When the hydrogels were printed, f-gelNB failed in all the printed designs. Part of the gels were on the building platform where the prints should be, but other parts were on the baseplate where the resin is. It was hypothesized that this occurred because f-gelNB reacts faster than f-GelMA, as it has no oxygen inhibition (30). Thus, it was thought that the bioresin placed at the beginning of the print gelated before the print finished, staying, in part, on the baseplate. Furthermore, when 15% f-GelMA prints were more brittle and the top layers (the ones that print in the end) were not well crosslinked. Therefore, almost all the gels were printed with 10% f-GelMA. The printing resolution was good, proven by the positive features, where 100 µm thick columns could be printed. However, not all channels from the negative features were open and perfusable, and energy was decreased to obtain more open channels. The best results were obtained with a 65 mJ/cm^2 irradiation energy, where 500 µm channels were

perfusable. Besides, branched channels of 1 mm, 800 µm and 600 µm diameter were successfully printed and perfused, demonstrating that a complex vascular model could be printed with the DLP. It has been previously demonstrated (18) that comparing hydrogel channelled constructs over non-channelled ones, cell viability (90% over 55% at day 7) and osteogenesis (40 times higher ALP activity in channelled ones at day 14) is significantly higher in the first ones. Therefore, the viability of printing channels with DLP implies a great advance for long-term 3D culture and tissue engineering

Apart from that, MSCs were printed with the DLP in hydrogel discs, where chondrogenesis and osteogenesis were checked at day 28. F-gelNB discs were not printed correctly and reliable results could not be obtained, so only differences among f-GelMA gels were compared. It was observed that ALP activity was significantly higher on gels cultured in osteogenic medium. However, ALP is an early osteogenic marker. Celikkin et al. (27) measured osteogenesis over time in GelMA hydrogels, noticing that ALP activity had a peak at day 14 but decreased afterwards. Thus, ALP measurement would be a more suitable approach for a day 14 timepoint, and a calcium deposition assay could be performed at day 28 instead, as Celikkin et al. showed (27). Despite this issue, it was proven that MSCs printed in hydrogels were able to undergo osteogenesis. Regarding chondrogenesis, there were significant differences among the 3 culture mediums at day 28, being the chondrogenic medium the best one. Nevertheless, these results were worse than the ones in the literature, where MSCs embedded in GelMA showed a ratio of GAGs/DNA of 125 (46). The difference could be related to the use of f-GelMA instead of p-GelMA, the photoinitiator or the printing process. Moreover, according to Li et al. (7), hydrogels with 30 kPa of stiffness show better results at maintaining a cartilaginous phenotype in MSCs, thus, stiffness of hydrogels should be also considered for this purpose. In any case, this experiment should be repeated to include a day 1 (and maybe a day 14) timepoint and include the f-gelNB gels.

Finally, the attachment of ECFCs and their ability to form monolayers on the f-GelMA surface was tested, with poor results. Cells did not attach and died over time and it was due to neither the use of fish GelMA (because tests were also performed in porcine GelMA and a fibrinogen coating, with similar results), nor the hydrogels releasing a toxic compound that killed ECFCs (because cells attached to the bottom of the plate and did not die when medium in contact with gels was added). Various authors worked on endothelial cell attachment to GelMA before. Klotz et al. (10) seeded GFP-ECFCs on GelMA 5% hydrogels, forming a confluent monolayer by day 10 in gels with 50% methacrylation degree. Cells detached from 30% methacrylated gels, and the experiment was not performed in highly methacrylated gels (the gels used in our experiments were 80%). Nichol et al. (36) seeded GFP-HUVECs on the surface of hydrogels with different GelMA concentrations, proving that cells adhered better to more concentrated GelMA gels, and Gauvin et al. (20) seeded the same cells on a GelMA scaffold with hexagonal pores, covering all the surface in 4 days. All these results were with porcine GelMA, which might differ to the use of fish GelMA. However, Yoon et al. (32) showed no difference between cell attachment to fish or porcine GelMA surface, and no difference between medium (55%) or high (90%) methacrylation degree (although they were fibroblasts, not endothelial cells). Moreover, it has also been shown that HUVECs attach to the channels inside p-GelMA (18,36). Bertassoni et al. (18) tested endothelial cell attachment to channels with different diameters, demonstrating that in all of them cells eventually form confluent monolayers. All these references share the use of Irgacure 2959 as a photoinitiator, so the use of ru/SPS might have a negative effect on the capacity of ECFCs to attach to hydrogels. Hence, a control with an Irgacure 2959 hydrogel should have been used to compare the effect of the photoinitiator on cell attachment.

5. Future prospects

Some experiments should be repeated or performed in the future to obtain vascularised hydrogels where MSCs could proliferate and derive into either bone or cartilage. First, the MSCs should be embedded again into both f-GelMA and f-gelNB hydrogels and cultured for 7 days to repeat the proliferation analysis. If the results show again that DNA concentration decreases in a week period, it means that cells do not survive in these gel formulations.

Second, the problem of 3D printing with f-gelNB should be solved. To do so, first gelNB gels should be casted with lower photoinitiator concentrations and see if there is little change in crosslinking efficiency and stiffness. This needs to be tested because literature shows that gelNB gels can be generated with lower photoinitiator concentrations (39). Once the formulation with the lowest acceptable photoinitiator concentrations is achieved, the gels should be 3D printed and whether the problem is solved or not should be checked. Lower printing energies could also be tested until obtaining the best printing parameters to achieve high resolution constructs.

Third, the chondrogenesis and osteogenesis assays should be repeated, this time with f-gelNB gels and new timepoints at day 1 and 14 apart from the day 28. A late osteogenic marker, like calcium deposition, could also be measured.

Finally, the endothelial cell attachment problem should be solved. More different conditions could be tested to find the reason why it did not work, including f-gelNB hydrogels, and a control with Irgracure 2959, which most of the attachment experiments are performed with in the literature.

Once all these problems are solved, the final experiment could be performed: printing both f-GelMA and f-gelNB hydrogels with embedded MSCs and complex channels. ECFCs would be then seeded in the surface of the channels and the constructs would be cultured to check the feasibility of the vascularisation and development of bone.

6. Conclusions

In summary, this study showed that fish GelMA hydrogels could be employed to print complex channelled structures with perfusable channels as small as 500 µm thick. Besides, these hydrogels could also be printed with MSCs and differentiate into osteocytes and chondrocytes. In general, gels crosslinked with ru/SPS photoinitiators showed better results than the ones with LAP. These were similar in crosslinking efficiency and mechanical properties, but better in cell viability and proliferation. On the other hand, there were no differences among GelMA and gelNB hydrogels, proving that gelNB gels can be used instead of GelMA ones due to the oxygen inhibition that the latter show. Apart from that, the 3D printing of the hydrogels with the DLP printer was optimised, with positive results for f-GelMA ru/SPS but poor results for f-gelNB ru/SPS. Finally, the attachment of endothelial cells to the surface of the GelMA ru/SPS hydrogels was not achieved.

In conclusion, f-GelMA crosslinked with ruthenium and SPS is an adequate hydrogel to print complex channelled and perfusable constructs with the DLP, and it is also capable of embedding MSCs that grow and differentiate. However, the gelNB with ruthenium and SPS still needs to be optimised for printing, and endothelial cells cannot attach to the surface of the hydrogels. Once these two problems are solved, f-GelMA and f-gelNB with ruthenium

and SPS will be promising bioinks to print vascularised models with embedded MSCs and endothelial cells seeded on the surface of the channels.

7. References

1. Bishop ES, Mostafa S, Pakvasa M, Luu HH, Lee MJ, Wolf M, et al. 3-D bioprinting technologies in tissue engineering and regenerative medicine: Current and future trends. Genes Dis. 2017;4(4):185–95.

2. Donderwinkel I, Hest CM Van, Cameron NR. Bio-inks for 3D bioprinting: recent advances and future prospects. Polym Chem. 2017;8:4451–71.

3. Melchels FPW, Feijen J, Grijpma DW. A review on stereolithography and its applications in biomedical engineering. Biomaterials [Internet]. 2010;31(24):6121–30. Available from: http://dx.doi.org/10.1016/j.biomaterials.2010.04.050

4. Panwar A, Tan LP. Current status of bioinks for micro-extrusion-based 3D bioprinting. Molecules. 2016;21(6):665–91.

5. Greene T, Lin CC. Modular Cross-Linking of Gelatin-Based Thiol-Norbornene Hydrogels for in Vitro 3D Culture of Hepatocellular Carcinoma Cells. ACS Biomater Sci Eng. 2015;1(12):1314–23.

6. Hribar KC, Soman P, Warner J, Chung P, Chen S. Light-assisted direct-write of 3D functional biomaterials. Lab Chip. 2014;14(2):268–75.

7. Li J, Chen M, Fan X, Zhou H. Recent advances in bioprinting techniques : approaches , applications and future prospects. J Transl Med. 2016;1–15.

8. Lin H, Zhang D, Alexnder PG, Yang G, Tan J, Cheng AW-M, et al. Application of visible light-based projection stereolithography for live cell-scaffold fabrication with designed architechture. Biomaterials. 2013;34(2):331–9.

9. Kim SH, Yeon YK, Lee JM, Chao JR, Lee YJ, Seo YB, et al. Precisely printable and biocompatible silk fibroin bioink for digital light processing 3D printing. Nat Commun [Internet]. 2018;9(1):1–14. Available from: http://dx.doi.org/10.1038/s41467-018-03759-y

10. Klotz BJ, Lim KS, Chang YX, Soliman BG, Pennings I, Malda J, et al. Engineering of a complex bone tissue model with endothelialised channels and capillary-like networks. Eur cells Mater. 2018;35:335–49.

11. Novosel EC, Kleinhans C, Kluger PJ. Vascularization is the key challenge in tissue engineering. Adv Drug Deliv Rev [Internet]. 2011;63(4):300–11. Available from: http://dx.doi.org/10.1016/j.addr.2011.03.004

12. Hoch E, Tovar GEM, Borchers K. Bioprinting of artificial blood vessels: Current approaches towards a demanding goal. Eur J Cardio-thoracic Surg. 2014;46(5):767–78.

13. Asakawa N, Shimizu T, Tsuda Y, Sekiya S, Sasagawa T, Yamato M, et al. Pre-vascularization of in vitro three-dimensional tissues created by cell sheet engineering. Biomaterials [Internet]. 2010;31(14):3903–9. Available from: http://dx.doi.org/10.1016/j.biomaterials.2010.01.105

14. Carmeliet P, Jain RK. Angiogenesis in cancer and other diseases. Nature. 2000;407(6801):249–57.

15. Kolesky DB, Truby RL, Gladman AS, Busbee TA, Homan KA, Lewis JA. 3D bioprinting of vascularized, heterogeneous cell-laden tissue constructs. Adv Mater. 2014;26(19):3124–30.

16. Byambaa B, Annabi N, Yue K, Trujillo-de Santiago G, Alvarez MM, Jia W, et al. Bioprinted Osteogenic and Vasculogenic Patterns for Engineering 3D Bone Tissue. Adv Healthc Mater. 2017;6(16):1–15.

17. Chen Y, Lin R, Qi H, Yang Y, Bae H, Melero-Martin JM, et al. Functional human vascular network generated in photocrosslinkable gelatin methacrylate hydrogels. Adv Funct Mater. 2012;22(10):2027–39.

18. Bertassoni LE, Cecconi M, Manoharan V, Nikkhah M, Hjortnes J, Cristino AL, et al. Hydrogel bioprinted microchannel networks for vascularization of tissue engineering constructs. Lab Chip. 2014;14(13):2202–11.

19. Lee VK, Lanzi AM, Haygan N, Yoo S-S, Vincent PA, Dai G. Generation of multi-scale vascular network system within 3D hydrogel using 3D bio-printing technology. Cell Mol Bioeng. 2014;7(3):460–72.

20. Gauvin R, Chen Y, Lee JW, Soman P, Zorlutuna P, Nichol JW, et al. Microfabrication of complex porous tissue engineering scaffolds using 3D projection stereolithography. Biomaterials. 2012;33(15):3824–34.

21. Wang Z, Kumar H, Tian Z, Jin X, Holzman JF, Menard F, et al. Visible Light Photoinitiation of Cell Adhesive Gelatin Methacryloyl Hydrogels for Stereolithography 3D Bioprinting. ACS Appl Mater Interfaces. 2018;

22. Lim KS, Levato R, Costa PF, Castilho MD, Alcala-Orozco CR, Van Dorenmalen KMA, et al. Bio-resin for high resolution lithography-based biofabrication of complex cell-laden constructs. Biofabrication. 2018;10(3).

23. DLP scheme [Internet]. Available from: http://www.3dprinting.lighting/3d-printing-technologies/stereolithography/%0A

24. Lin C-C, Ki CS, Shih H. Thiol-norbornene photo-click hydrogels for tissue engineering applications. J Appl Polym Sci. 2015;132(8).

25. Noshadi I, Hong S, Sullivan KE, Sani ES, Portillo-lara R, Tamayol A, et al. In vitro and in vivo analysis of visible light crosslinkable gelatin methacrylolyl (GelMA) hydrogels. Biomater Sci. 2017;5(i):2093–105.

26. Nguyen KT, West JL. Photopolymerizable hydrogels for tissue engineering applications. Biomaterials. 2002;23(22):4307–14.

27. Celikkin N, Mastrogiacomo S, Jaroszewicz J, Walboomers XF, Swieszkowski W. Gelatin methacrylate scaffold for bone tissue engineering: The influence of polymer concentration. J Biomed Mater Res - Part A. 2018;106(1):201–9.

28. Shih H, Liu HY, Lin CC. Improving gelation efficiency and cytocompatibility of visible light polymerized thiol-norbornene hydrogels via addition of soluble tyrosine. Biomater Sci. 2017;5(3):589–99.

29. Fedorovich NE, Oudshoorn MH, van Geemen D, Hennink WE, Alblas J, Dhert WJA. The effect of photopolymerization on stem cells embedded in hydrogels. Biomaterials [Internet]. 2008;30(3):344–53. Available from: http://dx.doi.org/10.1016/j.biomaterials.2008.09.037

30. Muñoz Z, Shih H, Lin C-C. Gelatin hydrogels formed by orthogonal thiol-norbornene photochemistry for cell encapsulation. Biomater Sci. 2014;2(8):1063–72.

31. Lim KS, Schon BS, Mekhileri N V., Brown GCJ, Chia CM, Prabakar S, et al. New Visible-Light Photoinitiating System for Improved Print Fidelity in Gelatin-Based Bioinks. ACS Biomater Sci Eng. 2016;2(10):1752–62.

32. Yoon HJ, Shin SR, Cha JM, Lee S, Kim J, Do T, et al. Cold Water Fish Gelatin Methacryloyl Hydrogel for Tissue Engineering Application. PLoS One. 2016;11(10):1–18.

33. Wang Z, Tian Z, Menard F, Kim K. Comparative study of gelatin methacrylate hydrogels from different sources for biofabrication applications. Biofabrication. 2017;9(4).

34. Singh S, Rao KVR, Venugopal K, Manikandan R. Alteration in Dissolution Characteristics of Gelatin-Containing Formulations. A Review of the Problem, Test Methods, and Solutions. Pharm Technol. 2002;23(April):36–58.

35. Van Den Bulcke AI, Bogdanov B, De Rooze N, Schacht EH, Cornelissen M, Berghmans H. Structural and rheological properties of methacrylamide modified gelatin hydrogels. Biomacromolecules. 2000;1(1):31–8.

36. Nichol JW, Koshy S, Bae H, Hwang CM, Khademhosseini A. Cell-laden microengineered gelatin methacrylate hydrogels. Biomaterials. 2010;31(21):5536–44.

37. Yue K, Santiago GT, Alvarez MM, Tamayol A, Annabi N, Khademhosseini A, et al. Synthesis, properties, and biomedical applications of gelatin methacrylolyl (GelMA) hydrogels. Biomaterials. 2015;73:254–71.

38. Shih H, Lin CC. Crosslinking and degradation of step-growth hydrogels formed by thiol-ene photo-click chemistry. Biomacromolecules. 2012;13(7):2003–17.

39. McCall JD, Anseth KS. Thiol-ene photopolymerizations provide a facile method to encapsulate proteins and maintain their bioactivity. Biomacromolecules. 2012;13(8):2410–7.

40. Fairbanks B, Schwartz M, Bowman C, Anseth K. Photoinitiated polymerisation of PEG-diacrylate with lithium phenyl-2,4,6-trimethylbenzoylphosphinate: polymerisation rate ans cytocompatibility. Biomaterials. 2009;30(35):6702–7.

41. Bryant SJ, Nuttelman CR, Anseth KS. Cytocompatibility of UV and visible light photoinitiating systems on cultured NIH/3T3 fibroblasts in vitro. J Biomater Sci Polym Ed. 2000;11(5):439–57.

42. Odadek THK. Chemistry for the analysis of protein – protein interactions : Rapid and efficient cross-linking triggered by long wavelength light. Proc Natl Acad Sci. 1999;96(May):6020–4.

43. Omidian H, Hasherni S, Askari F, Nafisi S. Swelling and Crosslink Density Measurements for Hydrogels. Iran J Polym Sci Technol. 1994;3(June 1994):115–9.

44. Anseth KS, Metters AT, Bryant SJ, Martens PJ, Elisseeff JH, Bowman CN. In situ forming degradable networks and their application in tissue engineering and drug delivery. J Control Release. 2008;78(1–3):199–209.

45. Li X, Chen S, Li J, Wang X, Zhang J, Kawazoe N, et al. 3D Culture of Chondrocytes in Gelatin Hydrogels with Different Stiffness. Polymers (Basel). 2016;8:269–84.

46. Levato R, Webb WR, Otto IA, Mensinga A, Zhang Y, van Rijen M, et al. The bio in the ink: cartilage regeneration with bioprintable hydrogels and articular cartilage-derived progenitor cells. Acta Biomater. 2017;61:41–53.